

# Coupled electron-phonon hydrodynamics and viscous thermoelectric equations

Jennifer Coulter,<sup>1,\*</sup> Bogdan Rajkov,<sup>2,\*</sup> and Michele Simoncelli<sup>2,3,†</sup>

<sup>1</sup>*Center for Computational Quantum Physics, Flatiron Institute, New York 10010, USA*

<sup>2</sup>*Theory of Condensed Matter Group of the Cavendish Laboratory, University of Cambridge (UK)*

<sup>3</sup>*Department of Applied Physics and Applied Mathematics, Columbia University, New York (USA)*

Non-diffusive, hydrodynamic-like transport of charge or heat has been observed in several materials, and recent, pioneering experiments have suggested the possible emergence of electron-phonon bifluids. Here we introduce the first-principles theory and computational framework to describe these phenomena, showing that the viscosity of electron-phonon bifluids is microscopically determined by composite “relaxon” electron-phonon excitations that also describe electron-phonon drag effects on thermoelectric transport coefficients. We show that these composite excitations emerge from the microscopic coupled electron-phonon Boltzmann transport equation, and demonstrate that the latter can be coarse-grained into a set of mesoscopic Viscous Thermoelectric Equations (VTE). The VTE unify the established hydrodynamic equation for electrons derived by Gurzhi [Sov. Phys. Usp. 11 1968], and the recently developed Viscous Heat Equations for phonons [PRX 10, 2020], while also extending them to cover the mixed electron-phonon bifluid regime. We employ this framework to elucidate from first principles the conditions under which electron and phonon fluids can coexist and mix, as well as to rationalize experimental signatures of electron-phonon drag in graphite.

## I. INTRODUCTION

Hydrodynamic transport for heat or charge in solids was theoretically predicted in the sixties [1–3] to occur when phonons or electrons exhibit crystal-momentum-conserving “normal” collisions much more frequently than momentum-dissipating “Umklapp” collisions, leading them to assume a collective drift velocity bearing analogies to the velocity field in a classical fluid. Pioneering experiments found unambiguous hallmarks of hydrodynamic thermal transport in dielectric solids. Mezhov-Deglin [1] measured a steady-state heat-flow profile akin to the typical parabolic “Poiseuille” profile of a viscous fluid that slows down in proximity of the boundaries of a pipe. Meanwhile, several other works [2, 4–7] observed transient heat propagation in the form of a coherent “second sound” temperature wave — an oscillatory evolution in which heat transiently backflows from colder to hotter regions, violating the smoothing property of diffusive transport [8, 9].

Observing hydrodynamic behavior for electrons initially proved more challenging. The first measurement was made three decades after heat hydrodynamics [10], and the field did not receive much attention until 2016, when electron-only hydrodynamics was predicted [11] and observed in graphene [12, 13], and simultaneously detected in PdCoO<sub>2</sub> [14], renewing interest in the field. Since then, several experiments have observed viscous behavior for electrons in graphene [15], and for phonons in graphite [16–20], always in micrometre-sized devices and at temperatures around 70-120 K. Very recently, hydrodynamic behavior has been observed at 300 K for electrons in graphene [21], and at 200 K for phonons in isotopically pure graphite [22].

Because this regime in which phonons or electrons behave fluid-like, rather than diffusively, shares formal analogies with fluid dynamics, several theoretical works have attempted to predict geometry- or boundary-condition-induced signatures of hydrodynamic transport using continuum Navier-Stokes-like partial differential equations. In the sixties, Gurzhi [3] coarse-grained the microscopic electron Boltzmann transport equation (eBTE) into continuum equations for hydrodynamic charge current and potential, which are still used nowadays to describe electron hydrodynamics [12, 23–26]. Similarly, Guyer and Krumhansl [27], Hardy and Albers [28], and others [27, 29, 30] derived from the phonon Boltzmann transport equation (pBTE) continuum models for heat hydrodynamics. Coarse-graining microscopic partial differential equations into continuum models requires performing approximations, whose practical accuracy is difficult to control a priori. Recent computational advances have enabled to solve from first principles the eBTE [31–35], the pBTE [34, 36–45], as well as coupled electron-phonon Boltzmann transport equation (epBTE) [46–49]. These insights have motivated reexamining the approximations involved in the derivation of continuum hydrodynamic models. For heat transport, this has led to extension of Fourier’s law [50, 51] or of the Guyer-Krumhansl equation [52, 53] to describe non-local heat transport in nanostructures, as well as a set of Viscous Heat Equations (VHE) [54] that encompass previous models as special limits [9] and, most importantly, describe with first-principles accuracy thermal transport from the hydrodynamic to the diffusive regime.

These developments have spurred the exploration of a physically richer phenomenon — the possibility of simultaneous electron and phonon hydrodynamics [55] — highlighting challenges in achieving a theoretically rigorous and quantitatively accurate description. In particular, several theoretical works have considered the single electron-phonon fluid regime, where continuous

\* These authors contributed equally to this work.

† michele.simoncelli@columbia.edu

momentum exchange between electrons and phonons through normal collisions results in a fluid in which they are perfectly mixed and share the same drift velocity [56, 57]. A recent experimental study [58] suggested the existence of an electron-phonon bifluid regime, where electron and phonon hydrodynamics occur concurrently but do not necessarily exhibit single-fluid physics. These experiments investigated heat transport in antimony upon lowering temperature, and attributed the absence of a hydrodynamic-to-ballistic transition [59] to the emergence of a two-component (not necessarily mixed) electron-phonon fluid. Additionally, these recent experiments [55, 58] have pointed to a possible connection between hallmarks of electron-phonon hydrodynamics and electron-phonon drag — the phenomenon in which out-of-equilibrium electrons induce out-of-equilibrium phonons via electron-phonon scattering, and vice-versa [60]. Drag has been extensively discussed in the literature in connection to redistribution of energy — but not momentum — between electrons and phonons [49, 60, 61]. Interestingly, several experiments have reported signatures of electron-phonon drag on the thermoelectric response of graphite [62–69] in the same temperature range where phonon-only hydrodynamics has been observed [16–20], suggesting it as a candidate for the observation of the electron-phonon bi-fluid regime. However, so far the relation between electron-phonon drag and bifluid hydrodynamics has been beyond the reach of first-principles accurate theoretical studies.

In summary, significant theoretical and experimental work has been done for single electronic, phononic fluids, or an idealized (perfectly mixed) single electron-phonon fluid. Yet, several critical questions remain unanswered: (i) Can semimetallic solids display the transport physics of multi-component fluids; in particular, can heat hydrodynamics drive charge hydrodynamics, and vice-versa? (ii) Can electron-phonon drag influence heat hydrodynamics, or even induce thermoelectric hydrodynamics? (iii) What is the influence of the boundary conditions applied to experimental devices on the hallmarks of electron-phonon hydrodynamics?

In this work, we introduce the first-principles theoretical and computational framework to quantitatively address these questions. We start by recasting the electron-phonon Boltzmann transport equation (epBTE) in a form amenable to be treated within the relaxon kinetic theory framework [70]. This enables us to discuss how microscopic conservation laws govern local equilibrium and transport, showing that standard diffusive thermoelectric coefficients (electrical and thermal conductivity, Seebeck and Peltier coefficients) are not sufficient to fully characterize conduction, and electron and phonon viscosities must be taken into account. We formally demonstrate this from a parity argument: electrons and phonons form coupled relaxon excitations that have well-defined (odd or even) parity. Odd components determine standard diffusive heat and charge flows, while the complementary even components determine hydrodynamic viscous flows.

We demonstrate that electron-phonon drag induces a change in the structure of relaxons, mixing otherwise independent electron and phonon relaxon excitations. We rely on these insights to coarse-grain the integro-differential epBTE into mesoscopic viscous thermoelectric equations (VTE) that unify Gurzhi’s [3] equation for electron fluids and the VHE for phonon fluids [54], and, most importantly, extend them to cover the coupled thermoelectric hydrodynamic regime. We rely on the VTE to explore electron-phonon bifluids in graphite, demonstrating that thermoelectric hydrodynamics induces measurable signatures, such as heat and charge flows that violate the similarity property characteristic of diffusive transport. Finally, we discuss possible experiments to probe electron-phonon hydrodynamics, as well as potential technological applications in electronics.

The manuscript is organized as follows. In Section II we introduce the epBTE and analyze its symmetries within the relaxon framework. In Sec. III we present the relation between microscopic electron-phonon relaxon excitations, their parity, and the macroscopic transport coefficients. In Sec. IV we rely on microscopic (quasi) conservation laws to coarse-grain the microscopic epBTE into the mesoscopic VTE. In Sec. V we show an application of our theoretical and computational framework to graphite, discussing how heat hydrodynamics is influenced by electron-phonon couplings as a function of doping. Finally, in Sec. VI we summarize results and discuss conceptual overlaps of our derivation with other coupled transport phenomena in solids, or with the framework used to describe classical fluids flowing through porous media.

## II. ELECTRON-PHONON TRANSPORT, FROM DIFFUSION TO HYDRODYNAMICS

### A. Electron-phonon Boltzmann transport equation

We describe the microscopic drift and scattering of electrons and phonons using the semiclassical Boltzmann transport framework. Specifically, we consider the linearized epBTE in the steady-state and in the absence of magnetic fields. Furthermore, we rewrite the integro-differential epBTE [60] in a physically insightful and numerically amenable matrix form, working in a vector space that is a direct sum of the electron and phonon subspaces [60, 71]:

$$\begin{aligned} & \left[ \begin{array}{c} \mathbf{v}_{\mathbf{k}m}^{\text{el}} \cdot \nabla_{\mathbf{r}} + \frac{e}{\hbar} [\nabla_{\mathbf{r}} V_{\text{eff}}] \cdot \nabla_{\mathbf{k}} \\ \mathbf{v}_{\mathbf{q}s}^{\text{ph}} \cdot \nabla_{\mathbf{r}} \end{array} \right] \left| \begin{array}{c} \mathbf{f}_{\mathbf{k}m} \\ \mathbf{n}_{\mathbf{q}s} \end{array} \right\rangle \\ &= - \left[ \begin{array}{c|c} S_{\mathbf{k}m,\mathbf{k}'m'}^{\text{el}} & D_{\mathbf{k}m,\mathbf{q}'s'}^{\text{el-ph}} \\ \hline D_{\mathbf{q}s,\mathbf{k}'m'}^{\text{ph-el}} & S_{\mathbf{q}s,\mathbf{q}'s'}^{\text{ph}} \end{array} \right] \left| \begin{array}{c} \mathbf{f}_{\mathbf{k}'m'} \\ \mathbf{n}_{\mathbf{q}'s'} \end{array} \right\rangle, \end{aligned} \quad (1)$$

where  $\mathbf{f}_{\mathbf{k}m}$  ( $\mathbf{n}_{\mathbf{q}s}$ ) denotes the deviation of the electron (phonon) population from equilibrium, with  $\mathbf{k}$  and  $m$  ( $\mathbf{q}$  and  $s$ ) being the wave vector and band index of the

electron (phonon) state. These deviations are defined as  $f_{\mathbf{k}m} = F_{\mathbf{k}m} - \bar{F}_{\mathbf{k}m}$  ( $n_{\mathbf{q}s} = N_{\mathbf{q}s} - \bar{N}_{\mathbf{q}s}$ ), where  $F_{\mathbf{k}m}$  ( $N_{\mathbf{q}s}$ ) is the total out-of-equilibrium electron (phonon) population and  $\bar{F}_{\mathbf{k}m} = (\exp[(\varepsilon_{\mathbf{k}m} - \bar{\mu})/(k_B\bar{T})] + 1)^{-1}$  ( $\bar{N}_{\mathbf{q}s} = (\exp[\hbar\omega_{\mathbf{q}s}/(k_B\bar{T})] - 1)^{-1}$ ) is the Fermi-Dirac (Bose-Einstein) equilibrium population at temperature  $\bar{T}$  for Bloch electrons with energy  $\varepsilon_{\mathbf{k}m}$  and chemical potential  $\bar{\mu}$  (phonons with energy  $\hbar\omega_{\mathbf{q}s}$ ).  $\mathbf{v}_{\mathbf{k}m}$  and  $\mathbf{v}_{\mathbf{q}s}$  are electron and phonon group velocities, respectively, and  $V_{\text{eff}} = V - \mu/e$  denotes the effective electric potential that accounts both for the external electric field and the variations in chemical potential [60]. In the linear regime, the force term in the electronic BTE is determined by spatial variations of the total chemical potential  $\mu_{\text{tot}} = -eV_{\text{eff}} = \mu - eV$ . The square brackets on the left-hand side denotes a matrix that is diagonal in both the electron and phonon subspaces. We employ the repeated-index summation convention, implying that the matrix-vector multiplication appearing on the scattering side of Eq. (1) has to be interpreted as follows:

$$\left[ \begin{array}{c|c} S_{\mathbf{k}m,\mathbf{k}'m'}^{\text{el}} & D_{\mathbf{k}m,\mathbf{q}'s'}^{\text{el-ph}} \\ \hline D_{\mathbf{q}s,\mathbf{k}'m'}^{\text{ph-el}} & S_{\mathbf{q}s,\mathbf{q}'s'}^{\text{ph}} \end{array} \right] \left| \begin{array}{c} f_{\mathbf{k}'m'} \\ n_{\mathbf{q}'s'} \end{array} \right\rangle = \left| \begin{array}{c} S_{\mathbf{k}m,\mathbf{k}'m'}^{\text{el}} f_{\mathbf{k}'m'} + D_{\mathbf{k}m,\mathbf{q}'s'}^{\text{el-ph}} n_{\mathbf{q}'s'} \\ D_{\mathbf{q}s,\mathbf{k}'m'}^{\text{ph-el}} f_{\mathbf{k}'m'} + S_{\mathbf{q}s,\mathbf{q}'s'}^{\text{ph}} n_{\mathbf{q}'s'} \end{array} \right\rangle, \quad (2)$$

which implies the following scalar product in the phonon-electron space:

$$\left\langle \begin{array}{c} f_{\mathbf{k}m} \\ n_{\mathbf{q}s} \end{array} \middle| \begin{array}{c} f'_{\mathbf{k}m} \\ n'_{\mathbf{q}s} \end{array} \right\rangle = \sum_{\mathbf{k}m} f_{\mathbf{k}m} f'_{\mathbf{k}m} + \sum_{\mathbf{q}s} n_{\mathbf{q}s} n'_{\mathbf{q}s}. \quad (3)$$

The notation used for the electron-phonon scattering matrix above highlights the various microscopic mechanisms that we are accounting for. The electronic quadrant  $S_{\mathbf{k}m,\mathbf{k}'m'}^{\text{el}}$  accounts for: (a) depumping and repumping scattering events involving electrons only, e.g. due to electron-electron interactions [72]; (b) electron depumping due to their interactions with phonons in an equilibrium bath state [60, 73]. Similarly, the phonon quadrant  $S_{\mathbf{q}s,\mathbf{q}'s'}^{\text{ph}}$  accounts for: (c) depumping and repumping scattering events involving phonons only, e.g. due to anharmonic phonon-phonon interactions [73]; (d) phonon depumping due to their interactions with electrons in an equilibrium bath state [60]. The off-diagonal quadrants account for electron-phonon drag effects, which are repumping scattering events that balance events (b) and (d). In particular,  $D_{\mathbf{k}m,\mathbf{q}'s'}^{\text{el-ph}}$  describes phonons' drag on electrons (i.e., out-of-equilibrium phonons that scatter with equilibrium electrons and drive them into an out-of-equilibrium state); analogously,  $D_{\mathbf{q}s,\mathbf{k}'m'}^{\text{ph-el}}$  describes electrons' drag on phonons (i.e., out-of-equilibrium electrons that scatter with phonons at equilibrium, driving the latter into an out-of-equilibrium state). The derivation of the expressions for scattering rates is discussed in Appendix A.

One can directly verify that neglecting the drag terms in Eq. (1) implies that the equations in the two rows decouple: the first row reduces to the well-known eBTE for

out-of-equilibrium electrons interacting with a phonon bath [31, 35, 74, 75] [76]; the second row reduces to the well-known pBTE for out-of-equilibrium phonons interacting among themselves due to anharmonic interactions [36, 37, 77–80] and with an electron bath [81]. The approximation of neglecting drag fails to capture the microscopic redistribution of energy and momentum between electrons and phonons, and consequently misses two physical effects: (i) the conservation of the total energy of the electron-phonon system [60], which is necessary for rigorously defining temperature [40]; (ii) the possibility that the total crystal momentum of the electron-phonon system is quasi-conserved in the presence of normal scattering dominating over Umklapp scattering. Including these drag terms  $D_{\mathbf{k}m,\mathbf{q}'s'}^{\text{el-ph}}$ ,  $D_{\mathbf{q}s,\mathbf{k}'m'}^{\text{ph-el}}$  rigorously overcomes both these two limitations. While recent developments [48, 49] have thoroughly investigated from first principles the effect (i) through an iterative solution of the epBTE, effect (ii) remains, to the best of our knowledge, largely unexplored with quantitative first-principles accuracy. In the following, we will address effect (ii) relying on the microscopic kinetic theory of relaxons [54, 70].

## B. Local thermoelectric equilibrium

When microscopic collisions between carriers conserve energy, charge, and (quasi) conserve momentum, the local equilibrium (LE) of electrons [56, 82, 83] and phonons [3, 28, 54] is described by “drifting” Fermi-Dirac and Bose-Einstein distributions, respectively. These are parametrized by a local temperature  $T(\mathbf{r})$  (emerging from the microscopic conservation of energy [60]), chemical potential  $\mu_{\text{tot}}(\mathbf{r})$  (stemming from charge conservation), and drift velocities for electrons  $\mathbf{u}_e(\mathbf{r})$  and phonons  $\mathbf{u}_p(\mathbf{r})$  (emerging from the possibly different quasi-conservation of momentum for electrons and phonons):

$$\left| \begin{array}{c} F_{\mathbf{k}m}^{\text{LE}}(\mathbf{r}) \\ N_{\mathbf{q}s}^{\text{LE}}(\mathbf{r}) \end{array} \right\rangle = \left| \begin{array}{c} \left( \exp \left[ \frac{\varepsilon_{\mathbf{k}m} - \mu_{\text{tot}}(\mathbf{r}) - \hbar\mathbf{k} \cdot \mathbf{u}_e(\mathbf{r})}{k_B T(\mathbf{r})} \right] + 1 \right)^{-1} \\ \left( \exp \left[ \frac{\hbar\omega_{\mathbf{q}s} - \hbar\mathbf{q} \cdot \mathbf{u}_p(\mathbf{r})}{k_B T(\mathbf{r})} \right] - 1 \right)^{-1} \end{array} \right\rangle \quad (4)$$

$$= \left| \begin{array}{c} \bar{F}_{\mathbf{k}m} \\ \bar{N}_{\mathbf{q}s} \end{array} \right\rangle + \left| \begin{array}{c} f_{\mathbf{k}m}^T(\mathbf{r}) + f_{\mathbf{k}m}^\mu(\mathbf{r}) + f_{\mathbf{k}m}^{u_e}(\mathbf{r}) \\ n_{\mathbf{q}s}^T(\mathbf{r}) + n_{\mathbf{q}s}^{u_p}(\mathbf{r}) \end{array} \right\rangle.$$

In the second line, we express the local equilibrium as a deviation from the global equilibrium  $\left| \begin{array}{c} \bar{F}_{\mathbf{k}m} \\ \bar{N}_{\mathbf{q}s} \end{array} \right\rangle$ , a form that is particularly useful in the regime of small deviations from the global equilibrium defined by  $\bar{T}$ ,  $\bar{\mu}$ ,  $\mathbf{u}_e = 0$ ,  $\mathbf{u}_p = 0$ . In fact, in such a regime one can expand the first line to linear order obtaining  $f_{\mathbf{k}m}^T = \partial_T F_{\mathbf{k}m}^{\text{LE}}|_{\text{eq}}[T(\mathbf{r}) - \bar{T}]$ ,  $f_{\mathbf{k}m}^\mu = \partial_\mu F_{\mathbf{k}m}^{\text{LE}}|_{\text{eq}}[\mu(\mathbf{r}) - \bar{\mu}]$ ,  $f_{\mathbf{k}m}^{u_e} = \partial_{u_e} F_{\mathbf{k}m}^{\text{LE}}|_{\text{eq}} \mathbf{u}_e(\mathbf{r})$ , and similarly for  $n_{\mathbf{q}s}^T$  and  $n_{\mathbf{q}s}^{u_p}$ .

We note that electrons are conserved in number and hence have a macroscopic chemical potential  $\mu(\mathbf{r})$  that can be different from zero; in contrast, phonons are not

conserved in number and hence have zero chemical potential. Importantly, in the expression above we used two different drift velocities for electrons and phonons to be able to describe the most general case in which they obey different quasi conservation laws. Specifically, in a system in which electrons and phonons are perfectly decoupled (i.e., featuring electron-electron and phonon-phonon scattering, but no electron-phonon scattering), electrons and phonons could in principle have different temperature and different drift velocities. To a good approximation, this is the case of an electrically insulating system, where phonon-phonon scattering dominates over electron-phonon and electron-electron scattering, and one obtains  $|\mathbf{u}_p(\mathbf{r})| \gg |\mathbf{u}_e(\mathbf{r})|$  and  $T(\mathbf{r})_{\text{ph}} \approx \bar{T} + T(\mathbf{r})$  and  $T(\mathbf{r})_{\text{el}} \approx \bar{T}$ . Conversely, in a metallic system at ultralow temperatures, one expects electron-electron scattering to be the dominant mechanisms, and a potential gradient  $\nabla V_{\text{eff}}$  implies  $|\mathbf{u}_e(\mathbf{r})| \gg |\mathbf{u}_p(\mathbf{r})|$ ,  $T(\mathbf{r})_{\text{el}} \approx \bar{T} + T(\mathbf{r})$ , and  $T(\mathbf{r})_{\text{ph}} \approx \bar{T}$ . Here, we account for the full scattering matrix that includes off-diagonal self terms [40] as well as off-diagonal drag terms [60], ensuring that microscopic electron-phonon and phonon-phonon scattering events perfectly conserve energy and enable its redistribution between electrons and phonons. This implies that the microscopic energy conservation law involves both electrons and phonons, and yields one single macroscopic temperature that is the Lagrange multiplier that ensures the microscopic conservation of energy [40, 84]. In contrast, the quasi conservation of crystal momentum is asymmetric between electrons and phonons — for example, the phonon-phonon quadrant includes Umklapp scattering events that do not involve electrons — and this asymmetry implies that one can have two fluid components, i.e. two different drift velocities  $\mathbf{u}_p(\mathbf{r})$  and  $\mathbf{u}_e(\mathbf{r})$ . As we will see later, it is critical to account for the possibility of having very different drift velocities for electrons and phonons to be able to capture the transition from phonon-only hydrodynamics to coupled electron-phonon hydrodynamics in semiconducting systems upon increasing doping.

### C. Electron-phonon relaxons

Solving the full epBTE (1) is a computationally challenging task, due to the high dimensionality of the full scattering matrix that couples electrons and phonons. The first step to tackle this challenge is to recast the problem in a form that is amenable to numerical treatment. To this aim, we show in Appendix A 2 that the scattering matrix can be rewritten in a symmetric — thus diagonalizable — form by applying a similarity transformation  $\mathbf{g}_{q_s}^{km} = 2 \left( \sqrt{\frac{\mathcal{D}}{(\mathcal{V}\mathcal{N}_k)}} \cosh \left[ \frac{\beta}{2} (\varepsilon_{km} - \mu) \right] \right) \left[ \frac{\beta}{2} \hbar \omega_{q_s} \right]$  [85]:

$$\Omega_{q_s, k'm'}^{km, k's'} = \mathbf{g}_{q_s}^{km} \begin{bmatrix} \text{S}_{km, k'm'}^{\text{el}} & \text{D}_{km, q's'}^{\text{el-ph}} \\ \text{D}_{q_s, k'm'}^{\text{ph-el}} & \text{S}_{q_s, q's'}^{\text{ph}} \end{bmatrix} \mathbf{g}_{q's'}^{-1, k'm'} \quad (5)$$

where the combined index  $\frac{km}{q_s}$  runs through both the electron and phonon states,  $\frac{\mathcal{D}}{\mathcal{V}\mathcal{N}_k}$  and  $\frac{1}{\mathcal{V}\mathcal{N}_q}$  are normalization factors that account for the electron spin degeneracy  $\mathcal{D}$ , number of electron wavevectors  $\mathcal{N}_k$ , number of phonon wavevectors  $\mathcal{N}_q$ , and unit-cell volume  $\mathcal{V}$ . Performing a similarity transformation on the scattering matrix also induces a transformation on the population vector, which assumes the symmetrised form  $|z_{q_s}^{km}\rangle = \mathbf{g}_{q_s}^{km} \left| \begin{smallmatrix} f_{km} \\ n_{q_s} \end{smallmatrix} \right\rangle$ , allowing us to rewrite the epBTE (1) as:

$$\mathbf{v}_{q_s}^{km} \cdot \nabla |z_{q_s}^{km}\rangle = - \sum_{\substack{k'm' \\ q's'}} \Omega_{q_s, k'm'}^{km, k's'} |z_{q's'}^{k'm'}\rangle, \quad (6)$$

where  $\mathbf{v}_{q_s}^{km} = \begin{bmatrix} \mathbf{v}_{q_s}^{\text{el}} \\ \mathbf{v}_{q_s}^{\text{ph}} \end{bmatrix}$  is a vector in the electron-phonon space containing electrons' and phonons' group velocities. It is insightful to recast the symmetrised coupled electron-phonon scattering matrix (5) in terms of its eigenvectors  $|\theta_{q_s}^\gamma\rangle$  and eigenvalues  $\tau^\gamma$ ,

$$\Omega_{q_s, k'm'}^{km, k's'} = \sum_{\gamma} \frac{1}{\tau^\gamma} |\theta_{q_s}^\gamma\rangle \langle \theta_{q's'}^\gamma|. \quad (7)$$

In fact, it has been shown [70] that the eigenvectors of the Boltzmann scattering matrix have the physical meaning of collective “relaxon” excitations that relax towards equilibrium with a lifetime  $\tau^\gamma$  determined by the inverse of the corresponding eigenvalue. In our case, relaxons are collective excitations involving mixtures of out-of-equilibrium electrons and phonons.

In the relaxon picture, quantities that are conserved by the microscopic epBTE dynamics (i.e., energy, charge, and quasi-conserved electron and phonon momentum) become apparent as they are related to eigenvectors of the scattering matrix with zero eigenvalue. In particular, the microscopic conservation of energy implies the emergence of the null “energy” eigenvector  $\Omega_{q_s, k'm'}^{km, k's'} |\theta_{q's'}^0\rangle = 0$  [60, 86], whose entries are related to the electron and phonon energies:

$$|\theta_{q_s}^0\rangle = \sqrt{\frac{1}{k_B \bar{T}^2 C_{\text{tot}}}} \left| \begin{smallmatrix} \sqrt{\frac{\mathcal{D}}{\mathcal{V}\mathcal{N}_k}} \sqrt{\bar{F}_{km}(1 - \bar{F}_{km})} (\varepsilon_{km} - \bar{\mu}) \\ \sqrt{\frac{1}{\mathcal{V}\mathcal{N}_q}} \sqrt{\bar{N}_{q_s}(1 + \bar{N}_{q_s})} \hbar \omega_{q_s} \end{smallmatrix} \right\rangle,$$

and  $C_{\text{tot}} = C_{\text{el}} + C_{\text{ph}}$  is the sum of the electron  $C_{\text{el}} = \frac{\mathcal{D}}{\mathcal{V}\mathcal{N}_k} \sum_{\mathbf{k}m} \frac{(\varepsilon_{km} - \mu)^2}{k_B T^2} \bar{F}_{km}(1 - \bar{F}_{km})$  and phonon  $C_{\text{ph}} = \frac{1}{\mathcal{V}\mathcal{N}_q} \sum_{\mathbf{q}s} \frac{\hbar^2 \omega_{q_s}^2}{k_B T^2} \bar{N}_{q_s}(1 + \bar{N}_{q_s})$  specific heat at constant volume. Similarly, the null eigenvector accounting for the conservation of charge is  $\Omega_{q_s, k'm'}^{km, k's'} |\theta_{q's'}^e\rangle = 0$ , which features nonzero entries only in the electron subspace and related to the constant electron charge  $-e$  [60]:

$$|\theta_{q_s}^e\rangle = \sqrt{\frac{e^2}{k_B \bar{T} \mathcal{U}}} \sqrt{\frac{\mathcal{D}}{\mathcal{V}\mathcal{N}_k}} \left| \begin{smallmatrix} \sqrt{\bar{F}_{km}(1 - \bar{F}_{km})} \\ 0 \end{smallmatrix} \right\rangle, \quad (9)$$

where  $\mathfrak{U} = \frac{e^2}{k_B T} \frac{\mathfrak{D}}{\mathcal{V} \mathcal{N}_k} \sum_{\mathbf{k}m} \bar{F}_{\mathbf{k}m} (1 - \bar{F}_{\mathbf{k}m})$  is a normalization constant related to the concentration of free carriers — at zero temperature it is proportional to the electronic density of states at the Fermi level [31].

In the diffusive regime, electron and phonon momentum is quickly dissipated by strong Umklapp scattering, and therefore the local equilibrium is fully described by the energy  $|\theta_{\mathbf{k}m}^0\rangle$  and charge  $|\theta_{\mathbf{k}m}^e\rangle$  eigenvectors. In contrast, in the hydrodynamic regime, we can expand the scattering matrix as  $\Omega = \Omega^N + \Omega^U$ , where  $\Omega^N$  is the dominant component containing normal collisions and  $\Omega^U$  is the component accounting for Umklapp collisions [87]. In an idealized system featuring only normal processes one would obtain null phonon momentum eigenvectors  $\Omega_{\mathbf{k}m, \mathbf{k}'m'}^N |\phi_{\mathbf{k}m}^{i,p}\rangle = 0$  for each  $i = 1, 2, 3$  Cartesian direction of the system, and null electron momentum eigenvectors  $\Omega_{\mathbf{k}m, \mathbf{k}'m'}^N |\phi_{\mathbf{k}m}^{i,e}\rangle = 0$ ; these eigenvectors have entries related to the phonon and electron momentum:

$$|\phi_{\mathbf{k}m}^{i,p}\rangle = \sqrt{\frac{1}{k_B T A_{\text{ph}}^i}} \sqrt{\frac{1}{\mathcal{V} \mathcal{N}_q}} \left| \begin{array}{c} 0 \\ \sqrt{\bar{N}_{qs}(1 + \bar{N}_{qs})} \hbar q^i \end{array} \right\rangle, \quad (10)$$

$$|\phi_{\mathbf{k}m}^{i,e}\rangle = \sqrt{\frac{1}{k_B T A_{\text{el}}^i}} \sqrt{\frac{\mathfrak{D}}{\mathcal{V} \mathcal{N}_k}} \left| \begin{array}{c} \sqrt{\bar{F}_{\mathbf{k}m}(1 - \bar{F}_{\mathbf{k}m})} \hbar k^i \\ 0 \end{array} \right\rangle. \quad (11)$$

Here,  $A_{\text{ph}}^i = \frac{1}{\mathcal{V} \mathcal{N}_q} \sum_{qs} \frac{(\hbar q^i)^2}{k_B T} \bar{N}_{qs}(1 + \bar{N}_{qs})$  is the phonon specific momentum [54], and, analogously,  $A_{\text{el}}^i = \frac{\mathfrak{D}}{\mathcal{V} \mathcal{N}_k} \sum_{\mathbf{k}m} \frac{(\hbar k^i)^2}{k_B T} \bar{F}_{\mathbf{k}m}(1 - \bar{F}_{\mathbf{k}m})$  is the electronic specific momentum.

In real systems Umklapp processes are present and imply that: (i) crystal momentum is not perfectly conserved, hence the vectors (10,11) cannot be null eigenvectors of  $\Omega$ ; (ii) the quasi-conservation of momentum can differ between the electron and phonon subsystems; (iii) by decreasing the strength of Umklapp collisions with respect to normal collisions, the momentum vectors (10,11) will progressively become eigenvectors of the full collision matrix, and their eigenvalue will progressively approach zero. Specifically, Umklapp scattering lifts the sixfold degeneracy of unperturbed momentum eigenvectors  $\{|\phi^\alpha\rangle\}_\alpha = \{|\phi^{i,e}\rangle, |\phi^{i,p}\rangle\}_{i=1,2,3}$ . The perturbed momentum eigenvectors  $\{|\theta^m\rangle\}_m$  and the associated momentum relaxation times  $\tau^m$  are calculated within first order degenerate perturbation theory (DPT). Any contributions to  $\{|\theta^m\rangle\}_m$  from non-special relaxons are, within DPT, proportional to the short lifetime of those non-special relaxons and are hence neglected in the limit of weak Umklapp scattering. This implies that taking linear combinations of the six vectors (10,11) approximatively yields six eigenvectors  $|\theta_{\mathbf{k}m}^m\rangle$  of the full collision scattering matrix with finite lifetime  $\tau^m$  with  $m = 1, \dots, 6$ , where the latter is obtained from the inverse eigenvalue of the 6x6 matrix

$$\langle \phi_{\mathbf{k}m}^{i,c_1} | \Omega_{\mathbf{k}m, \mathbf{k}'m'} | \phi_{\mathbf{k}m}^{j,c_2} \rangle = \frac{D_{c_1, c_2}^{ij}}{\sqrt{A_{c_1}^i A_{c_2}^j}}, \quad (12)$$

where  $c_1, c_2$  are carrier indexes that select the electron ('e') or phonon ('p') subspaces, while  $i, j = 1, 2, 3$  are Cartesian directions; the normalization constant  $\sqrt{A_{c_1}^i A_{c_2}^j}$  is discussed in Appendix C 3 and ensures that  $D_{c_1, c_2}^{ij}$  has physical units describing the momentum dissipation rate. As we see in Section IV, the rate of decay of momentum density related to the carrier  $c_1$  is given by  $\sum_{c_2=e,p} D_{c_1, c_2}^{ij} u_{c_2}^j$ , so  $D_{c_1, c_2}^{ij}$  has units of momentum density over length. Finally, we note that, since the  $|\theta_{\mathbf{k}m}^m\rangle$  are linear combinations of odd momentum eigenvectors, they remain odd.

The considerations above imply that in the hydrodynamic regime the electron-phonon system will have a local-equilibrium state described by: (a) two special eigenvectors with zero eigenvalue, related to conservation of charge and energy, respectively; (b) six special eigenvectors with finite eigenvalue related to quasi-conservation of electron and phonon momentum, each along the three Cartesian directions  $i = 1, 2, 3$ .

### III. CONDUCTIVITIES, VISCOSITIES, AND CROSS-TRANSPORT COEFFICIENTS

#### A. Heat and charge currents

Refs. [9, 54] discussed how in the hydrodynamic regime of thermal transport the heat current is made up of a diffusive and a hydrodynamic component, which share formal analogies to the diffusive and hydrodynamic flux components that appear in the description of transport for rarefied classical fluids [88–92]. To show that these two heat-flux components emerge also in the thermoelectric regime, we express the deviation from global equilibrium of the electron-phonon system in terms of relaxons:

$$\begin{aligned} |z_{\mathbf{k}m}^m\rangle &= \mathfrak{g}_{qs}^m \left| \begin{array}{c} \mathfrak{f}_{\mathbf{k}m}(\mathbf{r}) \\ \mathfrak{n}_{qs}(\mathbf{r}) \end{array} \right\rangle \\ &= \sqrt{\frac{C_{\text{tot}}}{k_B T^2}} |\theta_{\mathbf{k}m}^0\rangle [T(\mathbf{r}) - \bar{T}] - \sqrt{\frac{\mathfrak{U}}{k_B T}} |\theta_{\mathbf{k}m}^e\rangle V_{\text{eff}}(\mathbf{r}) \\ &\quad + \sqrt{\frac{A_{\text{el}}^i}{k_B T}} |\phi_{\mathbf{k}m}^{i,e}\rangle u_e^i(\mathbf{r}) + \sqrt{\frac{A_{\text{ph}}^i}{k_B T}} |\phi_{\mathbf{k}m}^{i,p}\rangle u_p^i(\mathbf{r}) + |z_{\mathbf{k}m}^\delta\rangle, \end{aligned} \quad (13)$$

where the terms proportional to  $|\theta_{\mathbf{k}m}^0\rangle$ ,  $|\theta_{\mathbf{k}m}^e\rangle$ ,  $|\phi_{\mathbf{k}m}^{i,e}\rangle$ ,  $|\phi_{\mathbf{k}m}^{j,p}\rangle$  describe the local equilibrium, and  $|z_{\mathbf{k}m}^\delta\rangle$  is the linear deviation from the local equilibrium, i.e., proportional to the gradient of the local-equilibrium fields  $\nabla T$ ,  $\nabla V_{\text{eff}}$ ,  $\nabla \mathbf{u}_e$ ,  $\nabla \mathbf{u}_p$ . Eq. (13) highlights the close relationship between conservation laws that underlie local equilibrium and special relaxons: changing the electron-phonon distribution proportionally to the special energy, charge, phonon or electron momentum relaxon, induces changes in the corresponding conjugate variable (in order,  $T(\mathbf{r})$ ,  $V_{\text{eff}}(\mathbf{r})$ ,  $\mathbf{u}_p(\mathbf{r})$ ,  $\mathbf{u}_e(\mathbf{r})$ ).

The special relaxons describing local equilibrium in Eq. (13) have well defined parity — one can directly verify from Eq. (8) that the even parity of the electron and phonon energies ( $\varepsilon_{\mathbf{k}m} = \varepsilon_{-\mathbf{k}m}$ ,  $\omega_{\mathbf{q}s} = \omega_{-\mathbf{q}s}$ ) implies that the energy  $|\theta_{\mathbf{q}s}^0\rangle$  relaxon is even, i.e.  $|\theta_{\mathbf{q}s}^0\rangle = |\theta_{-\mathbf{q}s}^0\rangle$ . Similarly, one can directly verify from Eq. (9) that because the electron's charge does not depend on the wavevector  $\mathbf{k}$ , the charge relaxon is also even ( $|\theta_{\mathbf{q}s}^e\rangle = |\theta_{-\mathbf{q}s}^e\rangle$ ). In contrast, the phonon momentum and electron momentum relaxons Eqs. (10) and (11) are proportional to the crystal momentum and therefore both odd:  $|\phi_{\mathbf{q}s}^{i,e}\rangle = -|\phi_{-\mathbf{q}s}^{i,e}\rangle$  and  $|\phi_{\mathbf{q}s}^{i,p}\rangle = -|\phi_{-\mathbf{q}s}^{i,p}\rangle$ . To investigate the parity properties of the deviation from equilibrium  $|z_{\mathbf{q}s}^\delta\rangle$ , we recall that in a system having time-reversal symmetry the scattering matrix is even under inversion of wavevectors' signs, i.e.,  $\Omega_{\mathbf{k}m, \mathbf{k}'m'} = \Omega_{-\mathbf{k}m, -\mathbf{k}'m'}$ . This property implies that relaxons, as eigenvectors of the scattering matrix, have well-defined (odd or even) parity, i.e. they satisfy  $|\theta_{\mathbf{q}s}^\gamma\rangle = \pm |\theta_{-\mathbf{q}s}^\gamma\rangle$  [54, 93]. Therefore by writing the deviation from equilibrium in the relaxons basis,

$$|z_{\mathbf{q}s}^\delta\rangle = \sum_{\xi \neq \text{LE}} d^\xi |\theta_{\mathbf{q}s}^\xi\rangle = |z_{\mathbf{q}s}^{\delta,E}\rangle + |z_{\mathbf{q}s}^{\delta,O}\rangle \quad (14)$$

one can decompose the deviation from equilibrium into the sum of even ( $|z_{\mathbf{q}s}^{\delta,E}\rangle$ ) and odd ( $|z_{\mathbf{q}s}^{\delta,O}\rangle$ ) components. In Eq. (14),  $\xi \neq \text{LE}$  means that the sum does not include the local equilibrium subspace spanned by the special eigenvectors related to conservation of energy (8), charge (9), and quasi conservation of momentum (11, 10). For later convenience we also mention that the group velocity,  $v_{\mathbf{q}s}^i$ , being the derivative of the even-parity dispersion, has odd parity,  $v_{-\mathbf{q}s}^i = -v_{\mathbf{q}s}^i$ .

The reasoning above and Eq. (13) can be exploited to express the microscopic heat flux for a system involving phonons [94] and electrons [60] in terms of relaxons:

$$\begin{aligned} Q^i &= \frac{1}{\mathcal{V}\mathcal{N}_q} \sum_{\mathbf{q}s} \hbar\omega_{\mathbf{q}s} v_{\mathbf{q}s}^i n_{\mathbf{q}s} + \frac{\mathcal{D}}{\mathcal{V}\mathcal{N}_k} \sum_{\mathbf{k}m} (\varepsilon_{\mathbf{k}m} - \bar{\mu}) v_{\mathbf{k}m}^i \mathbf{f}_{\mathbf{k}m} \\ &= \sqrt{k_B \bar{T}^2 C_{\text{tot}}} \langle \theta_{\mathbf{q}s}^0 | v_{\mathbf{q}s}^i | z_{\mathbf{q}s}^{\delta,O} \rangle \\ &= \chi_e^{ji} \bar{T} u_e^j + \chi_p^{ji} \bar{T} u_p^j - \tilde{\alpha}^{ij} \frac{\partial V_{\text{eff}}}{\partial r^j} - \tilde{\kappa}^{ij} \frac{\partial T}{\partial r^j}, \end{aligned} \quad (15)$$

where the first line is the usual expression for the phonon [94] and electron [60] heat flux, which can be intuitively resolved in terms of  $n_{\mathbf{q}s}$  phonons (and  $\mathbf{f}_{\mathbf{k}m}$  electrons) that propagate with velocity  $v_{\mathbf{q}s}^i$  ( $v_{\mathbf{k}m}^i$ ) and carry the energy  $\hbar\omega_{\mathbf{q}s}$  ( $\varepsilon_{\mathbf{k}m} - \bar{\mu}$ ). The second line is the total heat flux written in the relaxon formalism; its equivalence with the first line can be directly verified by using the energy eigenvector (8), the deviation from equilibrium (13), and the bracket notation introduced in Eq. (3). Only the odd-parity component  $|z_{\mathbf{q}s}^{\delta,O}\rangle$  contributes to the heat flux, because

in Eq. (15)  $|\theta_{\mathbf{q}s}^0\rangle$  has even parity,  $v_{\mathbf{q}s}^i$  has odd parity, and the scalar product involves summation over a domain having time-reversal symmetry. Finally, the third line follows from the form of the deviation from global equilibrium (13) in the linear-response regime. It highlights how in general the heat flux has two components: (i) an hydrodynamic component, which is determined by the local-equilibrium drift velocities for electrons and phonons; (ii) a diffusive component determined by the gradients of the temperature and potential fields. The coefficients  $\chi_e^{ji} \bar{T}$  and  $\chi_p^{ji} \bar{T}$  determine the contributions that electrons and phonons give to the hydrodynamic heat-flux component, respectively; their expressions can be directly derived from Eq. (13) and Eq. (8), and are reported in Tab. I. The determination of the Peltier coefficient  $\tilde{\alpha}^{ij}$  and thermal conductivity  $\tilde{\kappa}^{ij}$  will be discussed later in Sec. III C.

The description of the charge flux is analogous, and starts from the expression that relates the microscopic electronic distribution to the macroscopic charge flux,

$$\begin{aligned} J^i &= -\frac{\mathcal{D}e}{\mathcal{V}\mathcal{N}_k} \sum_{\mathbf{k}m} v_{\mathbf{k}m} \mathbf{f}_{\mathbf{k}m} \\ &= -\sqrt{k_B \bar{T} \mathcal{U}} \langle \theta_{\mathbf{q}s}^e | v_{\mathbf{q}s}^i | z_{\mathbf{q}s}^e \rangle \\ &= -\psi^{ji} u_e^j - \tilde{\sigma}^{ij} \frac{\partial V_{\text{eff}}}{\partial r^j} - \tilde{\sigma}^{ij} \tilde{S}^{jk} \frac{\partial T}{\partial r^k}. \end{aligned} \quad (16)$$

In total analogy to Eq. (15), the first line is the usual expression for the charge flux [31, 60, 71], which can be intuitively resolved in terms of  $\mathbf{f}_{\mathbf{k}m}$  electrons that propagate with velocity  $v_{\mathbf{q}s}^i$  and carry charge  $-e$ . The second line is the total charge flux written in the relaxon formalism, relying on Eq. (9) and the deviation from equilibrium (13). Expanding  $|z_{\mathbf{q}s}^e\rangle$  as in Eq. (13), even contributions vanish by parity, and the  $|z_{\mathbf{q}s}^p\rangle$  component vanishes because phonons are charge neutral. Therefore, the total charge current receives contributions from an electron-momentum current (originating from  $|z_{\mathbf{q}s}^e\rangle$  and proportional to  $\mathbf{u}_e$ ) and a diffusive current (originating from  $|z_{\mathbf{q}s}^{\delta,O}\rangle$  and proportional to  $\nabla T$  and  $\nabla V_{\text{eff}}$ ). The expression for the coefficient  $\psi^{ji}$  appearing in Eq. 16 can be readily computed contracting Eq. (13) and Eq. (9), and is reported in Tab. I; the determination of the electrical conductivity  $\tilde{\sigma}^{ij}$  and Seebeck coefficient  $\tilde{S}$  will be discussed later in Sec. III C.

Eqs. (15,16) describe the heat and charge flux in general, covering both the hydrodynamic and the diffusive regimes, as well as the intermediate cases. In the hydrodynamic regime of transport,  $\mathbf{u}_p$ ,  $\mathbf{u}_e$ ,  $\nabla T$ , and  $\nabla V_{\text{eff}}$  are independent. We will demonstrate later in Sec. IV C that in the diffusive regime of strong Umklapp dissipation, or when the second derivatives of the drift velocities are negligible, one has that the electron and phonon drift velocities can be written as linear combination of the temperature and potential gradients. Under these conditions, the terms  $\chi_e^{ji} \bar{T} u_e^j + \chi_p^{ji} \bar{T} u_p^j$  in Eq. (15) give additive contri-

butions to  $\tilde{\kappa}^{ij}$  and  $\tilde{\alpha}^{ij}$ , and the term  $-\psi^j u_e^j$  in Eq. (16) gives additive contributions to  $\tilde{\sigma}^{ij}$  and  $\tilde{S}^{ij}$ . Therefore, in the diffusive or negligible-viscosity regime, we will see that the heat and the charge fluxes Eqs. (15,16) reduce to the standard, gradient-driven diffusive form.

## B. Electron and phonon momentum currents

We start by recalling that to describe hydrodynamic transport for heat and/or charge in materials ranging from metals to insulators, it is necessary to have a formalism that allows phonons and electrons to have different drift velocities. Ref. [95] discussed how in the out-of-equilibrium transport regime where drift velocity is non-uniform in space, a non-zero momentum-flux emerges. For phonons, the momentum-flux tensor is [54]:

$$\begin{aligned}\Pi_p^{ij} &= \frac{1}{\mathcal{V}\mathcal{N}_q} \sum_{q^s} \hbar q^i v_{q^s}^j n_{q^s} \\ &= -\sqrt{k_B \bar{T}} A_{\text{ph}}^i \langle \phi_{\mathbf{k}m}^{i,p} | v_{\mathbf{k}m}^j | z_{q^s}^{\delta E} \rangle \\ &= \chi_p^{ij} [T(\mathbf{r}) - \bar{T}] - \zeta_{\text{pp}}^{ijkl} \frac{\partial u_p^k(\mathbf{r})}{\partial r^l} - \zeta_{\text{pe}}^{ijkl} \frac{\partial u_e^k(\mathbf{r})}{\partial r^l},\end{aligned}\quad (17)$$

and the first line shows that it is determined by  $n_{q^s}$  phonons having momentum  $q^i$  and propagating with velocity  $v_{q^s}^j$ . The second line is obtained from the first relying on Eqs. (10), Eq. (13), and some algebra. The third line follows from Eq. (13), and shows that the phonon momentum flux tensor receives contributions from the local temperature  $\bar{T}$  proportionally to the coefficient  $\chi_p^{ij}$ , as well as from the gradient of the phonon drift velocity through the ‘self’ phonon viscosity  $\zeta_{\text{pp}}^{ijkl}$  (which originates from exchange of momentum within the phonon subspace), and the gradient of the electron drift velocity through the phonon ‘drag’ viscosity  $\zeta_{\text{pe}}^{ijkl}$  (which originates from exchange of momentum between phonons and electrons).

Analogous considerations hold for the electron momentum flux tensor, which is defined as

$$\begin{aligned}\Pi_e^{ij}(\mathbf{r}) &= \frac{\mathcal{D}}{\mathcal{V}\mathcal{N}_k} \sum_{\mathbf{k}m} \hbar k^i v_{\mathbf{k}m}^j f_{\mathbf{k}m} \\ &= \sqrt{k_B \bar{T}} A_{\text{el}}^i \langle \phi_{\mathbf{k}m}^{i,e} | v_{\mathbf{k}m}^j | z_{q^s}^{\delta E} \rangle \\ &= \chi_e^{ij} [T(\mathbf{r}) - \bar{T}] - \psi^{ij} V_{\text{eff}}(\mathbf{r}) - \zeta_{\text{ee}}^{ijkl} \frac{\partial u_e^k(\mathbf{r})}{\partial r^l} - \zeta_{\text{ep}}^{ijkl} \frac{\partial u_p^k(\mathbf{r})}{\partial r^l}.\end{aligned}\quad (18)$$

It is apparent from the first line that  $\Pi_e^{ij}(\mathbf{r})$  is determined by  $f_{\mathbf{k}m}$  electrons having momentum  $k^i$  and propagating with velocity  $v_{\mathbf{k}m}^j$ . The second line shows that  $\Pi_e^{ij}(\mathbf{r})$  is related to the momentum eigenvectors via Eq. (11). Finally, the third line shows that  $\Pi_e^{ij}(\mathbf{r})$  receives contributions from: (i) the local potential  $V_{\text{eff}}(\mathbf{r})$  — this is an important difference from phonons and stems from the fact that electrons carry charge; (ii) the local temperature  $\bar{T}$

proportionally to the coefficient  $\chi_e^{ij}$ ; (iii) the gradients of the phonon and electron drift velocities through the self electron viscosity  $\zeta_{\text{ee}}^{ijkl}$  (which originates from exchange of momentum within the electron subspace) and electron drag viscosity  $\zeta_{\text{ep}}^{ijkl}$  (which originates from exchange of momentum between electrons and phonons; we will show later that  $\zeta_{\text{ep}}^{ijkl} = \zeta_{\text{pe}}^{klji}$ ). The subscript indices on the viscosity refer to the carrier of the momentum flux and the carrier of the drift velocity:  $\zeta_{\text{ee}}$  relates the electron momentum flux to the electron drift velocity, while  $\zeta_{\text{ep}}$  relates the electron momentum flux to the phonon drift velocity.

In Eqs. (17, 18) we have highlighted that only the even contributions of the population  $|z_{q^s}^{\delta E}\rangle$  contribute to the momentum-flux tensors, which is a direct consequence of the momentum eigenvectors having odd parity. Later in Sec. IV we will discuss the relevance of viscosities in the hydrodynamic regime, as well as the negligible influence that they have on transport in the diffusive regime.

## C. Conductivities from odd relaxons, and viscosities from even relaxons

In the previous sections we laid out the description of transport within linear response theory, where the heat, charge, and momentum fluxes are determined by the local-equilibrium fields and their gradients. Here, we discuss how to determine the transport coefficients that parametrize these fluxes.

Equation (13) shows the general relation between the local-equilibrium fields  $T(\mathbf{r})$ ,  $V_{\text{eff}}(\mathbf{r})$ ,  $u_p^i(\mathbf{r})$ ,  $u_e^j(\mathbf{r})$  ( $i, j = 1, 2, 3$ ) and the eight special relaxons. To compute the transport coefficients, we employ the standard procedure of inserting the deviation from equilibrium (13) into the epBTE (6), and considering an out-of-equilibrium state  $|z_{q^s}^{\delta}\rangle$  that is spatially homogeneous and linearly proportional to the first derivative of the local fields [37, 54]. Then, rewriting Eq. (6) using the eigenvectors and eigenvalues of the collision matrix (7) enables to directly determine  $|z_{q^s}^{\delta}\rangle$ :

$$|z_{q^s}^{\delta}\rangle = - \sum_{\xi \neq \text{LE}} \sum_{\mathbf{k}'m'} |\theta_{\mathbf{k}m}^{\xi}\rangle \tau^{\xi} \langle \theta_{\mathbf{k}'m'}^{\xi} | \mathbf{v}_{\mathbf{k}'m'} \cdot \nabla | z_{q^s}^{\text{LE}} \rangle, \quad (19)$$

where  $\sum_{\xi \neq \text{LE}} |\theta_{\mathbf{k}m}^{\xi}\rangle \tau^{\xi} \langle \theta_{\mathbf{k}'m'}^{\xi} |$  is the inverse of the scattering matrix  $\Omega$  restricted to the subspace orthogonal to the local-equilibrium subspace (since  $\xi \neq \text{LE}$ ), and  $|z_{q^s}^{\text{LE}}\rangle = |z_{q^s}^T\rangle + |z_{q^s}^{\mu}\rangle + |z_{q^s}^e\rangle + |z_{q^s}^p\rangle$  is the local-equilibrium state. Recalling that the out-of-equilibrium distribution can be decomposed in odd and even components,  $|z_{q^s}^{\delta}\rangle = |z_{q^s}^{\delta,O}\rangle + |z_{q^s}^{\delta,E}\rangle$ , respectively, one has that the aforementioned inversion symmetry of the scattering matrix implies that: (i) the odd part of the response  $|z_{q^s}^{\delta,O}\rangle$  gives non-zero contributions only when contracted

with the even special relaxons  $|\theta_{q_s}^0\rangle$ ,  $|\theta_{q_s}^e\rangle$ , hence proportional to  $\nabla T$  and  $\nabla V_{\text{eff}}$ ; (ii) the even response  $|z_{q_s}^{\delta,E}\rangle$  gives non-zero contributions only when contracted with the odd special eigenvectors  $|z_{q_s}^e\rangle$ ,  $|z_{q_s}^p\rangle$  and is proportional to  $\nabla \mathbf{u}_e$  and  $\nabla \mathbf{u}_p$ .

To determine the thermal conductivity  $\tilde{\kappa}$  and Peltier coefficient  $\tilde{\alpha}$ , we insert Eq. (13) and Eq. (19) into Eq. (15), obtaining

$$\tilde{\kappa}^{ij} = C_{\text{tot}} \sum_{\xi \neq \text{LE}} \langle \theta_{q_s}^0 | v_{q_s}^i | \theta_{q_s}^\xi \rangle \langle \theta_{q_s'}^\xi | v_{q_s'}^j | \theta_{q_s'}^0 \rangle \tau^\xi, \quad (20)$$

$$\tilde{\alpha}^{ij} = -\sqrt{C_{\text{tot}} \mathcal{U} \bar{T}} \sum_{\xi \neq \text{LE}} \langle \theta_{q_s}^e | v_{q_s}^i | \theta_{q_s}^\xi \rangle \langle \theta_{q_s'}^\xi | v_{q_s'}^j | \theta_{q_s'}^0 \rangle \tau^\xi. \quad (21)$$

These expressions allow us to determine macroscopic transport coefficients from a full solution of epBTE (i.e., beyond the single-mode relaxation-time approximation [71]), and, most importantly, to resolve them in terms of microscopic electron-phonon relaxon excitations. For example, the thermal conductivity Eq. (20) is determined by relaxon excitations that carry heat  $C_{\text{tot}} = C_{\text{el}} + C_{\text{ph}}$ , by propagating with velocity  $\langle \theta_{q_s'}^\xi | v_{q_s'}^j | \theta_{q_s'}^0 \rangle$  over the lifetime  $\tau^\xi$ . The Peltier coefficient (21) is determined by relaxons excitations that, over the lifetime  $\tau^\xi$ , carry charge (related to  $\mathcal{U}$ ) with velocity  $\langle \theta_{q_s}^e | v_{q_s}^i | \theta_{q_s}^\xi \rangle$ , and heat (related to  $C_{\text{tot}}$ ) with velocity  $\langle \theta_{q_s'}^\xi | v_{q_s'}^j | \theta_{q_s'}^0 \rangle$ .

All other transport coefficients can be found following the procedure used to determine  $\tilde{\kappa}^{ij}$  and  $\tilde{\alpha}^{ij}$ . The full derivation is given in Appendix B, while Table I contains a summary of the results. We note, firstly, that the heat conductivity  $\tilde{\kappa}$ , electrical conductivity  $\tilde{\sigma}$ , Peltier  $\tilde{\alpha}$  and Seebeck  $\tilde{S}$  coefficients are determined only by the odd relaxons. In contrast, the calculation of the viscosity of the electron fluid  $\zeta_{\text{ee}}^{ijkl}$  (phonon fluid  $\zeta_{\text{pp}}^{ijkl}$ ), which describes the momentum flux tensor for electrons (phonons) generated in response to a perturbation of the corresponding electron (phonon) drift velocity, requires contraction with the odd momentum eigenvectors, and therefore is determined only by even components of  $|z_{q_s}^\delta\rangle$ .  $\zeta_{\text{pe}}^{ijkl} = \zeta_{\text{ep}}^{klij}$  is the drag viscosity, which describes the momentum flux tensor for electrons generated in response to a perturbation of the phonon drift velocity, and vice-versa, and is also determined only by even components of  $|z_{q_s}^\delta\rangle$  (see Appendix B). The expression for all the transport coefficients can be written in a compact form by defining a relaxon response operator (RRO):

$$\Delta_{q_s, q_s'}^{ij} = \sum_{\xi \neq \text{LE}} v_{q_s}^i | \theta_{q_s}^\xi \rangle \langle \theta_{q_s'}^\xi | v_{q_s'}^j \tau^\xi. \quad (22)$$

RRO exposes the relation between special eigenvectors and transport coefficients:

$$\tilde{\kappa}^{ij} = C_{\text{tot}} \langle \theta_{q_s}^0 | \Delta_{q_s, q_s'}^{ij} | \theta_{q_s'}^0 \rangle, \quad (23)$$

$$\tilde{\sigma}^{ij} = \mathcal{U} \langle \theta_{q_s}^e | \Delta_{q_s, q_s'}^{ij} | \theta_{q_s'}^e \rangle, \quad (24)$$

$$\tilde{\alpha}^{ij} = [\tilde{\sigma} \tilde{S}]^{ij} \bar{T} = -\sqrt{\mathcal{U} C_{\text{tot}} \bar{T}} \langle \theta_{q_s}^e | \Delta_{q_s, q_s'}^{ij} | \theta_{q_s'}^0 \rangle, \quad (25)$$

$$\zeta_{\text{ee}}^{ijkl} = \sqrt{A_{\text{el}}^i A_{\text{el}}^k} \langle \phi_{q_s}^{i,e} | \Delta_{q_s, q_s'}^{jl} | \phi_{q_s'}^{k,e} \rangle, \quad (26)$$

$$\zeta_{\text{pp}}^{ijkl} = \sqrt{A_{\text{ph}}^i A_{\text{ph}}^k} \langle \phi_{q_s}^{i,p} | \Delta_{q_s, q_s'}^{jl} | \phi_{q_s'}^{k,p} \rangle, \quad (27)$$

$$\zeta_{\text{pe}}^{ijkl} = \zeta_{\text{ep}}^{klij} = \sqrt{A_{\text{ph}}^i A_{\text{el}}^k} \langle \phi_{q_s}^{i,p} | \Delta_{q_s, q_s'}^{jl} | \phi_{q_s'}^{k,e} \rangle, \quad (28)$$

in particular, we see that thermal conductivity  $\tilde{\kappa}^{ij}$  emerges from bracketing RRO between energy eigenvectors; the electrical conductivity  $\tilde{\sigma}^{ij}$  originates from bracketing RRO between charge eigenvectors; the Peltier  $\tilde{\alpha}$  and Seebeck  $\tilde{S}$  coefficients derive from RRO coupling charge and energy eigenvectors; the self viscosity for the electron  $\zeta_{\text{ee}}^{ijkl}$  (phonon  $\zeta_{\text{pp}}^{ijkl}$ ) fluid emerge from bracketing RRO between electron (phonon) momentum eigenvectors; finally, the drag viscosities derive from RRO coupling momentum eigenvectors for electrons and phonons. These expressions show that electron-phonon drag influences transport coefficients both through a change in the eigenvalues of the scattering matrix, as well as through a change in the structure of relaxons, mixing otherwise independent electron and phonon relaxon excitations. In the next section we will show that these transport coefficients enter as parameters into partial-differential equations that describe thermoelectric hydrodynamic transport in devices.

#### IV. VISCOUS THERMOELECTRIC EQUATIONS

In this section we discuss how to exploit the microscopic symmetries and (quasi) conservation laws of the electron-phonon system to coarse-grain the microscopic epBTE (6) into a set of mesoscopic Viscous Thermoelectric Equations (VTE), which allow to accurately predict the behavior of the local fields  $T, V_{\text{eff}}, \mathbf{u}_e, \mathbf{u}_p$  in devices.

We start by considering the heat flux, as given in the second line of Eq. (15); such an expression shows that the evolution of the heat-flux field in space can be determined by contracting both sides of the coupled epBTE Eq. (6) with  $\langle \theta_{q_s}^0 |$  (Eq. (8)). Specifically, we show in Appendix C that the contraction with the drift side of the epBTE yields a term proportional to the divergence of the energy flux  $\nabla \cdot \mathbf{Q}(\mathbf{r})$ . The product between  $\langle \theta_{q_s}^0 |$  and the scattering matrix yields zero, since the energy relaxon (8) is a null eigenvector of the scattering matrix (this stems from the fact that energy is conserved in all microscopic scattering mechanisms). Therefore, we find the continuity equation for energy flow in the steady-state regime  $\nabla \cdot \mathbf{Q}(\mathbf{r}) = 0$ . Expanding  $\mathbf{Q}(\mathbf{r})$  in terms of fields, as in the last line of Eq. (15), we find energy balance equation Eq. (30).



Parity	Perturbation	Proportional to conjugate variable	Contributes to flux	Determines transport coefficient
odd	Odd out-of-equilibrium $ z_{\mathbf{q}s}^{\delta,O}\rangle$	$\nabla V$	$\mathbf{J}$	$\bar{\sigma}^{ij} = \mathfrak{U} \langle \theta^e   \Delta^{ij}   \theta^e \rangle$
			$\mathbf{Q}$	$\tilde{\alpha}^{ij} = \sqrt{\mathfrak{U} C_{\text{tot}} \bar{T}} \langle \theta^e   \Delta^{ij}   \theta^0 \rangle$
		$\nabla T$	$\mathbf{J}$	$\bar{\sigma}^{ik} \tilde{S}^{kj} = \frac{\tilde{\alpha}^{ij}}{T}$
			$\mathbf{Q}$	$\tilde{\kappa}^{ij} = C_{\text{tot}} \langle \theta^0   \Delta^{ij}   \theta^0 \rangle$
	Electron momentum $ \phi_{\mathbf{q}s}^{i,e}\rangle, i=1,2,3$	$\mathbf{u}_e(\mathbf{r})$	$\mathbf{J}$	$\psi^{ij} = \sqrt{\mathfrak{U} A_{\text{el}}^i} \langle \phi^{i,e}   v^j   \theta^e \rangle$
			$\mathbf{Q}$	$\chi_e^{ij} \bar{T} = \sqrt{C_{\text{tot}} A_{\text{el}}^i \bar{T}} \langle \phi^{i,e}   v^j   \theta^0 \rangle$
Phonon momentum $ \phi_{\mathbf{q}s}^{i,p}\rangle, i=1,2,3$	$\mathbf{u}_p(\mathbf{r})$	$\mathbf{Q}$	$\chi_p^{ij} \bar{T} = \sqrt{C_{\text{tot}} A_{\text{ph}}^i \bar{T}} \langle \phi^{i,p}   v^j   \theta^0 \rangle$	
even	Even out-of-equilibrium $ z_{\mathbf{q}s}^{\delta,E}\rangle$	$\nabla \mathbf{u}_e$	$\Pi_e$	$\zeta_{\text{ee}}^{ijkl} = \sqrt{A_{\text{el}}^i A_{\text{el}}^k} \langle \phi^{i,e}   \Delta^{jl}   \phi^{k,e} \rangle$
				$\zeta_{\text{ep}}^{ijkl} = \sqrt{A_{\text{el}}^i A_{\text{ph}}^k} \langle \phi^{i,e}   \Delta^{jl}   \phi^{k,p} \rangle$
		$\nabla \mathbf{u}_p$	$\Pi_p$	$\zeta_{\text{pp}}^{ijkl} = \sqrt{A_{\text{ph}}^i A_{\text{ph}}^k} \langle \phi^{i,p}   \Delta^{jl}   \phi^{k,p} \rangle$
				$\zeta_{\text{pe}}^{ijkl} = \zeta_{\text{ep}}^{klij}$
	Temperature $ \theta_{\mathbf{q}s}^0\rangle$	$T(\mathbf{r})$	$\Pi_e$	$\chi_e^{ij} = \sqrt{\frac{C_{\text{tot}} A_{\text{el}}^i}{T}} \langle \phi^{i,e}   v^j   \theta^0 \rangle$
			$\Pi_p$	$\chi_p^{ij} = \sqrt{\frac{C_{\text{tot}} A_{\text{ph}}^i}{T}} \langle \phi^{i,p}   v^j   \theta^0 \rangle$
Effective potential $ \theta_{\mathbf{q}s}^e\rangle$	$V_{\text{eff}}(\mathbf{r})$	$\Pi_e$	$\psi^{ij} = \sqrt{\mathfrak{U} A_{\text{el}}^i} \langle \phi^{i,e}   v^j   \theta^e \rangle$	

TABLE I. Summary of the coefficients appearing in the VTE, and of their physical meaning.

An analogous reasoning can be applied to coarse-grain the epBTE into an equation for the charge flux. Multiplying Eq. (6) by  $\langle \theta_{\mathbf{q}s}^e |$ , and comparing with the second line of Eq. (16), directly gives  $\nabla \cdot \mathbf{J}(\mathbf{r}) = 0$ . As with the heat flux, the zero on the right-hand side is obtained because scattering perfectly conserves charge. Expanding  $\mathbf{J}(\mathbf{r})$  as in the last line of Eq. (16) gives the second of four equations (31). In contrast to Eq. (30), the charge equation does not contain any direct macroscopic contribution from the phonon drift velocity, since phonons are charge neutral. Phonons affect the charge flow only through microscopic interactions with electrons, which determine the Seebeck coefficient and also influence the electrical conductivity.

In the case of electron (phonon) momentum, we can as before multiply Eq. (6) with  $\langle \phi_{\mathbf{q}s}^{i,e} |$  ( $\langle \phi_{\mathbf{q}s}^{i,p} |$ ), obtaining on the left-hand side the divergence of  $\partial_{r_j} \Pi_e^{ij}$  ( $\partial_{r_j} \Pi_p^{ij}$ ). In this case, the behavior on the right-hand scattering side is different from that obtained for the energy and charge eigenvectors; in fact, electron and phonon momentum are dissipated by Umklapp scattering, thus a non-zero value is obtained when  $\langle \phi_{\mathbf{q}s}^{i,e} |$  ( $\langle \phi_{\mathbf{q}s}^{i,p} |$ ) multiply the scattering side. These terms are in general proportional to  $\langle \phi^{i,e(p)} | \Omega | \theta_{\mathbf{q}s}^e \rangle$ , where  $|\theta_{\mathbf{q}s}^e\rangle$  is any relaxon. Considering the regime anticipated in Sec. IIC — in which Umklapp causes predominantly momentum dissipation or redistribution within the momentum subspaces, and negligible momentum redistribution between the momentum and the other subspaces — we keep only  $|z_{\mathbf{q}s}^e\rangle$  and  $|z_{\mathbf{q}s}^p\rangle$

terms and neglect  $|z_{\mathbf{q}s}^{\delta}\rangle$  on the right-hand side of Eq. (6) multiplied by  $\langle \phi_{\mathbf{q}s}^{i,e} |$  or  $\langle \phi_{\mathbf{q}s}^{i,p} |$ . [96]. Expanding the momentum fluxes as in Eqs. (17) and (18) yields the macroscopic momentum balance equations for electrons (32) and phonons (33).

We also note from Eqs. (17,18) that, because the divergence of the momentum flux tensor depends on the index  $i$  only, the viscosity can be symmetrized as follows:

$$\eta_{c_1, c_2}^{ijkl} = \frac{1}{2} (\zeta_{c_1, c_2}^{ijkl} + \zeta_{c_1, c_2}^{ilkj}), \quad (29)$$

where  $c_1, c_2$  are generic carrier indexes that can assume the electronic ‘e’ or phononic ‘p’ values. The viscosity symmetrization (29) is performed to make the symmetries of transport more apparent; for example, it shows that is not necessary to resolve the  $ii jj$  and  $ij ji$  viscosity components but it is sufficient to know their average. In practice, one can directly verify from the momentum balance equations for electrons (32) and phonons (33) that Schwartz theorem on symmetry of second partial derivatives implies that the physical behavior is unaffected by this symmetrization.

In summary, by contracting the microscopic epBTE with the special eigenvectors describing local equilibrium for energy, charge, electron and phonon momentum, we have obtained the following set of mesoscopic Viscous Thermoelectric Equations:

$$\bar{T}\chi_e^{ij}\frac{\partial u_e^i}{\partial r^j} + \bar{T}\chi_p^{ij}\frac{\partial u_p^i}{\partial r^j} - \tilde{\alpha}^{ij}\frac{\partial^2 V_{\text{eff}}}{\partial r^i\partial r^j} - \tilde{\kappa}^{ij}\frac{\partial^2 T}{\partial r^i\partial r^j} = 0, \quad (30)$$

$$-\psi^{ij}\frac{\partial u_e^i}{\partial r^j} - \tilde{\sigma}^{ij}\frac{\partial^2 V_{\text{eff}}}{\partial r^i\partial r^j} - [\tilde{\sigma}\tilde{S}]^{ij}\frac{\partial^2 T}{\partial r^i\partial r^j} = 0, \quad (31)$$

$$\chi_e^{ij}\frac{\partial T}{\partial r^j} - \psi^{ij}\frac{\partial V_{\text{eff}}}{\partial r^j} - \eta_{ee}^{ijkl}\frac{\partial u_e^k}{\partial r^j\partial r^l} - \eta_{ep}^{ijkl}\frac{\partial u_p^k}{\partial r^j\partial r^l} = -D_{ee}^{ij}u_e^j - D_{ep}^{ij}u_p^j, \quad (32)$$

$$\chi_p^{ij}\frac{\partial T}{\partial r^j} - \eta_{pp}^{ijkl}\frac{\partial u_p^k}{\partial r^j\partial r^l} - \eta_{pe}^{ijkl}\frac{\partial u_e^k}{\partial r^j\partial r^l} = -D_{pp}^{ij}u_p^j - D_{pe}^{ij}u_e^j, \quad (33)$$

where the matrices  $D_{ee}$ ,  $D_{ep}$ ,  $D_{pe}$ ,  $D_{pp}$  are momentum dissipation rates, accounting for the decay of electron and phonon momentum defined in Eq. (12). All the coefficients appearing in the VTE can be resolved in terms of microscopic relaxon properties and evaluated from first principles; their expressions are reported in Tab. I. We note that Eqs. (30) and (31) for charge and energy are scalar equations, while Eqs. (32) and (33) for electron and phonon momentum are vector equations, with one equation for each Cartesian component of the electron or phonon drift velocity ( $i, j = 1, 2, 3$ ). The details of the derivation of the VTE are given in Appendix C.

The VTE give a full description of transport in a coupled electron-phonon system, covering all the regimes ranging from the hydrodynamic to the diffusive one. In the following we show that the VTE incorporate as a special limits the Viscous Heat Equations, describing hydrodynamic phonon transport of heat [54, 97], Gurzhi's equations for hydrodynamic electron transport [3], as well as the standard Diffusive Thermoelectric Equations (DTE) [60].

### A. Viscous Heat Equations

The VHE describes heat-only transport in electrical insulators, we can neglect transport by electrons, and the charge and electron momentum relaxons trivially become zero vectors. This means that Eqs. (31) and (32) are trivially satisfied, and additionally  $\chi_e$ ,  $\tilde{\alpha}$ ,  $\eta_{pe}$ , and  $D_{pe}$  vanish. Therefore, under these conditions, the VTE simplify to:

$$\bar{T}\chi_p^{ij}\frac{\partial u_p^i}{\partial r^j} - \tilde{\kappa}^{ij}\frac{\partial^2 T}{\partial r^i\partial r^j} = 0, \quad (34)$$

$$\chi_p^{ij}\frac{\partial T}{\partial r^j} - \eta_{pp}^{ijkl}\frac{\partial u_p^k}{\partial r^j\partial r^l} = -D_{pp}^{ij}u_p^j, \quad (35)$$

which are the Viscous Heat Equations [9].

### B. Gurzhi's Equations

As in the original paper by Gurzhi [3], and in more recent works [12, 24, 25], we consider an isotropic system

where all the transport tensors are proportional to the identity (e.g.  $\tilde{\sigma}^{ij} = \tilde{\sigma}\delta^{ij}$ ). The Gurzhi limit is obtained from the VTE by considering the limiting case of metallic system where: (i) phonons are at equilibrium, so that temperature is considered constant and the phonon drift velocity can be neglected; (ii) electron-phonon drag can be neglected, i.e.,  $D_{ep/pe} = \eta_{ep/pe} = 0$  and (iii) thermoelectric effects are neglected, so that  $\tilde{\alpha} \approx 0$  and  $\tilde{S} \approx 0$ . Conditions (i) and (ii), along with Eq. (33), imply that  $T$  is constant. Eq. (30) gives the incompressibility condition for the electronic drift velocity,  $\nabla \cdot \mathbf{u}_e = 0$ . Additionally, considering  $\tilde{S} = 0$  in Eq. (31) and in Eq. (16) yields  $\mathbf{J} = -\psi\mathbf{u}_e - \tilde{\sigma}\nabla V_{\text{eff}}$  and

$$\nabla \cdot \mathbf{J} = 0, \quad (36)$$

which is the first Gurzhi equation. We note that due to the incompressibility of  $\mathbf{u}_e$ , Eq. (36) and Eq. (16) with  $S = 0$  imply the electrical potential to be a harmonic function  $\nabla^2 V_{\text{eff}} = 0$ . Now using Eq. (16) with  $\tilde{S} = 0$  to rewrite Eq. (32) in terms of  $\mathbf{J}$  (as in Refs. [12, 25]), and accounting for the aforementioned incompressibility condition, one obtains,

$$-\frac{\eta_{ee}}{D_{ee}}\nabla^2 \mathbf{J} + \mathbf{J} = -\left(\frac{\psi^2}{D_{ee}} + \tilde{\sigma}\right)\nabla V_{\text{eff}}, \quad (37)$$

where we will show in the next section that  $\left(\frac{\psi^2}{D_{ee}} + \tilde{\sigma}\right) = \sigma$  is the standard diffusive electrical conductivity, and  $\frac{\eta_{ee}}{D_{ee}} = l_G^2$  is the square of the Gurzhi length [3]. Eq. (37) coincides with the Gurzhi or Navier-Stokes equation with an ohmic term used to model hydrodynamic transport for electrons (see for example Eq. (1) in Ref. [25]).

### C. Diffusive Thermoelectric Equations

Here we show that in the limiting case of momentum dissipation dominating over viscous effects, and when drag effects on the dissipation of the drift velocity can be neglected, the VTE reduce to the DTE. In particular, one has that Eq. (32) reduces to (also in this case we consider an isotropic solid for simplicity)

$$-D_{pp}^{-1}\chi_p\nabla T = \mathbf{u}_p. \quad (38)$$

Similarly, under these conditions, Eq. (33) reduces to

$$-D_{ee}^{-1}\chi_e\nabla T + D_{ee}^{-1}\psi\nabla V_{\text{eff}} = \mathbf{u}_e. \quad (39)$$

Inserting Eq. (38) into Eq. (30) yields the energy DTE,

$$(\tilde{\alpha} - \bar{T}\frac{\chi_e\psi}{D_{ee}})\nabla^2 V_{\text{eff}} + (\tilde{\kappa} + \bar{T}\frac{\chi_p^2}{D_{pp}} + \bar{T}\frac{\chi_e^2}{D_{ee}})\nabla^2 T = 0. \quad (40)$$

Similarly, inserting Eq. (39) into Eq. (31) yields

$$(\tilde{\sigma} + \frac{\psi^2}{D_{ee}})\nabla^2 V_{\text{eff}} + (\tilde{\sigma}\tilde{S} - \frac{\psi\chi_e}{D_{ee}})\nabla^2 T = 0. \quad (41)$$

Eqs. (40) and (41) are the standard diffusive thermoelectric equations. As anticipated in Section III C, the transport coefficients appearing in these equations are determined by the addition of two terms: (i) the terms with tilde originate from the microscopic diffusion of charge and/or energy; (ii) an additive contribution that originates from momentum behaving diffusively in the regime where Umklapp dissipation is strong. In formulas, within our formalism the standard thermal conductivity, electrical conductivity, and Peltier coefficients measured in diffusive experiments are

$$\sigma = \tilde{\sigma} + \frac{\psi^2}{D_{ee}}, \quad (42)$$

$$\kappa = \tilde{\kappa} + \bar{T}\frac{\chi_p^2}{D_{pp}} + \bar{T}\frac{\chi_e^2}{D_{ee}}, \quad (43)$$

$$S = \frac{1}{\sigma\bar{T}}\left(\tilde{\alpha} - \bar{T}\frac{\chi_e\psi}{D_{ee}}\right). \quad (44)$$

Full details of the derivation of these transport coefficients are given in Appendix B.

## V. CASE STUDY: ELECTRON-PHONON BIFLUID IN GRAPHITE

Experimental work from the 1970s suggested that signatures of electron-phonon drag manifest in undoped graphite as an anomalous dip in the temperature dependence of the Seebeck coefficient [62–64]. Subsequent experiments found the Seebeck coefficient to be highly sensitive to doping impurities and carrier concentration, revealing an increase in  $S$  upon hole doping [65, 67–69] and a decrease upon electron doping [98].

In addition to displaying thermoelectric anomalies, graphite has recently gained attention as a target system for the observation of transient fluid-like heat transport phenomena such as second sound [16, 22], lattice cooling [18, 99], as well as steady-state heat hydrodynamic phenomena such as Poiseuille heat flow [19], thickness-dependent Poiseuille conductivity peak [17], and Tesla-valve rectification of heat flow [20]. In spite of the combined evidence of heat hydrodynamics and the strong influence of electron-phonon drag on thermoelectric properties, the possible interplay between phonon hydrodynamics and electronic transport in graphite has never

been investigated with first-principles accuracy. These past findings, and the possibility to tuning the electronic-transport properties of graphite via doping [67–69, 98], make graphite an ideal system to investigate the possibility of simultaneous heat and charge hydrodynamics.

### A. Transport coefficients from first principles

We relied on density-functional theory (DFT) to compute for graphite all the electronic and phononic properties appearing in the epBTE (6) (i.e., electron and phonon bands, phonon-phonon and electron-phonon couplings that determine the full collision matrix with drag terms, see Appendix D for details [100]), and implemented in the open-source Phoebe code [34] the numerical infrastructure to diagonalize the coupled collision matrix and evaluate all the transport coefficients in Tab. I.

We show in Fig. 1 the transport coefficients as a function of temperature, also evaluating their dependence on charge carrier concentration by comparing three different doping levels:  $-10^{20}\text{cm}^{-3}$  (strongly electron-doped),  $-2.5 \times 10^{18}\text{cm}^{-3}$  (weakly electron-doped), and  $+2.5 \times 10^{18}\text{cm}^{-3}$  (weakly hole-doped). Additionally, to quantify the impact of electron-phonon drag on the transport coefficients, we compare predictions obtained considering the full electron-phonon collision matrix appearing in the coupled epBTE (5), against those obtained neglecting the drag quadrants in the scattering matrix and corresponding to solving decoupled eBTE and pBTE.

Panel **a** shows a strong impact of electron-phonon drag on the diffusive Seebeck coefficient (44) for all doping concentrations analyzed. First, for the strongly electron-doped case (orange), we see that the influence of electron-phonon drag is maximized at lower temperatures, and decreases steadily with increasing temperature. The decreasing behavior of  $S$  upon increasing temperature qualitatively matches the behavior observed in samples with electron doping [98]. Upon progressively reducing the concentration of electrons, to weak electron doping (blue) or even weak hole doping (red), the curve  $S(T)$  reverses its concavity and progressively shifts towards more positive values. The overall behavior matches the upward shift in  $S$  experimentally observed upon increasing hole concentration [65, 66]. We note that these experiments discuss defects that increase hole concentration, but do not report the exact dopant concentration. Thus, our comparison with experiments is meaningful at the level of the observed trend upon increasing hole concentration.

Predictions for the diffusive electrical conductivity (42) are shown in **b**, and display a significant dependence on doping — samples with strong electron doping ( $-10^{20}\text{cm}^{-3}$ ) show a conductivity that is about one order of magnitude larger than weakly electron-doped and weakly hole-doped samples over the entire temperature range analyzed. For all doping concentrations, predictions for the electrical conductivity are negligibly affected by considering or not electron-phonon drag.

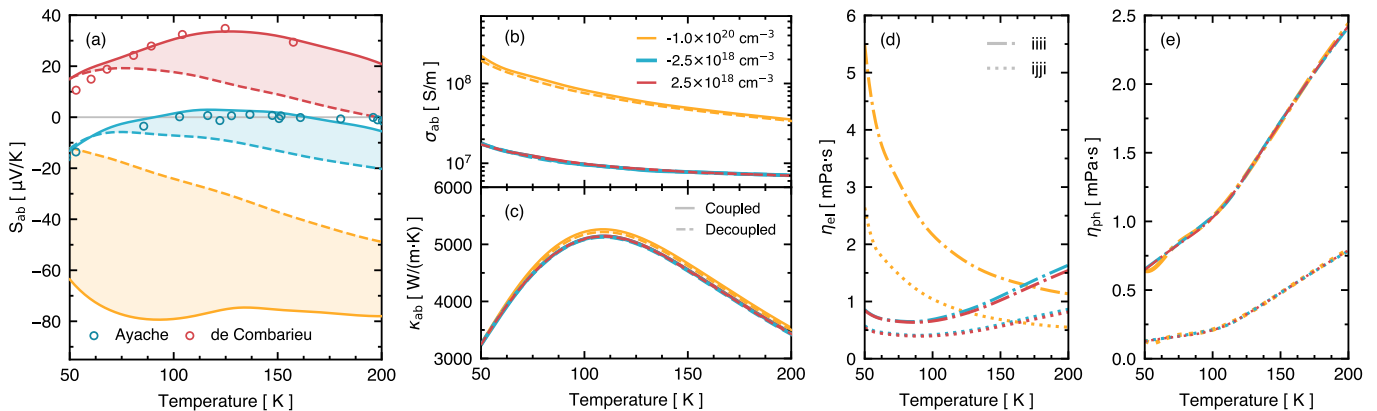


FIG. 1. **Influence of electron-phonon drag and doping on bulk transport coefficients in graphite.** We show first-principles predictions for the Seebeck coefficient (a), electrical conductivity (b), and total thermal conductivity (c), accounting for electron-phonon drag (solid lines) or not (dashed lines) — the shaded area quantifies the contribution of electron-phonon drag. (d) and (e) show the independent components of the electronic and phononic viscosities from the coupled BTE solution. Colors distinguish three doping concentrations,  $-1 \times 10^{20} \text{ cm}^{-3}$  (yellow),  $-2.5 \times 10^{18} \text{ cm}^{-3}$  (blue), and  $+2.5 \times 10^{18} \text{ cm}^{-3}$  (red). Empty blue circles are experimental data from Ref [66], and empty red circles from Ref [65] (annealed 520K sample).

The total diffusive thermal conductivity (43) includes electronic and phononic contributions, and is shown in c. Strong electronic doping induces a small but noticeable ( $< 5\%$ ) increase compared to weakly electron- or hole-doped samples. Similarly to the electronic conductivity, electron-phonon drag has a negligible influence on the thermal conductivity.

Finally, the electron and phonon viscosities are shown in d and e (Eqs. (26,27)). We see that doping strongly impacts the electronic viscosity: in strongly electron-doped samples, the electronic viscosity decreases with temperature as in typical liquids; in weakly hole-doped samples, the electronic viscosity increases with temperature, mirroring the behavior of classical gases. In contrast, the phonon viscosity is negligibly impacted by doping, always maintaining an increasing-with-temperature trend that mirrors classical gases. We note that for the viscosity we reported only predictions from the full coupled calculations with drag, since viscosity is relevant only in the hydrodynamic regime that requires to account for the drag quadrants to be accurately described. We note that graphite in-plane is isotropic, and this implies that there can in general be three different non-zero viscosity components:  $\eta^{iiii}$ ,  $\eta^{ijjj} = \eta^{jjji}$ , and  $\eta^{jjij}$ . These components satisfy the following relation  $\eta^{iiii} = 2\eta^{ijji} + \eta^{jjij}$ , and therefore in Fig. 1 we report only two independent components.

## B. Electron-phonon hydrodynamics in devices

The transport coefficients predicted in the previous section are necessary for parametrizing the VTE with quantitative accuracy, enabling us to solve them in realistic device geometries and predict macroscopic signatures of thermoelectric hydrodynamic transport.

Since previous works have studied devices containing phonon-only fluids [9, 54, 97, 101], or electron-only fluids [11, 12, 21, 25], the most natural device to investigate electron-phonon bifluids should allow verification of both the known phonon-only and electron-only fluid limits, and also illustrate what happens when these coexist, interact, or mix. The two-fluid-mixing device made of highly doped graphite shown in Fig. 2 is an ideal setup to investigate all these regimes. In fact, in this device we employ boundary conditions (BCs, discussed in Fig. 2) that drive a phonon-dominated hydrodynamic heat flow in the upper channel as well as a hydrodynamic electron flow in the lower channel, and the forced merging of the two flows at the intersection of the channels enables us to investigate how electron-phonon bifluids emerge from mixing electronic and phononic fluids with non-negligible viscosity. We highlight how the phonon-dominated hydrodynamic heat flow in the upper channel and the electronic hydrodynamic flow in the lower channel, each displays the characteristic Poiseuille hydrodynamic profile, where the flow is faster at the center of the channel and slower at the boundaries (colormaps in panels a and d, respectively). We also note that both these flows in the narrow channels are symmetric relative to the boundaries. In addition, it is worth noting that in the upper narrow channel the charge current is much smaller compared to the lower one — as expected from having smaller potential difference applied to the upper channel compared to the lower one — but the heat flux in the lower channel is larger than in the upper one, despite having a stronger temperature difference applied at the boundaries of the upper channel. This large heat flux in the lower channel is dominated by a diffusive component that is driven by the potential difference through the Peltier coefficient  $\tilde{\alpha}$  in Eq. (34). In the wide mixing channel, the heat and charge currents exhibit the viscous hydrodynamic fea-

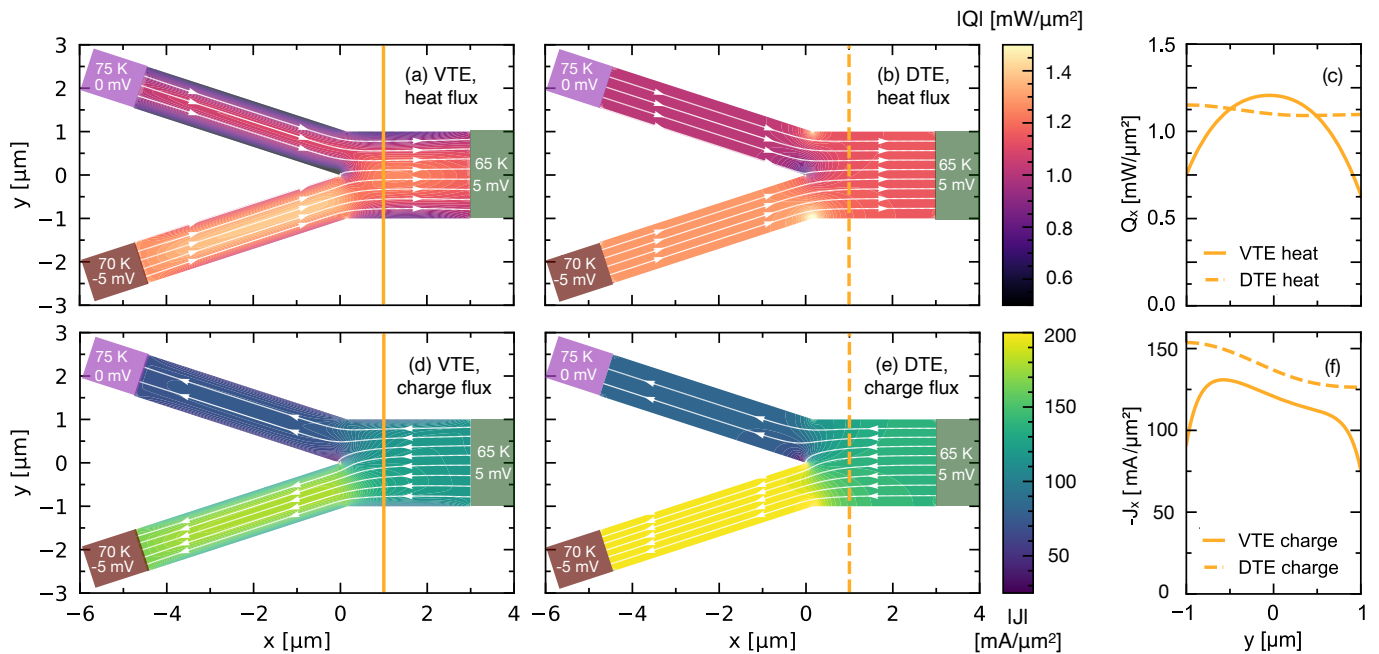


FIG. 2. **Macroscopic signatures of viscous electron-phonon hydrodynamics**, in fluid-mixing device made of highly electron-doped graphite ( $-10^{20} \text{ cm}^{-3}$ ). Boundary conditions are as follows: temperature (potential) is set at 75 K (0 mV) on the upper thin terminal, 70 K ( $-5 \text{ mV}$ ) on the lower thin terminal, and at 65 K (5 mV) at the wide terminal. The other boundaries are assumed to be electrically insulating and adiabatic (i.e., no heat and charge flux is flowing through them), and, in the VTE case, electron and phonon drift velocities are zero on all boundaries (no-slip BCs). Top row, heat flux predicted from the VTE (a), or DTE (b) and their comparison along the section  $x=1\mu\text{m}$  (c). Bottom row, charge flux predicted from the VTE (d), DTE (e), and their comparison along the section  $x=1\mu\text{m}$  (f). We show the in-plane ( $x-y$ ) components of the fluxes for a three dimensional device that can be treated as bulk (infinitely long) in the  $z$  direction.

ture of being minimized at the boundaries; however, in contrast to the symmetric behavior observed in the narrow channels, we see that in the wide mixing channel the shapes for the heat and charge currents are visibly different, with an asymmetry that is much more pronounced in the charge flux compared to the heat flux (Fig. 2c and f show the heat and charge fluxes, respectively, along the section  $x = 1\mu\text{m}$ ).

To confirm that these observable macroscopic features originate from microscopic electron and phonon hydrodynamics, we compare the heat and charge fluxes of the VTE (Fig. 2a,d), which accounts for hydrodynamic effects, with the heat and charge fluxes predicted by the standard diffusive DTE (Fig. 2b,e). We confirm that the hydrodynamic features observed in the VTE fluxes are absent in the DTE results; in particular, the heat and charge fluxes emerging from the DTE approach the boundaries with zero derivative [102]. We conclude by noting that in all the simulations in Fig. 2 finite-size (ballistic) corrections on the transport coefficients are accounted for following the approach of Ref. [54], which is formally analogous to the Bosanquet-type approximation used to describe corrections to fluids' viscosities in the transition regime [103], see Appendix B3 for details.

In summary, the VTE demonstrate the possible coexistence of electron and phonon bifluids at conditions where electron-phonon drag has a significant influence

on transport coefficients such as the Seebeck coefficients. In the weakly electron- or hole-doped samples, we found that transport is hydrodynamic for phonons only. This suggests that having strong electron-phonon drag effect on the thermoelectric coefficients is a necessary condition for the emergence of electron-phonon bifluids. In the next section, we discuss in detail how they interact and the signatures they produce.

### C. Hydrodynamic violations of the similarity between heat and charge flows

Expanding the results for specific boundary conditions shown in Fig. 2, we investigate how different kinds of boundary conditions influence the shape (in the mathematical sense) of the heat and charge current profiles.

In Fig. 3 we show that the behavior predicted by the VHE violates the mathematical similarity property that relates the heat and charge fluxes emerging from the DTE. Specifically, in the steady-state, the DTE imply that both temperature and electrical potential are harmonic functions, i.e.,  $\nabla^2 V = 0$  and  $\nabla^2 T = 0$ , and therefore they cannot have local maximum or local minimum other than on the boundary of the domain. It is particularly insightful to consider the solution of the DTE in two special cases: (i) potential-only difference BCs,

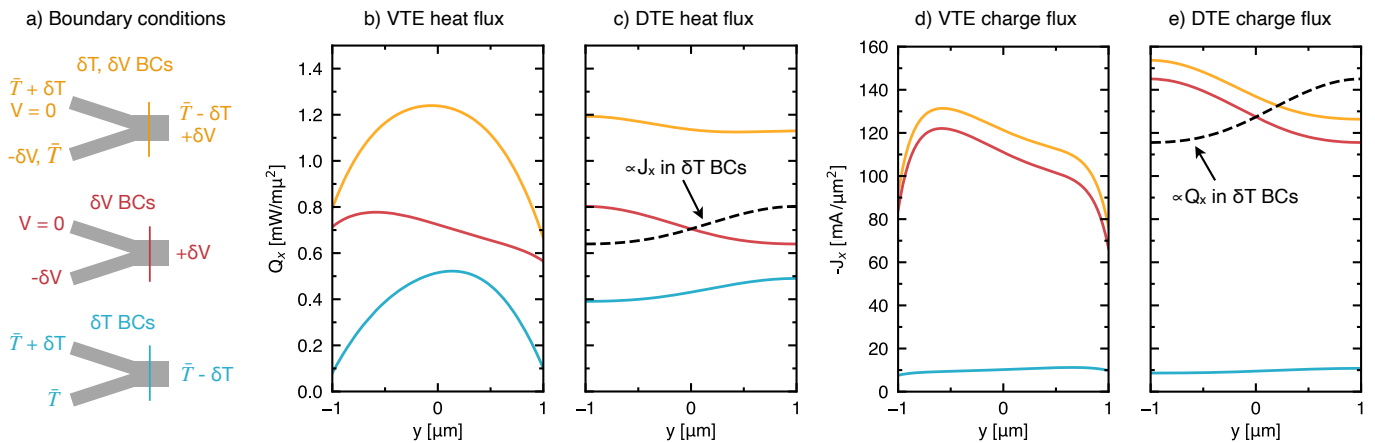


FIG. 3. **Violation of the similarity between heat and charge flow in the thermoelectric hydrodynamic regime.** We show the horizontal heat ( $Q^x(y)$ ) and charge ( $J^x(y)$ ) flux along the section  $x = 1\mu\text{m}$  (vertical dashed slice of the device, as shown in **a**) predicted by the VTE (**b** and **d**) or DTE (**c** and **e**) in the presence of different boundary conditions (BCs), which are detailed in the schematic shown in **a**). The flux for temperature-difference only BCs is blue (lowest inset in **a**), for potential-difference only BCs is red (central inset in **a**), and for combined temperature- and potential-difference BCs is yellow (upper inset in **a**) as in Fig. 2. In the VTE, the boundary conditions influence the shape of the non-diffusive flux profile. In contrast, in the DTE, the type of boundary conditions affects the magnitude but not the shape of the flux profile. This is demonstrated by the dashed line in panel **b** (**d**), which shows that rescaling and mirroring with respect to  $y$  the heat (charge) flux obtained in the presence of temperature-only boundary conditions yields a heat (charge) flux that is mathematically similar the one obtained from the potential-only boundary conditions.

which imply that the temperature remains equal to zero everywhere in the domain; (ii) temperature-only difference BCs, which imply the potential remains equal to zero everywhere. In case (i) the electrical potential fully determines the profile for both the charge ( $\mathbf{J} = -\sigma\nabla V$ ) and heat flux ( $\mathbf{Q} = -\alpha\nabla V$ ), which will consequently have mathematically similar profiles, related by a rescaling.

Analogously, in case (ii) the temperature fully determines the profile of both the heat ( $\mathbf{Q} = -\kappa\nabla T$ ) and charge flux ( $\mathbf{J} = -\sigma S\nabla T$ ), which will consequently also have mathematically similar profiles. In addition, because in case (i) one has that  $T(\mathbf{r}) = \bar{T}$  and  $V(\mathbf{r})$  is determined by the solution of  $\nabla^2 V(\mathbf{r}) = 0$  in the presence of potential-only BCs, and in case (ii) one has that  $V(\mathbf{r}) = 0$  and  $T(\mathbf{r})$  is determined by the solution of  $\nabla^2 T$  with temperature-only BCs, choosing mathematically analogous conditions for case (i) and (ii) will lead to mathematically similar profiles in the two cases.

We demonstrate these properties in Fig. 3. Specifically, panel **c** and **e** numerically confirm these analytical properties. First, we confirm that the heat-flux profile obtained in case (i) (red line in panel **c**) is mathematically similar to the charge flux obtained in case (i), (red line in panel **e**); analogously, the heat-flux profile obtained in case (ii) (blue line in panel **c**) is mathematically similar to the charge flux obtained in case (ii) (blue line in panel **e**). Second, since the potential-only BCs of case (i) are mathematically related to the temperature-only BCs of case (ii) by a mirror operation of the  $y$  coordinate, we also confirm that applying the same mirroring operation to the heat and charge profiles obtained in case (i), yields profiles mathematically similar to case (ii), confirming

our analytical expectations.

Most importantly, panel **b** and **d** show that this similarity property between heat and charge fluxes no longer holds in the hydrodynamic VTE case. In particular, applying temperature-only difference BCs and no-slip boundary conditions for both electronic and phononic drift velocity, one clearly sees that the heat flux profile (blue line in panel **b**) is not mathematically similar to the charge flux profile (blue line in panel **d**). Analogous considerations hold for potential-only difference BCs and no-slip boundary conditions for both electronic and phononic drift velocity: the VTE heat flux profile (red line in panel **b**) is not mathematically similar to the VTE charge flux profile (red line in panel **d**). We conclude by noting that in Fig. 3, finite-size (ballistic) corrections on the transport coefficients are taken into account following the approach discussed in Appendix B3 and employed also in Fig. 2.

## VI. CONCLUSIONS

We have introduced a theoretical framework to describe with first-principles accuracy thermoelectric transport beyond the diffusive regime, elucidating the conditions under which phonons, electrons, or a mixture of them can behave as a bifluid, rather than diffusively. Starting from the coupled electron-phonon Boltzmann transport equation (epBTE), we have exposed the microscopic symmetries and (quasi) conservation laws that determine transport of heat in phonon-only systems, of charge in electron-only systems, and thermoelectric phe-

nomena in coupled electron-phonon systems. Specifically, we have elucidated how out-of-equilibrium mixtures of electrons and phonons form relaxon excitations with well-defined parity, with odd relaxons determining the standard diffusive thermoelectric transport coefficients — electrical conductivity ( $\sigma$ ), thermal conductivity ( $\kappa$ ), Peltier and Seebeck coefficients ( $\alpha$  and  $S$ , respectively) — while the complementary set of even relaxons determine the viscosities of the electron and phonon components of the bifluid.

These microscopic insights have allowed us to coarse-grain the epBTE into Viscous Thermoelectric Equations (VTE) that formally unify Gurzhi’s [3] equation for electron-only hydrodynamics and the Viscous Heat Equations for phonon-only hydrodynamics [54], and most importantly, extend them to cover the mixed electron-phonon bifluid regime as well as its transition into the diffusive limit in large devices or at high temperature. According to the VTE, when electrons and phonons are negligibly coupled, the heat and charge fluxes can sustain different temperatures and drift velocities. This is the case, e.g., in: (i) electrical insulators, where phonon-phonon scattering is the dominant interaction and determines both temperature gradient and phonon drift velocity, while electrons are at equilibrium; (ii) metals at low temperature having electron-electron scattering as dominant interaction mechanism, implying that temperature gradients and electron drift velocity are exclusively determined by electrons while phonons are at equilibrium. Most importantly, the VTE extend beyond these limiting cases, also describing mixed regimes where momentum-conserving electron-phonon interactions are dominant, as well as regimes where they compete with phonon-phonon or electron-electron scattering. Under these conditions, electrons and phonons can exchange energy and momentum, implying that both contribute to temperature gradients, as well as to electronic and phononic drift velocities. We have shown that in general the drift velocities for the electron and phonon fluids can be different, since Umklapp processes can impact phonons and electrons in different ways.

We have discussed the emergence and coexistence of diffusive and hydrodynamic behavior for both heat and charge currents, showing that conduction in solids can become formally analogous to transport phenomena in rarefied classical fluids [88–92]. We have demonstrated that the hydrodynamic components of the charge and heat fluxes are, at the micrometre lengthscale, strongly influenced by devices’ boundary conditions and shape. It is worth noting that the presence of weak but non-zero Umklapp processes implies that the hydrodynamic component of the charge and heat currents are subject to dissipation, an effect that formally appears in the VTE as a linear term in the drift velocities, which competes with the viscous term involving second derivatives of the drift velocities. The mathematical form of the dissipation shares analogies to the damping term appearing in the extended Navier-Stokes equations used to describe fluids

that dissipate momentum when flowing through porous media [104–108].

We have applied our quantitatively accurate, first-principles framework to several graphite samples with different dopings as a case study, finding agreement between our predictions for the influence of electron-phonon drag on the Seebeck coefficient and experiments [65, 66]. Importantly, we have shown that the influence of electron-phonon drag on the Seebeck coefficient strongly depends on doping, and it is most prominent in samples with high electron doping. We have relied on these findings to identify the temperature and doping conditions under which heat hydrodynamics in graphite is influenced by electrons. Specifically, we have shown that highly doped graphite displays heat hydrodynamic signatures similar to natural graphite, and, most importantly, that it also permits coexistence of unmixed hydrodynamic phonon and electron fluids. We discussed unambiguous, experimentally observable hallmarks of the electron-phonon bifluid: (i) emergence of Poiseuille-like profiles for both charge and heat currents in micrometric devices with rough (non-slipping) boundaries, which can be detected by measuring the scaling with size of the heat [109] and charge [110] transported through devices having fixed geometry and different sizes, or even from visualizing microscopic carrier dynamics [111]; (ii) violation of the mathematical similarity constraint between heat and charge profiles typical of thermoelectric diffusive flows, a feature that can be detected, e.g., through spatially-resolved heat or charge current measurements [15, 21, 25, 112].

We have demonstrated that the electron and phonon fluids can have very different viscosities, which can be exploited to control the relation between charge and heat flux in micrometric devices. Notably, we found that viscosities can be controlled through doping. In weakly doped graphitic devices, electrons and phonons both display a viscosity increasing with temperature and reminiscent of the behavior of gases; upon increasing electron doping, the electronic viscosity reverse trend in temperature, displaying a decreasing-with-temperature trend reminiscent of the one observed in typical liquids, while phonons viscosities are negligibly affected by doping and always increase with temperature, as in gases.

Additionally, it is worth noting that the theory and methodology developed here for thermoelectric hydrodynamics shares several formal analogies with other coupled transport phenomena in solids — e.g., involving drag between phonons and photons [113], magnons and electrons [114], or phonons and magnons [115] — thus will inspire further novel developments and applications. We also release these developments open-source to the community in an extension of the Phoebe software suite [34], enabling future investigations of electron-phonon drag effects and thermoelectric hydrodynamics.

We conclude by noting that our fundamental findings and methodological developments may also have direct technological applications. For example, in power electronics, where viscous violations of the diffusive energy-

charge flux similarity property could be exploited to focus the charge flux and the parasitic heat flux in different device's regions. As such, our findings open new avenues to tackle the overheating problem in electronics, or even to design novel devices where viscous degrees of freedom allows unprecedented control and management on mixed heat and charge flows.

## VII. CODE AVAILABILITY

The numerical infrastructure to solve from first principles the microscopic coupled electron-phonon Boltzmann transport equation in the linear-response regime is released as a major version update of the open-source Phoebe [34] software suite, available at <https://github.com/phoebe-team/>. The SOLver for Viscous Thermoelectric Equations (SolViTE) is interfaced with the Phoebe suite and will be released in a format compatible with standard finite-element solvers.

## VIII. ACKNOWLEDGMENTS

We gratefully acknowledge Bo Peng, Samuel Huberman, and Aleksei Sokolov for the useful discussions. The computational resources were provided by: (i) the Sulis Tier 2 HPC platform (funded by EPSRC Grant EP/T022108/1 and the HPC Midlands+consortium); (ii) the UK National Supercomputing Service ARCHER2, for which access was obtained via the UKCP consortium and funded by EPSRC [EP/X035891/1]; (iii) the Kelvin2 HPC platform at the NI-HPC Centre (funded by EPSRC and jointly managed by Queen's University Belfast and Ulster University); (iv) The Flatiron Institute, which is a division of the Simons Foundation. B. R. acknowledges support from Trinity College at University of Cambridge. M. S. acknowledges support from: (i) the Swiss National Science Foundation (SNSF) project P500PT\_203178; (ii) Gonville and Caius College at University of Cambridge.

### Appendix A: Coupled electron-phonon scattering matrix

In this Appendix we derive the scattering rates for electrons and phonons, including drag effects. These determine the scattering matrix on the right-hand side of the epBTE, Eq. (1). Self quadrants  $S_{\mathbf{k}m, \mathbf{k}'m'}^{\text{el}}$ ,  $S_{\mathbf{q}s, \mathbf{q}'s'}^{\text{ph}}$  of the electron-phonon scattering matrix are reported in Cepellotti *et al.* [34]; we derive the complementary expressions for the drag quadrants  $D_{\mathbf{k}m, \mathbf{q}'s'}^{\text{el-ph}}$ ,  $D_{\mathbf{q}s, \mathbf{k}'m'}^{\text{el-ph}}$  [56, 71], and then apply them a two-carrier generalization of the symmetrization transformation discussed by Hardy [93].

#### 1. Electron-phonon scattering rates

In considering the electron-phonon interaction, we restrict ourselves to the lowest-order collisions, in which a phonon is absorbed or emitted by an electron, followed by an appropriate change of state of the electron. The net scattering rate of the  $\mathbf{k}m$  state into the  $\mathbf{k}'m'$  state due to the  $\mathbf{q}s$  phonon is given by Fermi's golden rule [73]. In the linearized epBTE, we consider only the rates at leading linear order in  $f_{\mathbf{k}m}$ ,  $n_{\mathbf{q}s}$ , and  $f_{\mathbf{k}'m'}$ :

$$W_{\mathbf{k}m, \mathbf{q}s; \mathbf{k}'m'} = \frac{2\pi}{\hbar} |g_{m, m', s}(\mathbf{k}, \mathbf{k}', \mathbf{q})|^2 \delta_{\mathbf{k}' - \mathbf{k} - \mathbf{q}, G} \delta(\varepsilon_{\mathbf{k}'m'} - \varepsilon_{\mathbf{k}m} - \hbar\omega_{\mathbf{q}s}) \times \left[ (\bar{N}_{\mathbf{q}s} + \bar{F}_{\mathbf{k}'m'}) f_{\mathbf{k}m} + (\bar{F}_{\mathbf{k}m} - \bar{F}_{\mathbf{k}'m'}) n_{\mathbf{q}s} - (1 - \bar{F}_{\mathbf{k}m} + \bar{N}_{\mathbf{q}s}) f_{\mathbf{k}'m'} \right]. \quad (\text{A1})$$

The Kronecker delta and the Dirac delta function enforce the conservation of momentum and energy, respectively, and  $g_{m, m', s}(\mathbf{k}, \mathbf{k}', \mathbf{q})$  is the electron-phonon matrix element [32]. We note that the linearization of the scattering rate requires choosing an equilibrium point; in this equilibrium point all scattering rates must vanish. We write the net rate as  $W_{\mathbf{k}m, \mathbf{q}s; \mathbf{k}'m'} = \mathcal{P}_{\mathbf{k}m, \mathbf{q}s; \mathbf{k}'m'}^{\mathbf{k}m} f_{\mathbf{k}m} + \mathcal{P}_{\mathbf{k}m, \mathbf{q}s; \mathbf{k}'m'}^{\mathbf{q}s} n_{\mathbf{q}s} - \mathcal{P}_{\mathbf{k}m, \mathbf{q}s; \mathbf{k}'m'}^{\mathbf{k}'m'} f_{\mathbf{k}'m'}$ , where  $\mathcal{P}$  are equilibrium transition rates [73]. These rates do not depend on the deviation from equilibrium and are always non-negative. We can then express the scattering rates due to the electron-phonon interaction, starting with electrons:

$$\left. \frac{df_{\mathbf{k}m}}{dt} \right|_{\text{coll}} = - \frac{1}{\mathcal{V} \mathcal{N}_{\mathbf{k}}} \sum_{\mathbf{k}'m', \mathbf{q}s} \left( \mathcal{P}_{\mathbf{k}m, \mathbf{q}s; \mathbf{k}'m'}^{\mathbf{k}m} + \mathcal{P}_{\mathbf{k}'m', \mathbf{q}s; \mathbf{k}m}^{\mathbf{k}m} \right) f_{\mathbf{k}m} + \frac{1}{\mathcal{V} \mathcal{N}_{\mathbf{k}}} \sum_{\mathbf{k}'m', \mathbf{q}s} \left( \mathcal{P}_{\mathbf{k}m, \mathbf{q}s; \mathbf{k}'m'}^{\mathbf{k}'m'} + \mathcal{P}_{\mathbf{k}'m', \mathbf{q}s; \mathbf{k}m}^{\mathbf{k}'m'} \right) f_{\mathbf{k}'m'} - \frac{1}{\mathcal{V} \mathcal{N}_{\mathbf{q}}} \sum_{\mathbf{q}s, \mathbf{k}'m'} \left( \mathcal{P}_{\mathbf{k}m, \mathbf{q}s; \mathbf{k}'m'}^{\mathbf{q}s} - \mathcal{P}_{\mathbf{k}'m', \mathbf{q}s; \mathbf{k}m}^{\mathbf{q}s} \right) n_{\mathbf{q}s}, \quad (\text{A2})$$

where the two rates in each bracket account for processes in which an electron absorbs or emits a phonon. We further separate the scattering-out terms, which are proportional to  $f_{\mathbf{k}m}$  itself, from the scattering-in terms that are



proportional to the populations of other electron states  $f_{\mathbf{k}'m'}$ . Comparing Eq. (A2) with the electron part of Eq. (1), we find the expressions for two quadrants of the unsymmetrized scattering matrix:

$$\begin{aligned} S_{\mathbf{k}m,\mathbf{k}'m'}^{\text{el}} &= \frac{1}{\mathcal{V}\mathcal{N}_{\mathbf{k}}} \sum_{\mathbf{k}''m'',\mathbf{q}s} \frac{2\pi}{\hbar} |g_{m,m'',s}(\mathbf{k},\mathbf{k}'',\mathbf{q})|^2 \delta_{\mathbf{k}''-\mathbf{k}-\mathbf{q},\mathbf{G}} \left[ \delta(\varepsilon_{\mathbf{k}''m''}-\varepsilon_{\mathbf{k}m}-\hbar\omega_{\mathbf{q}s}) + \delta(\varepsilon_{\mathbf{k}''m''}-\varepsilon_{\mathbf{k}m}+\hbar\omega_{\mathbf{q}s}) \right] \times \\ &\times \frac{1}{2 \sinh[\frac{\beta}{2}\hbar\omega_{\mathbf{q}s}]} \left[ \delta_{\mathbf{k}'m',\mathbf{k}m} \frac{\cosh[\frac{\beta}{2}(\varepsilon_{\mathbf{k}m}-\mu)]}{\cosh[\frac{\beta}{2}(\varepsilon_{\mathbf{k}'m''}-\mu)]} - \delta_{\mathbf{k}'m',\mathbf{k}''m''} \frac{\cosh[\frac{\beta}{2}(\varepsilon_{\mathbf{k}'m''}-\mu)]}{\cosh[\frac{\beta}{2}(\varepsilon_{\mathbf{k}m}-\mu)]} \right], \end{aligned} \quad (\text{A3})$$

$$\begin{aligned} D_{\mathbf{k}m,\mathbf{q}s}^{\text{el-ph}} &= \frac{1}{\mathcal{V}\mathcal{N}_{\mathbf{q}}} \sum_{\mathbf{k}'m'} \frac{2\pi}{\hbar} \left[ |g_{m,m',s}(\mathbf{k},\mathbf{k}',\mathbf{q})|^2 \delta_{\mathbf{k}'-\mathbf{k}-\mathbf{q},\mathbf{G}} \delta(\varepsilon_{\mathbf{k}'m'}-\varepsilon_{\mathbf{k}m}-\hbar\omega_{\mathbf{q}s}) \right. \\ &\left. - |g_{m',m,s}(\mathbf{k}',\mathbf{k},\mathbf{q})|^2 \delta_{\mathbf{k}'-\mathbf{k}+\mathbf{q},\mathbf{G}} \delta(\varepsilon_{\mathbf{k}'m'}-\varepsilon_{\mathbf{k}m}+\hbar\omega_{\mathbf{q}s}) \right] \frac{\sinh[\frac{\beta}{2}\hbar\omega_{\mathbf{q}s}]}{2 \cosh[\frac{\beta}{2}(\varepsilon_{\mathbf{k}m}-\mu)] \cosh[\frac{\beta}{2}(\varepsilon_{\mathbf{k}'m'}-\mu)]}, \end{aligned} \quad (\text{A4})$$

where we expanded the scattering rates using Eq. (A1) and expressed equilibrium populations in terms of Fermi-Dirac and Bose-Einstein populations. In the first bracket of Eq. (A3), we group together absorption of  $\mathbf{q}s$  and emission of  $-\mathbf{q}s$ , while in the second bracket the two terms determine the diagonal and off-diagonal terms of  $S_{\mathbf{k}m,\mathbf{k}'m'}^{\text{el}}$  [116]. In Eq. (A4), the two terms in the bracket account for absorption and emission of the  $\mathbf{q}s$  mode, exactly as in Eq. (A2).

We proceed in an analogous way to describe the scattering term for phonons:

$$\left. \frac{dn_{\mathbf{q}s}}{dt} \right|_{\text{coll}} = \frac{\mathfrak{D}}{\mathcal{V}\mathcal{N}_{\mathbf{k}}} \sum_{\mathbf{k}m,\mathbf{k}'m'} (\mathcal{P}_{\mathbf{k}'m',\mathbf{q}s;\mathbf{k}m}^{km} - \mathcal{P}_{\mathbf{k}m,\mathbf{q}s;\mathbf{k}'m'}^{km}) f_{\mathbf{k}m} - \frac{\mathfrak{D}}{\mathcal{V}\mathcal{N}_{\mathbf{k}}} \sum_{\mathbf{k}m,\mathbf{k}'m'} \mathcal{P}_{\mathbf{k}m,\mathbf{q}s;\mathbf{k}'m'}^{\mathbf{q}s} n_{\mathbf{q}s}; \quad (\text{A5})$$

here a single sum over electrons accounts for both absorption and emission, and we note also that the electron-phonon interaction is diagonal in the phonon subspace. The scattering matrix elements are then:

$$\begin{aligned} D_{\mathbf{q}s,\mathbf{k}m}^{\text{ph-el}} &= \frac{\mathfrak{D}}{\mathcal{V}\mathcal{N}_{\mathbf{k}}} \sum_{\mathbf{k}'m'} \frac{2\pi}{\hbar} \left[ |g_{m,m',s}(\mathbf{k},\mathbf{k}',\mathbf{q})|^2 \delta_{\mathbf{k}'-\mathbf{k}-\mathbf{q},\mathbf{G}} \delta(\varepsilon_{\mathbf{k}'m'}-\varepsilon_{\mathbf{k}m}-\hbar\omega_{\mathbf{q}s}) \right. \\ &\left. - |g_{m',m,s}(\mathbf{k}',\mathbf{k},\mathbf{q})|^2 \delta_{\mathbf{k}'-\mathbf{k}+\mathbf{q},\mathbf{G}} \delta(\varepsilon_{\mathbf{k}'m'}-\varepsilon_{\mathbf{k}m}+\hbar\omega_{\mathbf{q}s}) \right] \frac{\cosh[\frac{\beta}{2}(\varepsilon_{\mathbf{k}m}-\mu)]}{2 \sinh[\frac{\beta}{2}\hbar\omega_{\mathbf{q}s}] \cosh[\frac{\beta}{2}(\varepsilon_{\mathbf{k}'m'}-\mu)]}, \end{aligned} \quad (\text{A6})$$

$$S_{\mathbf{q}s,\mathbf{q}'s'}^{\text{ph}} = \delta_{\mathbf{q}s,\mathbf{q}'s'} \frac{\mathfrak{D}}{\mathcal{V}\mathcal{N}_{\mathbf{k}}} \sum_{\mathbf{k}m,\mathbf{k}'m'} \frac{2\pi}{\hbar} |g_{m',m,s}(\mathbf{k}',\mathbf{k},\mathbf{q})|^2 \delta_{\mathbf{k}'-\mathbf{k}-\mathbf{q},\mathbf{G}} \delta(\varepsilon_{\mathbf{k}'m'}-\varepsilon_{\mathbf{k}m}-\hbar\omega_{\mathbf{q}s}) \frac{\sinh[\frac{\beta}{2}\hbar\omega_{\mathbf{q}s}]}{2 \cosh[\frac{\beta}{2}(\varepsilon_{\mathbf{k}m}-\mu)] \cosh[\frac{\beta}{2}(\varepsilon_{\mathbf{k}'m'}-\mu)]}. \quad (\text{A7})$$

## 2. Symmetrization

As discussed in Section IIC, the first step of solving the epBTE is recasting the coupled scattering matrix in a symmetric form. We start by symmetrizing the self quadrants  $S_{\mathbf{k}m,\mathbf{k}'m'}^{\text{el}}, S_{\mathbf{q}s,\mathbf{q}'s'}^{\text{ph}}$ ; these transformations are taken from Cepellotti *et al.* [34] and Chaput [36], Hardy [93], respectively:

$$S_{\mathbf{k}m,\mathbf{k}'m'}^{\text{el}} = S_{\mathbf{k}m,\mathbf{k}'m'}^{\text{el}} \frac{\cosh[\frac{\beta}{2}(\varepsilon_{\mathbf{k}'m'}-\mu)]}{\cosh[\frac{\beta}{2}(\varepsilon_{\mathbf{k}m}-\mu)]}, \quad (\text{A8})$$

$$S_{\mathbf{q}s,\mathbf{q}'s'}^{\text{ph}} = S_{\mathbf{q}s,\mathbf{q}'s'}^{\text{ph}} \frac{\sinh[\frac{\beta}{2}\hbar\omega_{\mathbf{q}'s'}]}{\sinh[\frac{\beta}{2}\hbar\omega_{\mathbf{q}s}]}. \quad (\text{A9})$$

As can be verified from the expression above, this transformation produces symmetric self quadrants, so that  $S_{\mathbf{k}m,\mathbf{k}'m'}^{\text{el}} = S_{\mathbf{k}'m',\mathbf{k}m}^{\text{el}}, S_{\mathbf{q}s,\mathbf{q}'s'}^{\text{ph}} = S_{\mathbf{q}'s',\mathbf{q}s}^{\text{ph}}$ , while the symmetrised drag quadrants  $\mathcal{D}_{\mathbf{k}m,\mathbf{q}'s'}^{\text{el-ph}}, \mathcal{D}_{\mathbf{q}s,\mathbf{k}'m'}^{\text{ph-el}}$  need to satisfy  $\mathcal{D}_{\mathbf{k}m,\mathbf{q}s}^{\text{el-ph}} = \mathcal{D}_{\mathbf{q}s,\mathbf{k}m}^{\text{ph-el}}$ . Comparing with Eqs. (A4) and (A6), we find that this can be obtained through the following transformation:

$$D_{\mathbf{k}m,\mathbf{q}'s'}^{\text{el-ph}} = \mathcal{D}_{\mathbf{k}m,\mathbf{q}'s'}^{\text{el-ph}} \sqrt{\frac{\mathcal{N}_{\mathbf{k}}}{\mathfrak{D}\mathcal{N}_{\mathbf{q}}}} \frac{\sinh[\frac{\beta}{2}\hbar\omega_{\mathbf{q}'s'}]}{\cosh[\frac{\beta}{2}(\varepsilon_{\mathbf{k}m}-\mu)]}, \quad (\text{A10})$$

$$D_{\mathbf{q}s, \mathbf{k}'m'}^{\text{ph-el}} = \mathcal{D}_{\mathbf{q}s, \mathbf{k}'m'}^{\text{ph-el}} \sqrt{\frac{\mathfrak{D}\mathcal{N}_{\mathbf{q}}}{\mathcal{N}_{\mathbf{k}}}} \frac{\cosh[\frac{\beta}{2}(\varepsilon_{\mathbf{k}'m'} - \mu)]}{\sinh[\frac{\beta}{2}\hbar\omega_{\mathbf{q}s}]}.$$
 (A11)

The four relations above motivate the definition of the similarity transformation  $\mathfrak{g}_{\mathbf{q}s}^{km}$  discussed in Eq. (5) of the main text:

$$\mathfrak{g}_{\mathbf{q}s}^{km} = \begin{pmatrix} \sqrt{\frac{\mathfrak{D}}{\mathcal{V}\mathcal{N}_{\mathbf{k}}}} \frac{1}{\sqrt{\bar{F}_{\mathbf{k}m}[1-\bar{F}_{\mathbf{k}m}]}} \\ \sqrt{\frac{1}{\mathcal{V}\mathcal{N}_{\mathbf{q}}}} \frac{1}{\sqrt{\bar{N}_{\mathbf{q}s}[\bar{N}_{\mathbf{q}s}+1]}} \end{pmatrix} = 2 \begin{pmatrix} \sqrt{\frac{\mathfrak{D}}{\mathcal{V}\mathcal{N}_{\mathbf{k}}}} \cosh[\frac{\beta}{2}(\varepsilon_{\mathbf{k}m} - \mu)] \\ \sqrt{\frac{1}{\mathcal{V}\mathcal{N}_{\mathbf{q}}}} \sinh[\frac{\beta}{2}\hbar\omega_{\mathbf{q}s}] \end{pmatrix}.$$
 (A12)

Note that we included a factor of  $\mathcal{V}$  in the definition of  $\mathfrak{g}_{\mathbf{q}s}^{km}$ , which has no effect on  $\Omega_{\mathbf{q}s, \mathbf{q}'s'}$ , but it will later simplify relations involving symmetrized populations  $|z_{\mathbf{k}m}\rangle$ . Thus, the final form of the symmetrized electron-phonon scattering rates is:

$$\begin{aligned} \mathcal{S}_{\mathbf{k}m, \mathbf{k}'m'}^{\text{el}} &= \frac{1}{\mathcal{V}\mathcal{N}_{\mathbf{k}}} \sum_{\mathbf{k}''m'', \mathbf{q}s} \frac{2\pi}{\hbar} |g_{m, m'', s}(\mathbf{k}, \mathbf{k}'', \mathbf{q})|^2 \delta_{\mathbf{k}'' - \mathbf{k} - \mathbf{q}, \mathbf{G}} \left[ \delta(\varepsilon_{\mathbf{k}''m''} - \varepsilon_{\mathbf{k}m} - \hbar\omega_{\mathbf{q}s}) + \delta(\varepsilon_{\mathbf{k}''m''} - \varepsilon_{\mathbf{k}m} + \hbar\omega_{\mathbf{q}s}) \right] \times \\ &\times \frac{1}{2 \sinh[\frac{\beta}{2}\hbar\omega_{\mathbf{q}s}]} \left[ \delta_{\mathbf{k}'m', \mathbf{k}m} \frac{\cosh[\frac{\beta}{2}(\varepsilon_{\mathbf{k}m} - \mu)]}{\cosh[\frac{\beta}{2}(\varepsilon_{\mathbf{k}'m'} - \mu)]} - \delta_{\mathbf{k}'m', \mathbf{k}'m'} \right], \end{aligned}$$
 (A13)

$$\begin{aligned} \mathcal{D}_{\mathbf{k}m, \mathbf{q}s}^{\text{el-ph}} &= \frac{1}{\mathcal{V}} \sqrt{\frac{\mathfrak{D}}{\mathcal{N}_{\mathbf{k}}\mathcal{N}_{\mathbf{q}}}} \sum_{\mathbf{k}'m'} \frac{2\pi}{\hbar} \left[ |g_{m, m', s}(\mathbf{k}, \mathbf{k}', \mathbf{q})|^2 \delta_{\mathbf{k}' - \mathbf{k} - \mathbf{q}, \mathbf{G}} \delta(\varepsilon_{\mathbf{k}'m'} - \varepsilon_{\mathbf{k}m} - \hbar\omega_{\mathbf{q}s}) \right. \\ &\left. - |g_{m', m, s}(\mathbf{k}', \mathbf{k}, \mathbf{q})|^2 \delta_{\mathbf{k}' - \mathbf{k} + \mathbf{q}, \mathbf{G}} \delta(\varepsilon_{\mathbf{k}'m'} - \varepsilon_{\mathbf{k}m} + \hbar\omega_{\mathbf{q}s}) \right] \frac{1}{2 \cosh[\frac{\beta}{2}(\varepsilon_{\mathbf{k}'m'} - \mu)]}, \end{aligned}$$
 (A14)

and  $\mathcal{S}_{\mathbf{q}s, \mathbf{q}'s'}^{\text{ph}} = \mathcal{S}_{\mathbf{q}s, \mathbf{q}'s'}^{\text{ph}}$  since this quadrant is diagonal.

### 3. Other scattering mechanisms

The phonon-phonon scattering matrix elements take into account the leading-order anharmonic three-phonon scattering events, i.e., coalescence ( $\dot{\mathbf{q}}\dot{s} + \ddot{\mathbf{q}}\ddot{s} \rightarrow \mathbf{q}s$ ) and decay ( $\mathbf{q}s \rightarrow \dot{\mathbf{q}}\dot{s} + \ddot{\mathbf{q}}\ddot{s}$ ). The resulting matrix element are [37]:

$$\begin{aligned} \mathcal{S}_{\mathbf{q}s, \dot{\mathbf{q}}\dot{s}}^{\text{ph-ph}} \bar{N}_{\dot{\mathbf{q}}\dot{s}} (\bar{N}_{\dot{\mathbf{q}}\dot{s}} + 1) \\ = \delta_{\mathbf{q}s, \dot{\mathbf{q}}\dot{s}} \mathcal{N}_{\mathbf{q}} \Gamma_{\mathbf{q}s}^{\text{ph-ph}} - \sum_{\ddot{\mathbf{q}}\ddot{s}} \left( P_{\mathbf{q}s, \dot{\mathbf{q}}\dot{s}}^{\dot{\mathbf{q}}\dot{s}} - P_{\mathbf{q}s, \dot{\mathbf{q}}\dot{s}}^{\ddot{\mathbf{q}}\ddot{s}} + P_{\dot{\mathbf{q}}\dot{s}, \dot{\mathbf{q}}\dot{s}}^{\mathbf{q}s} \right), \end{aligned}$$
 (A15)

$$\Gamma_{\mathbf{q}s}^{\text{ph-ph}} = \frac{1}{\mathcal{N}_{\mathbf{q}}} \sum_{\dot{\mathbf{q}}\dot{s}, \ddot{\mathbf{q}}\ddot{s}} \left( P_{\dot{\mathbf{q}}\dot{s}, \dot{\mathbf{q}}\dot{s}}^{\mathbf{q}s} + \frac{1}{2} P_{\dot{\mathbf{q}}\dot{s}, \dot{\mathbf{q}}\dot{s}}^{\mathbf{q}s} \right),$$
 (A16)

where  $\Gamma_{\mathbf{q}s}^{\text{ph-ph}}$  is the linewidth due to phonon-phonon scattering, and the scattering rates for coalescence and decay processes are respectively given by:

$$\begin{aligned} P_{\mathbf{q}s, \dot{\mathbf{q}}\dot{s}}^{\ddot{\mathbf{q}}\ddot{s}} &= \frac{2\pi}{\hbar} |V^{(3)}(\mathbf{q}s, \dot{\mathbf{q}}\dot{s}, -\ddot{\mathbf{q}}\ddot{s})|^2 \delta_{\mathbf{q} + \dot{\mathbf{q}} - \ddot{\mathbf{q}}, \mathbf{G}} \\ &\delta(\hbar\omega_{\mathbf{q}s} + \hbar\omega_{\dot{\mathbf{q}}\dot{s}} - \hbar\omega_{\ddot{\mathbf{q}}\ddot{s}}) \bar{N}_{\mathbf{q}s} \bar{N}_{\dot{\mathbf{q}}\dot{s}} (\bar{N}_{\ddot{\mathbf{q}}\ddot{s}} + 1), \end{aligned}$$
 (A17)

$$\begin{aligned} P_{\mathbf{q}s, \dot{\mathbf{q}}\dot{s}}^{\mathbf{q}s} &= \frac{2\pi}{\hbar} |V^{(3)}(\mathbf{q}s, -\dot{\mathbf{q}}\dot{s}, -\ddot{\mathbf{q}}\ddot{s})|^2 \delta_{\mathbf{q} - \dot{\mathbf{q}} - \ddot{\mathbf{q}}, \mathbf{G}} \\ &\delta(\hbar\omega_{\mathbf{q}s} - \hbar\omega_{\dot{\mathbf{q}}\dot{s}} - \hbar\omega_{\ddot{\mathbf{q}}\ddot{s}}) \bar{N}_{\mathbf{q}s} (\bar{N}_{\dot{\mathbf{q}}\dot{s}} + 1) (\bar{N}_{\ddot{\mathbf{q}}\ddot{s}} + 1). \end{aligned}$$
 (A18)

The phonon-phonon matrix element  $V^{(3)}$  is the Fourier transform of the third derivative of the total crystal

---

energy per unit cell  $\varepsilon^{\text{cell}}$  with respect to the atomic displacements[37].

Finally, the matrix elements accounting for scattering between phonons and mass-impurities are [37]:

$$\begin{aligned} \mathcal{S}_{\mathbf{q}s, \dot{\mathbf{q}}\dot{s}}^{\text{ph-isot}} &= \frac{\pi}{2} \omega_{\mathbf{q}s} \omega_{\dot{\mathbf{q}}\dot{s}} \left[ \bar{N}_{\mathbf{q}s} \bar{N}_{\dot{\mathbf{q}}\dot{s}} + \frac{1}{2} (\bar{N}_{\mathbf{q}s} + \bar{N}_{\dot{\mathbf{q}}\dot{s}}) \right] \\ &\times \sum_m g_m^{\text{isot}} \left| \sum_{\alpha} z_{\dot{\mathbf{q}}\dot{s}}^{m\alpha*} \cdot z_{\mathbf{q}s}^{m\alpha} \right|^2 \delta(\omega_{\mathbf{q}s} - \omega_{\dot{\mathbf{q}}\dot{s}}). \end{aligned}$$
 (A19)

## Appendix B: Derivation of the transport coefficients

### 1. Charge and heat currents from odd relaxons

We will show how the transport coefficients can be derived on the example of the charge current and electrical conductivity; all other transport coefficients are derived in an analogous fashion, and their form is stated for completeness. Throughout this derivation, we will rely on the fact that the epBTE can be split into an even and an odd part, assuming inversion symmetry is obeyed (see main text and [54, 93]).

We start from Eq. (6), considering only the part with

odd parity, and inserting Eq. (13):

$$\begin{aligned} \mathbf{v}_{q^s}^{k_m} \cdot \nabla \left[ T \sqrt{\frac{C_{\text{tot}}}{k_B \bar{T}^2}} |\theta_{q^s}^0\rangle - V_{\text{eff}} \sqrt{\frac{\mathfrak{U}}{k_B \bar{T}}} |\theta_{q^s}^e\rangle + |z_{q^s}^{\delta, E}\rangle \right] \\ = - \sum_{\substack{k'm' \\ q's'}} \Omega_{k_m, k'm'} \left( |z_{q^s}^e\rangle + |z_{q^s}^p\rangle + |z_{q^s}^{\delta, O}\rangle \right). \end{aligned} \quad (\text{B1})$$

To derive the transport coefficients, we need describe the out-of-equilibrium state of the system  $|\theta_{q^s}^\xi\rangle$  as a linear combination of relaxons, i.e.

$$|z_{q^s}^{\delta, O}\rangle = \sum_{\xi \neq \text{LE}} c_\xi |\theta_{q^s}^\xi\rangle, \quad (\text{B2})$$

where  $\xi$  runs only over non-special odd relaxons, determining the coefficients  $c_\xi$  by projecting Eq. (B1) onto the relaxon  $|\theta_{q^s}^\xi\rangle$ . We focus on determining the linear-response transport coefficients, thus in this projection we neglect contributions proportional to second (or higher-order) gradients in the local-equilibrium fields. Since relaxons are exactly the spectrum of  $\Omega_{k_m, k'm'}$ , on the right-hand side this projection isolates only the relaxon  $|\theta_{q^s}^\xi\rangle$ . Repeating this for every odd non-special relaxon  $|\theta_{q^s}^\xi\rangle$ , we find that the odd diffusive response is given by:

$$\begin{aligned} |z_{q^s}^{\delta, O}\rangle = - \sqrt{\frac{C_{\text{tot}}}{k_B \bar{T}^2}} \sum_{\xi \neq \text{LE}} \tau^\xi |\theta_{q^s}^\xi\rangle \langle \theta_{q^s}^\xi | v_{q^s}^i | \theta_{q^s}^0 \rangle \frac{\partial T}{\partial r^i} \\ + \sqrt{\frac{\mathfrak{U}}{k_B \bar{T}}} \sum_{\xi \neq \text{LE}} \tau^\xi |\theta_{q^s}^\xi\rangle \langle \theta_{q^s}^\xi | v_{q^s}^i | \theta_{q^s}^e \rangle \frac{\partial V_{\text{eff}}}{\partial r^i} \end{aligned} \quad (\text{B3})$$

#### a. Charge transport coefficients

Having solved for this part of the population perturbation, we can find the expression for the electrical current in terms of conjugate variables, starting from its microscopical definition (16):

$$\begin{aligned} J^i = - \frac{\mathfrak{D}e}{\mathcal{V} \mathcal{N}_{\mathbf{k}}} \sum_{k_m} v_{k_m}^i f_{k_m} \\ = - \sqrt{k_B \bar{T} \mathfrak{U}} \langle \theta_{q^s}^e | v_{k_m}^i | z_{q^s}^{k_m} \rangle \\ = - \sqrt{k_B \bar{T} \mathfrak{U}} \langle \theta_{q^s}^e | v_{k_m}^i \left( |z_{q^s}^e\rangle + |z_{q^s}^{\delta, O}\rangle \right), \end{aligned} \quad (\text{B4})$$

where we have introduced shorthands  $|z_{q^s}^e\rangle$ ,  $|z_{q^s}^p\rangle$  for the electron and phonon momentum terms in Eq. (13). In going to the second line, we exploited the fact that the charge eigenvector only has entries in the electron subspace, so we have effectively projected the deviation into the electron subspace. Then we note that only

the odd part of  $|z_{q^s}^{k_m}\rangle$  contributes to  $\mathbf{J}(\mathbf{r})$ ; additionally, the phonon momentum contribution vanishes because phonons carry no charge, implying  $\langle \theta_{q^s}^e | \mathbf{v}_{k_m} | \phi^p \rangle = 0$ . Finally, expanding  $|z_{q^s}^e\rangle$  as in Eq. (13) and  $|z_{q^s}^{\delta, O}\rangle$  as in Eqs. (13) and (B3), we find:

$$\begin{aligned} J^i = - \sqrt{\mathfrak{U} A_{\text{el}}^j} \langle \theta_{q^s}^e | v_{k_m}^i | \phi_{q^s}^{j, e} \rangle u_c^j(\mathbf{r}) \\ + \sqrt{\frac{\mathfrak{U} C_{\text{tot}}}{\bar{T}}} \sum_{\xi, j} \langle \theta_{q^s}^e | v_{k_m}^i | \theta_{q^s}^\xi \rangle \langle \theta_{q^s}^\xi | v_{k_m}^j | \theta_{q^s}^0 \rangle \tau^\xi \frac{\partial T}{\partial r^j} \\ - \mathfrak{U} \sum_{\xi, j} \langle \theta_{q^s}^e | v_{k_m}^i | \theta_{q^s}^\xi \rangle \langle \theta_{q^s}^\xi | v_{k_m}^j | \theta_{q^s}^e \rangle \tau^\xi \frac{\partial V_{\text{eff}}}{\partial r^j}. \end{aligned} \quad (\text{B5})$$

Comparing the form above to the last line of Eq. (16), we find the expressions for transport coefficients related to charge transport:

$$\psi^{ij} = \sqrt{\mathfrak{U} A_{\text{el}}^j} \langle \theta_{q^s}^e | v_{k_m}^i | \phi_{q^s}^{j, e} \rangle, \quad (\text{B6})$$

$$\tilde{\sigma}^{ij} = \mathfrak{U} \sum_{\xi \neq \text{el}} \langle \theta_{q^s}^e | v_{k_m}^i | \theta_{q^s}^\xi \rangle \langle \theta_{q^s}^\xi | v_{k_m}^j | \theta_{q^s}^e \rangle \tau^\xi, \quad (\text{B7})$$

$$[\tilde{\sigma}, \tilde{S}]^{ij} = - \sqrt{\frac{C_{\text{tot}} \mathfrak{U}}{\bar{T}}} \sum_{\xi \neq \text{el}} \langle \theta_{q^s}^e | v_{k_m}^i | \theta_{q^s}^\xi \rangle \langle \theta_{q^s}^\xi | v_{k_m}^j | \theta_{q^s}^0 \rangle \tau^\xi. \quad (\text{B8})$$

As noted in the main text, we exclude the momentum eigenvectors from the electrical conductivity  $\tilde{\sigma}$  and the Seebeck coefficient  $\tilde{S}$ . This is because the contributions to these two tensors are proportional to field gradients by definition, whereas the contribution from  $|z_{q^s}^e\rangle$  is not necessarily along the gradient of either field. Noting again that the charge eigenvector only has entries in the electron subspace, we see that  $\tilde{\sigma}$  depends only on the projection of the electron-phonon relaxons in the electronic subspace.

#### b. Heat transport coefficients

The heat current is determined in a way analogous to the charge current, since both depend only on the odd part of the deviation from equilibrium. Starting from the definition of the heat current (15):

$$\begin{aligned} Q^i = \frac{\mathfrak{D}}{\mathcal{V} \mathcal{N}_{\mathbf{k}}} \sum_{k_m} (\varepsilon_{k_m} - \mu) v_{k_m}^i f_{k_m} + \frac{1}{\mathcal{V} \mathcal{N}_{\mathbf{q}}} \sum_{q^s} \hbar \omega_{q^s} v_{q^s}^i n_{q^s} \\ = \sqrt{k_B \bar{T}^2 C_{\text{tot}}} \langle \theta_{q^s}^0 | v_{k_m}^i | z_{q^s}^{k_m} \rangle \\ = \sqrt{k_B \bar{T}^2 C_{\text{tot}}} \langle \theta_{q^s}^0 | v_{k_m}^i \left( |z_{q^s}^e\rangle + |z_{q^s}^p\rangle + |z_{q^s}^{\delta, O}\rangle \right). \end{aligned} \quad (\text{B9})$$

As before, we can find the heat current by plugging Eqs. (13) and (B3) into the above equation. We find the

form given in the last line of Eq. (15), with the transport coefficients given by the following expressions:

$$\chi_e^{ij} = \sqrt{\frac{C_{\text{tot}} A_{\text{el}}^j}{\bar{T}}} \langle \theta_{\mathbf{k}m}^0 | v_{\mathbf{q}s}^i | \phi_{\mathbf{k}m}^{j,e} \rangle, \quad (\text{B10})$$

$$\chi_p^{ij} = \sqrt{\frac{C_{\text{tot}} A_{\text{ph}}^j}{\bar{T}}} \langle \theta_{\mathbf{k}m}^0 | v_{\mathbf{q}s}^i | \phi_{\mathbf{k}m}^{j,p} \rangle, \quad (\text{B11})$$

$$\tilde{\kappa}^{ij} = C_{\text{tot}} \sum_{\xi \neq \text{el,ph}} \langle \theta_{\mathbf{k}m}^0 | v_{\mathbf{q}s}^i | \theta_{\mathbf{k}m}^\xi \rangle \langle \theta_{\mathbf{k}'m'}^\xi | v_{\mathbf{q}'s'}^j | \theta_{\mathbf{k}'m'}^0 \rangle \tau^\xi, \quad (\text{B12})$$

$$\tilde{\alpha}^{ij} = -\sqrt{C_{\text{tot}} \mathcal{U} \bar{T}} \sum_{\xi \neq \text{el,ph}} \langle \theta_{\mathbf{k}m}^e | v_{\mathbf{q}s}^i | \theta_{\mathbf{k}m}^\xi \rangle \langle \theta_{\mathbf{k}'m'}^\xi | v_{\mathbf{q}'s'}^j | \theta_{\mathbf{k}'m'}^0 \rangle \tau^\xi. \quad (\text{B13})$$

As with  $\tilde{\sigma}$ ,  $\tilde{S}$ , here we have explicitly separated the momentum contributions from the sum over relaxons, due to the difference in their response, as noted above. We note that the Peltier coefficient and the Seebeck coefficient, Eqs. (B8) and (B13), satisfy the Kelvin-Onsager relation by definition:  $\tilde{\alpha}^{ij} = \tilde{S}^{ik} \tilde{\sigma}^{kj} \bar{T}$ ; this an advantage compared to other methods that do not respect this relation by construction and have to employ numerical correction scheme to restore it [49].

## 2. Momentum fluxes from even relaxons

As anticipated in the main text, the response to drift-velocity perturbations is determined by the even part of the epBTE. To becomes apparent when Eq. (13) is inserted into the epBTE (Eq. (6)):

$$\begin{aligned} v_{\mathbf{k}m}^j \left( \sqrt{\frac{A_{\text{el}}^i}{k_B \bar{T}}} | \phi_{\mathbf{k}m}^{i,e} \rangle \frac{\partial u_e^i}{\partial r^j} + \sqrt{\frac{A_{\text{ph}}^i}{k_B \bar{T}}} | \phi_{\mathbf{q}s}^{i,p} \rangle \frac{\partial u_p^i}{\partial r^j} \right) = \\ = - \sum_{\substack{\mathbf{k}'m' \\ \mathbf{q}'s'}} \Omega_{\mathbf{k}m, \mathbf{k}'m'} \sum_{\mathbf{q}'s'} | z_{\mathbf{k}m}^{\delta,E} \rangle, \end{aligned} \quad (\text{B14})$$

since the left-hand side has now even parity, implying that also the right-hand side must have the same parity due to the wavevectors-inversion symmetry of the full collision matrix. For this reason, analogously to Eq. (B1), we have dropped  $| z_{\mathbf{k}m}^{\delta,O} \rangle$  on the left-hand side.

As before, we can expand  $| z_{\mathbf{k}m}^{\delta,E} \rangle$  in the relaxon basis,

$$| z_{\mathbf{k}m}^{\delta,E} \rangle = \sum_{\xi \neq \text{LE}} d^\xi | \theta_{\mathbf{k}m}^\xi \rangle, \quad (\text{B15})$$

where now  $\xi$  runs only over non-special even relaxons. We insert Eq. (B15) into Eq. (B14), and take the scalar product on both sides with a generic relaxon, obtaining the coefficients  $d^\xi$  that determine the even diffusive re-

sponse:

$$\begin{aligned} | z_{\mathbf{k}m}^{\delta,E} \rangle = & -\sqrt{\frac{A_{\text{el}}^i}{k_B \bar{T}}} \sum_{\xi \neq \text{LE}} \tau^\xi | \theta_{\mathbf{k}m}^\xi \rangle \langle \theta_{\mathbf{k}m}^\xi | v_{\mathbf{q}s}^j | \phi_{\mathbf{k}m}^{i,e} \rangle \frac{\partial u_e^i}{\partial r^j} \\ & -\sqrt{\frac{A_{\text{ph}}^i}{k_B \bar{T}}} \sum_{\xi \neq \text{LE}} \tau^\xi | \theta_{\mathbf{k}m}^\xi \rangle \langle \theta_{\mathbf{k}m}^\xi | v_{\mathbf{q}s}^j | \phi_{\mathbf{k}m}^{i,p} \rangle \frac{\partial u_p^i}{\partial r^j}. \end{aligned} \quad (\text{B16})$$

We now consider the crystal-momentum fluxes for electrons and phonons, which can be written in terms of the momentum special relaxons:

$$\Pi_e^{ij} = \frac{\mathfrak{D}}{\mathcal{V} \mathcal{N}_{\mathbf{k}}} \sum_{\mathbf{k}m} \hbar k^i v_{\mathbf{k}m}^j \mathbf{f}_{\mathbf{k}m} = \sqrt{k_B \bar{T} A_{\text{el}}^i} \langle \phi_{\mathbf{k}m}^{i,e} | v_{\mathbf{q}s}^j | z_{\mathbf{k}m}^{\delta,E} \rangle, \quad (\text{B17})$$

$$\Pi_p^{ij} = \frac{1}{\mathcal{V} \mathcal{N}_{\mathbf{q}}} \sum_{\mathbf{q}s} \hbar q^i v_{\mathbf{q}s}^j \mathbf{n}_{\mathbf{q}s} = \sqrt{k_B \bar{T} A_{\text{ph}}^i} \langle \phi_{\mathbf{q}s}^{i,p} | v_{\mathbf{q}s}^j | z_{\mathbf{q}s}^{\delta,E} \rangle. \quad (\text{B18})$$

We can proceed further by inserting Eq. (13) into the above equations, noting that odd relaxons vanish by symmetry, giving us three distinct flux components of the electron momentum flux:

$$\Pi_e^{ij} = \Pi_e^{ij,T} + \Pi_e^{ij,V_{\text{eff}}} + \Pi_e^{ij,\delta E}, \quad (\text{B19})$$

where we have defined, using Eq. (13):

$$\Pi_e^{ij,T} = \sqrt{\frac{C_{\text{tot}} A_{\text{el}}^i}{\bar{T}}} \langle \phi_{\mathbf{k}m}^{i,e} | v_{\mathbf{q}s}^j | \theta_{\mathbf{k}m}^0 \rangle T(\mathbf{r}) \quad (\text{B20})$$

$$\Pi_e^{ij,V_{\text{eff}}} = -\sqrt{\mathcal{U} A_{\text{el}}^i} \langle \phi_{\mathbf{k}m}^{i,e} | v_{\mathbf{q}s}^j | \theta_{\mathbf{k}m}^e \rangle V_{\text{eff}}(\mathbf{r}) \quad (\text{B21})$$

$$\Pi_e^{ij,\delta E} = \sqrt{k_B \bar{T} A_{\text{el}}^i} \langle \phi_{\mathbf{k}m}^{i,e} | v_{\mathbf{q}s}^j | z_{\mathbf{k}m}^{\delta,E} \rangle. \quad (\text{B22})$$

Note that we have dropped the  $\bar{T}$  and  $\bar{\mu}$  terms from the momentum fluxes; as with the flux of the equilibrium population, they are space-independent so they do not contribute to any transport phenomena [117]. Equation (B19) makes explicit the separation of different components of the flux:  $\Pi_e^{ij,T}$  and  $\Pi_e^{ij,\mu}$  are fluxes related to conjugate variables related to local equilibrium, i.e. the special eigenvectors, while  $\Pi_e^{ij,\delta E}$  represents the momentum flux carried by the out-of-equilibrium component of the perturbation. Using Eq. (B16), we can further express  $\Pi_e^{ij,\delta E}$  as:

$$\begin{aligned} \Pi_e^{ij,\delta E} = & - \sum_{\xi \neq \text{LE}} \sqrt{A_{\text{el}}^i A_{\text{el}}^k} \langle \phi_{\mathbf{k}m}^{i,e} | v_{\mathbf{q}s}^j | \theta_{\mathbf{k}m}^\xi \rangle y_{\xi,e}^{kl} \frac{\partial u_e^k}{\partial r^l} \\ & - \sum_{\xi \neq \text{LE}} \sqrt{A_{\text{el}}^i A_{\text{ph}}^k} \langle \phi_{\mathbf{k}m}^{i,e} | v_{\mathbf{q}s}^j | \theta_{\mathbf{k}m}^\xi \rangle y_{\xi,p}^{kl} \frac{\partial u_p^k}{\partial r^l}; \end{aligned} \quad (\text{B23})$$

which in turn determines the expression for the self and drag viscosities of the electron fluid:

$$\Pi_e^{ij,\delta E} = -\zeta_{\text{see}}^{ijkl} \frac{\partial u_e^k}{\partial r^l} - \zeta_{\text{ep}}^{ijkl} \frac{\partial u_p^k}{\partial r^l}, \quad (\text{B24})$$

with

$$\zeta_{\text{see}}^{ijkl} = \sqrt{A_{\text{el}}^i A_{\text{el}}^k} \sum_{\xi \neq \text{LE}} \langle \phi_{\mathbf{k}m}^{i,e} | v_{\mathbf{k}m}^j | \theta_{\mathbf{k}m}^\xi \rangle \langle \theta_{\mathbf{k}'m'}^\xi | v_{\mathbf{k}'m'}^l | \phi_{\mathbf{k}'m'}^{k,e} \rangle \tau^\xi \quad (\text{B25})$$

and

$$\zeta_{\text{sep}}^{ijkl} = \sqrt{A_{\text{el}}^i A_{\text{ph}}^k} \sum_{\xi \neq \text{LE}} \langle \phi_{\mathbf{k}m}^{i,e} | v_{\mathbf{k}m}^j | \theta_{\mathbf{k}m}^\xi \rangle \langle \theta_{\mathbf{k}'m'}^\xi | v_{\mathbf{k}'m'}^l | \phi_{\mathbf{k}'m'}^{k,p} \rangle \tau^\xi \quad (\text{B26})$$

Since we are considering two separate conjugate variables, we need to consider two different viscosities; the self viscosity is the one relating the electron drift velocity and the electron momentum flux, while the drag viscosity relates the phonon drift velocity to the electron momentum flux. The same naming convention is used later, in Eqs. (B31) and (B32), for the phonon self and drag viscosities.

For the phonon momentum flux, we can follow the same steps, giving:

$$\Pi_p^{ij} = \Pi_p^{ij,T} + \Pi_p^{ij,\delta E}, \quad (\text{B27})$$

$$\Pi_p^{ij,T} = \sqrt{\frac{C_{\text{tot}}^i A_{\text{ph}}^i}{\bar{T}}} \langle \phi_{\mathbf{k}m}^{i,p} | v_{\mathbf{k}m}^j | \theta_{\mathbf{k}m}^0 \rangle (T(\mathbf{r}) - \bar{T}), \quad (\text{B28})$$

$$\Pi_p^{ij,\delta E} = \sqrt{k_B \bar{T} A_{\text{ph}}^i} \langle \phi_{\mathbf{k}m}^{i,p} | v_{\mathbf{k}m}^j | z_{\mathbf{k}m}^{\delta,E} \rangle. \quad (\text{B29})$$

In this case, there is no flux associated with the effective potential because phonons are charge neutral,  $\langle \phi^p | \mathbf{v} | \theta^e \rangle = 0$ . The viscosities are found analogously to the electron case, by inserting Eq. (B16) into Eq. (B29):

$$\Pi_p^{ij,\delta E} = -\zeta_{\text{pe}}^{ijkl} \frac{\partial u_e^k}{\partial r^l} - \zeta_{\text{pp}}^{ijkl} \frac{\partial u_p^k}{\partial r^l}, \quad (\text{B30})$$

with

$$\zeta_{\text{pp}}^{ijkl} = \sqrt{A_{\text{ph}}^i A_{\text{ph}}^k} \sum_{\xi \neq \text{LE}} \langle \phi_{\mathbf{k}m}^{i,p} | v_{\mathbf{k}m}^j | \theta_{\mathbf{k}m}^\xi \rangle \langle \theta_{\mathbf{k}'m'}^\xi | v_{\mathbf{k}'m'}^l | \phi_{\mathbf{k}'m'}^{k,p} \rangle \tau^\xi, \quad (\text{B31})$$

and

$$\zeta_{\text{pe}}^{ijkl} = \sqrt{A_{\text{ph}}^i A_{\text{el}}^k} \sum_{\xi \neq \text{LE}} \langle \phi_{\mathbf{k}m}^{i,p} | v_{\mathbf{k}m}^j | \theta_{\mathbf{k}m}^\xi \rangle \langle \theta_{\mathbf{k}'m'}^\xi | v_{\mathbf{k}'m'}^l | \phi_{\mathbf{k}'m'}^{k,e} \rangle \tau^\xi. \quad (\text{B32})$$

Equations (B25), (B26), (B31) and (B32) show that in electron-phonon bifluids, the electron and phonon fluids can have different viscosities. Looking at drag viscosities in particular, Eqs. (B26) and (B32), we can see that these vanish identically in the absence of drag; as mentioned above, no-drag relaxons will belong either only to the electron or only to the phonon subspace.

We can summarize the results for momentum fluxes in the following form:

$$\Pi_e^{ij} = \chi_e^{ij} T(\mathbf{r}) - \psi^{ij} V_{\text{eff}}(\mathbf{r}) - \zeta_{\text{ee}}^{ijkl} \frac{\partial u_e^k}{\partial r^l} - \zeta_{\text{ep}}^{ijkl} \frac{\partial u_p^k}{\partial r^l} \quad (\text{B33})$$

$$\Pi_p^{ij} = \chi_p^{ij} T(\mathbf{r}) - \zeta_{\text{pp}}^{ijkl} \frac{\partial u_p^k}{\partial r^l} - \zeta_{\text{pe}}^{ijkl} \frac{\partial u_e^k}{\partial r^l}, \quad (\text{B34})$$

where we defined three additional parameters relevant for transport:

$$\chi_e^{ij} = \sqrt{\frac{C_{\text{tot}}^i A_{\text{el}}^i}{\bar{T}}} \langle \phi_{\mathbf{k}m}^{i,e} | v_{\mathbf{k}m}^j | \theta_{\mathbf{k}m}^0 \rangle, \quad (\text{B35})$$

$$\chi_p^{ij} = \sqrt{\frac{C_{\text{tot}}^i A_{\text{ph}}^i}{\bar{T}}} \langle \phi_{\mathbf{k}m}^{i,p} | v_{\mathbf{k}m}^j | \theta_{\mathbf{k}m}^0 \rangle, \quad (\text{B36})$$

$$\psi^{ij} = \sqrt{\mathcal{U} A_{\text{el}}^i} \langle \phi_{\mathbf{k}m}^{i,e} | v_{\mathbf{k}m}^j | \theta_{\mathbf{k}m}^e \rangle. \quad (\text{B37})$$

These coefficients determine both the momentum fluxes carried by the gradients of conjugate variables and the heat and charge fluxes carried by the drift velocities.

In conclusion, taking into account both the odd and the even part of the epBTE, we have found the linearly independent transport coefficients that are necessary to describe the mesoscopic hydrodynamic behavior of electron-phonon bifluids. These are summarized in Table I.

### 3. Finite size effects on transport coefficients

Here, we discuss an approximate approach to account for finite-size (ballistic) corrections to the transport coefficients. The approach is discussed in Ref. [54] and is formally analogous to the Bosanquet-type approximation used to describe corrections to fluids' transport coefficients in the transition regime [103] (corresponding  $0.1 \lesssim$  Knudsen number  $\lesssim 10$ , i.e. to mean free path of the fluid molecule of the order of the characteristic length of the device). In the following we summarize the salient features of this approximate treatment of ballistic effects.

In devices featuring smallest characteristic size  $L_S$  (for the geometry in Fig. 2 this is the width of the narrow tunnel) much larger than the mean free path of electrons and phonons, the transport coefficients are given by the bulk expressions derived in the previous Appendix. Conversely, in the opposite limit when  $L_S$  is much smaller than the carrier mean free path, the transport coefficients are dominated by boundary scattering, often described using the expression proposed by Casimir [73]  $\Omega_{\mathbf{k}m, \mathbf{k}'m'}^{\text{boundary}} = |\mathbf{v}_{\mathbf{k}m}^{\mathbf{q}s} / L_S \delta_{\mathbf{k}m, \mathbf{k}'m'}^{\mathbf{q}s, \mathbf{q}'s'}$ . When the two length-scales become comparable, one has to account for the interplay between these two scattering mechanisms.

In the ballistic limit, accounting only for  $\Omega^{\text{boundary}}$ , we find that the relaxon response operator (RRO), defined in Eq. (22), becomes diagonal and is given by:

$$\Delta_{\mathbf{k}m, \mathbf{k}'m'}^{\mathbf{q}s, \mathbf{q}'s'} = L_S \sum_{\mathbf{k}m, \mathbf{q}s} \frac{v_{\mathbf{k}m}^{\mathbf{q}s} v_{\mathbf{k}'m'}^{\mathbf{q}'s'}}{|\mathbf{v}_{\mathbf{k}m}^{\mathbf{q}s}|} \delta_{\mathbf{k}m, \mathbf{k}'m'}^{\mathbf{q}s, \mathbf{q}'s'}. \quad (\text{B38})$$

From here, we can find the ballistic limit of all transport coefficients by plugging in  $\Delta^{\text{ballistic}}$  into the expressions

given in Table I. For example, we find that the electrical conductivity is given by  $\sigma_{\text{ballistic}}^{ij} = R^{ij} L_S$ , where  $R^{ij}$  is the specific ballistic electrical conductivity:

$$R^{ij} = \frac{1}{\mathcal{N}_{\mathbf{k}} \mathcal{V}} \sum_{\mathbf{km}} \frac{e^2}{k_B \bar{T}} \bar{F}_{\mathbf{km}} (1 - \bar{F}_{\mathbf{km}}) \frac{v_{\mathbf{km}}^i v_{\mathbf{km}}^j}{|\mathbf{v}_{\mathbf{km}}|}. \quad (\text{B39})$$

Similarly, for the electron self viscosity we find  $\eta_{\text{ee,ballistic}}^{ijkl} = M_{\text{ee,ballistic}}^{ijkl} L_S$ , where  $M_{\text{ee,ballistic}}^{ijkl}$  is the specific ballistic electron self viscosity:

$$M_{\text{ee,ballistic}}^{ijkl} = \frac{\mathfrak{D}}{\mathcal{N}_{\mathbf{k}} \mathcal{V}} \sum_{\mathbf{km}} \frac{\hbar^2 k^i k^k}{k_B \bar{T}} \bar{F}_{\mathbf{km}} (1 - \bar{F}_{\mathbf{km}}) \frac{v_{\mathbf{km}}^i v_{\mathbf{km}}^j}{|\mathbf{v}_{\mathbf{km}}|}. \quad (\text{B40})$$

To simplify the discussion of the interpolation between the above limits, we focus on the case of tensors that are isotropic in the in-plane directions, which is sufficient for the scope of the present work. Starting from tensors of rank two, such as  $\sigma^{ij}$  and  $\kappa^{ij}$ , the general isotropic form is  $\sigma^{ij} = \sigma \delta^{ij}$ , i.e. the matrix is diagonal. We compute the effective conductivity using the common Matthiessen combination [54, 103]:

$$\frac{1}{\sigma_{\text{eff}}} = \frac{1}{\sigma} + \frac{1}{\sigma_{\text{ballistic}}}. \quad (\text{B41})$$

This expression smoothly interpolates between the two limits, giving an effective conductivity that is always lower than the bulk limit due to boundary scattering. It also tends to the bulk limit for large sample sizes, while for small sample sizes we recover the ballistic conductivity. The effective electrical conductivity also remains isotropic, as desired. We note that the expressions has been reported for the standard diffusive coefficient  $\sigma$ . To correct the coefficient  $\tilde{\sigma}$  (as well as  $\tilde{\kappa}$  and  $\tilde{S}$ ) appearing in the VTE, which is related to the standard  $\sigma$  via Eq. (42) (see Eq. (43) for the thermal conductivity, and Eq. (44) for the Seebeck), we assume that the relative weight of the momentum contribution in the ballistic case is the same as the relative weight of the momentum contribution in the bulk case. In formulas, we compute

$$\tilde{\sigma}_{\text{ballistic}} = \sigma_{\text{ballistic}} \frac{\tilde{\sigma}}{\sigma}, \quad (\text{B42})$$

and then we combine it with  $\tilde{\sigma}$  using the Mathiessen combination:

$$\frac{1}{\tilde{\sigma}_{\text{eff}}} = \frac{1}{\tilde{\sigma}} + \frac{1}{\tilde{\sigma}_{\text{ballistic}}}. \quad (\text{B43})$$

When the viscosities assume an isotropic form, there can in general be three different non-zero components:  $\eta^{iiii}$ ,  $\eta^{ijjj} = \eta^{jjji}$ , and  $\eta^{ijij}$ , which satisfy the following relation  $\eta^{iiii} = 2\eta^{ijjj} + \eta^{ijij}$ . Therefore, we interpolate the two independent components in the same way as above:

$$\frac{1}{\eta_{\text{eff}}^{\text{indices}}} = \frac{1}{\eta_{\text{bulk}}^{\text{indices}}} + \frac{1}{\eta_{\text{ballistic}}^{\text{indices}}}, \quad \text{indices} = \text{ijji, ijij}, \quad (\text{B44})$$

while for the  $iiii$  component we simply enforce the isotropy condition:  $\eta_{\text{eff}}^{iiii} = 2\eta_{\text{eff}}^{ijjj} + \eta_{\text{eff}}^{ijij}$ . The properties discussed for the rank two case hold also in the rank four case; notably, the effective viscosity remains isotropic. We also note that for drag viscosities the ballistic correction is zero, since  $\Delta^{\text{ballistic}}$  is diagonal while  $|\phi^{i,e}\rangle$  and  $|\phi^{j,p}\rangle$  lie in the electron and phonon subspace.

It is worth discussing a detail relevant for multi-carrier transport. The thermal conductivity is the only transport coefficient for which we have both an electron and a phonon ballistic component, found by splitting  $\Delta^{\text{ballistic}}$  into two sums over the electron and phonon subspaces, respectively:

$$\tilde{\kappa}_{\text{el,ballistic}}^{ij} = \frac{\mathfrak{D}}{\mathcal{N}_{\mathbf{k}} \mathcal{V}} \sum_{\mathbf{km}} \frac{(\varepsilon_{\mathbf{km}} - \bar{\mu})^2}{k_B \bar{T}^2} \bar{F}_{\mathbf{km}} (1 - \bar{F}_{\mathbf{km}}) \frac{v_{\mathbf{km}}^i v_{\mathbf{km}}^j}{|\mathbf{v}_{\mathbf{km}}|} L_S \frac{\tilde{\kappa}_{\text{el}}}{\kappa_{\text{el}}}, \quad (\text{B45})$$

$$\tilde{\kappa}_{\text{ph,ballistic}}^{ij} = \frac{1}{\mathcal{N}_{\mathbf{q}} \mathcal{V}} \sum_{\mathbf{qs}} \frac{\hbar \omega^2}{k_B \bar{T}^2} \bar{N}_{\mathbf{qs}} (1 + \bar{N}_{\mathbf{qs}}) \frac{v_{\mathbf{qs}}^i v_{\mathbf{qs}}^j}{|\mathbf{v}_{\mathbf{qs}}|} L_S \frac{\tilde{\kappa}_{\text{ph}}}{\kappa_{\text{ph}}}. \quad (\text{B46})$$

In graphite, the bulk thermal conductivity is dominated by phonons, while  $\kappa_{\text{el,ballistic}} \gg \kappa_{\text{ph,ballistic}}$ . To account that ballistic effects influence electrons and phonons independently, we correct the thermal conductivity for ballistic effects as:

$$\frac{1}{\tilde{\kappa}_{\text{eff}}} = \frac{1}{\tilde{\kappa}} + \frac{1}{\tilde{\kappa}_{\text{el,ballistic}}} + \frac{1}{\tilde{\kappa}_{\text{ph,ballistic}}}, \quad (\text{B47})$$

which ensures that ballistic effects have more weight in regularizing the phonon-dominated thermal conductivity of graphite. We conclude by noting that while the treatment above has been applied to the conductivity  $\tilde{\kappa}$  that appears within the VTE, it can be used also for the conductivity  $\kappa$  that appears in the DTE, Eq. (43). To determine ballistic corrections to the DTE conductivity, one has to replace  $\tilde{\kappa}_{\text{el}}$  with  $\kappa_{\text{el}}$  in Eq. (B45), and  $\tilde{\kappa}_{\text{ph}}$  with  $\kappa_{\text{ph}}$  in Eq. (B46), obtaining:

$$\kappa_{\text{el,ballistic}}^{ij} = \frac{\mathfrak{D}}{\mathcal{N}_{\mathbf{k}} \mathcal{V}} \sum_{\mathbf{km}} \frac{(\varepsilon_{\mathbf{km}} - \bar{\mu})^2}{k_B \bar{T}^2} \bar{F}_{\mathbf{km}} (1 - \bar{F}_{\mathbf{km}}) \frac{v_{\mathbf{km}}^i v_{\mathbf{km}}^j}{|\mathbf{v}_{\mathbf{km}}|} L_S, \quad (\text{B48})$$

$$\kappa_{\text{ph,ballistic}}^{ij} = \frac{1}{\mathcal{N}_{\mathbf{q}} \mathcal{V}} \sum_{\mathbf{qs}} \frac{\hbar \omega^2}{k_B \bar{T}^2} \bar{N}_{\mathbf{qs}} (1 + \bar{N}_{\mathbf{qs}}) \frac{v_{\mathbf{qs}}^i v_{\mathbf{qs}}^j}{|\mathbf{v}_{\mathbf{qs}}|} L_S. \quad (\text{B49})$$

### Appendix C: Deriving the Viscous Thermoelectric Equations

In the previous Appendix, we have derived the transport coefficients parametrizing the fluxes of conserved and quasi-conserved quantities. Here, we derive the set of mesoscopic partial differential equations describing the flow of (quasi) conserved quantities.

In the hydrodynamic regime, where most of the collisions conserve the crystal momentum, we decompose the full collision operator into the normal and Umklapp component, as in Section II C:  $\Omega_{\mathbf{k}m, \mathbf{q}^s}^{\mathbf{k}'m', \mathbf{q}'s'} = \Omega_{\mathbf{k}m, \mathbf{q}^s}^N{}^{\mathbf{k}'m', \mathbf{q}'s'} + \Omega_{\mathbf{k}m, \mathbf{q}^s}^U{}^{\mathbf{k}'m', \mathbf{q}'s'}$ . Then the electron-phonon epBTE, Eq. (6), becomes:

$$\mathbf{v}_{\mathbf{q}^s}^{\mathbf{k}m} \cdot \nabla_{\mathbf{r}} |z_{\mathbf{q}^s}^{\mathbf{k}m}\rangle = - \sum_{\substack{\mathbf{k}'m' \\ \mathbf{q}'s'}} \left( \Omega_{\mathbf{k}m, \mathbf{q}^s}^N{}^{\mathbf{k}'m', \mathbf{q}'s'} + \Omega_{\mathbf{k}m, \mathbf{q}^s}^U{}^{\mathbf{k}'m', \mathbf{q}'s'} \right) |z_{\mathbf{q}'s'}^{\mathbf{k}'m'}\rangle. \quad (\text{C1})$$

We expand  $|z_{\mathbf{q}^s}^{\mathbf{k}m}\rangle$  as in Eq. (13). Then, after noting that all the local-equilibrium terms are proportional to special eigenvectors that are all null eigenvectors of the normal collision matrix, we have that Eq. (C1) becomes:

$$\begin{aligned} \mathbf{v}_{\mathbf{q}^s}^{\mathbf{k}m} \cdot \nabla_{\mathbf{r}} |z_{\mathbf{q}^s}^{\mathbf{k}m}\rangle &= - \sum_{\substack{\mathbf{k}'m' \\ \mathbf{q}'s'}} \Omega_{\mathbf{k}m, \mathbf{q}^s}^N{}^{\mathbf{k}'m', \mathbf{q}'s'} |z_{\mathbf{q}'s'}^{\delta, \mathbf{k}'m'}\rangle \\ &\quad - \sum_{\substack{\mathbf{k}'m' \\ \mathbf{q}'s'}} \Omega_{\mathbf{k}m, \mathbf{q}^s}^U{}^{\mathbf{k}'m', \mathbf{q}'s'} \left( |z_{\mathbf{q}'s'}^{\mathbf{u}_e}\rangle + |z_{\mathbf{q}'s'}^{\mathbf{u}_p}\rangle + |z_{\mathbf{q}'s'}^{\delta, \mathbf{k}'m'}\rangle \right). \end{aligned} \quad (\text{C2})$$

To derive a set of mesoscopic viscous equations describing transport, we take the scalar product of Eq. (C2) with the  $2+2d$  special eigenvectors ( $d$  is the dimensionality of the system). As a result we obtain four coupled equations describing the evolution of local chemical potential (which is related to the electrical potential), local temperature, and local electron and phonon drift velocities (these last two are equations for vector fields, thus have  $d$  components).

### 1. Projection in the charge subspace

Taking the scalar product of Eq. (C2) with  $\langle \theta_{\mathbf{q}^s}^e |$ , and recalling Eq. (B4), we obtain:

$$\begin{aligned} \langle \theta_{\mathbf{q}^s}^e | \mathbf{v}_{\mathbf{q}^s}^{\mathbf{k}m} \cdot \nabla_{\mathbf{r}} |z_{\mathbf{q}^s}^{\mathbf{k}m}\rangle &= \nabla \cdot \langle \theta_{\mathbf{q}^s}^e | \mathbf{v}_{\mathbf{q}^s}^{\mathbf{k}m} |z_{\mathbf{q}^s}^{\mathbf{k}m}\rangle \\ &= (k_B \bar{T} \bar{\mathcal{U}})^{-1/2} \nabla \cdot \mathbf{J} \\ &= \langle \theta_{\mathbf{q}^s}^e | \Omega_{\mathbf{k}m, \mathbf{q}^s}^{\mathbf{k}'m', \mathbf{q}'s'} |z_{\mathbf{q}^s}^{\mathbf{k}m}\rangle \\ &= 0. \end{aligned} \quad (\text{C3})$$

In the last line, the scalar product vanishes because  $|\theta_{\mathbf{q}^s}^e\rangle$  is a zero eigenvector of  $\Omega$ . We can now scale all terms by  $\sqrt{k_B \bar{T} \bar{\mathcal{U}}}$  and insert the form for  $\mathbf{J}$  found in the Eq. (16), obtaining:

$$-\psi^{ij} \frac{\partial u_e^i}{\partial r^j} - \tilde{\sigma}^{ij} \frac{\partial^2 V_{\text{eff}}}{\partial r^i \partial r^j} - [\tilde{\sigma} \tilde{S}]^{ij} \frac{\partial^2 T}{\partial r^i \partial r^j} = 0. \quad (\text{C4})$$

The physical content of Eq. (C4) is that of a continuity equation for charge. We can rewrite the equation as  $\nabla \cdot \mathbf{J} = 0$ , where  $\mathbf{J}$  is defined in Eq. (16).

### 2. Projection in the energy subspace

Similarly, we can take the scalar product of Eq. (C2) with  $\sqrt{C_{\text{tot}} k_B \bar{T}^2} \langle \theta_{\mathbf{q}^s}^0 |$ , obtaining:

$$\begin{aligned} \sqrt{C_{\text{tot}} k_B \bar{T}^2} \langle \theta_{\mathbf{q}^s}^0 | \mathbf{v}_{\mathbf{q}^s}^{\mathbf{k}m} \cdot \nabla_{\mathbf{r}} |z_{\mathbf{q}^s}^{\mathbf{k}m}\rangle &= \nabla \cdot \left( \sqrt{C_{\text{tot}} k_B \bar{T}^2} \langle \theta_{\mathbf{q}^s}^0 | \mathbf{v}_{\mathbf{q}^s}^{\mathbf{k}m} |z_{\mathbf{q}^s}^{\mathbf{k}m}\rangle \right) \\ &= \nabla \cdot \mathbf{Q} \\ &= \sqrt{C_{\text{tot}} k_B \bar{T}^2} \langle \theta_{\mathbf{q}^s}^0 | \Omega_{\mathbf{k}m, \mathbf{q}^s}^{\mathbf{k}'m', \mathbf{q}'s'} |z_{\mathbf{q}^s}^{\mathbf{k}m}\rangle \\ &= 0. \end{aligned} \quad (\text{C5})$$

In going from the second to the third line we used Eq. (B9), and as for charge conservation, the right-hand side vanishes because the charge eigenvector is a zero eigenvector of  $\Omega$ . Now we can insert the form for  $\mathbf{Q}$  given in Eq. (15) to find:

$$\chi_e^{ij} \frac{\partial u_e^i}{\partial r^j} + \chi_p^{ij} \frac{\partial u_p^i}{\partial r^j} - \tilde{\alpha}^{ij} \frac{\partial^2 V_{\text{eff}}}{\partial r^i \partial r^j} - \tilde{\kappa}^{ij} \frac{\partial^2 T}{\partial r^i \partial r^j} = 0. \quad (\text{C6})$$

The physical meaning of Eq. (C6) is that of a continuity equation for energy. Using Eq. (15), it can be rewritten as  $\nabla \cdot \mathbf{Q} = 0$ .

### 3. Projection in the momentum subspace

#### a. Momentum in the electronic subspace

To describe the evolution of the electron momentum, we take the scalar product of Eq. (C2) with  $\langle \phi_{\mathbf{q}^s}^{i,e} |$  ( $i = 1, 2, 3$ ), finding:

$$\begin{aligned} \left\langle \phi_{\mathbf{q}^s}^{i,e} \left| v_{\mathbf{q}^s}^{\mathbf{k}m} \cdot \frac{\partial}{\partial r^j} \right| z_{\mathbf{q}^s}^{\mathbf{k}m} \right\rangle &= \frac{1}{\sqrt{k_B \bar{T} A_{\text{el}}^i}} \frac{\partial \Pi_e^{ij}}{\partial r^j} \\ &= - \langle \phi_{\mathbf{q}^s}^{i,e} | \Omega_{\mathbf{k}m, \mathbf{q}^s}^U{}^{\mathbf{k}'m', \mathbf{q}'s'} \left( |z_{\mathbf{q}'s'}^{\mathbf{u}_e}\rangle + |z_{\mathbf{q}'s'}^{\mathbf{u}_p}\rangle + |z_{\mathbf{q}'s'}^{\delta, \mathbf{k}'m'}\rangle \right) \\ &\approx - \langle \phi_{\mathbf{q}^s}^{i,e} | \Omega_{\mathbf{k}m, \mathbf{q}^s}^U{}^{\mathbf{k}'m', \mathbf{q}'s'} \left( |z_{\mathbf{q}'s'}^{\mathbf{u}_e}\rangle + |z_{\mathbf{q}'s'}^{\mathbf{u}_p}\rangle \right) \\ &= - \sqrt{\frac{A_{\text{el}}^j}{k_B \bar{T}}} \langle \phi_{\mathbf{q}^s}^{i,e} | \Omega_{\mathbf{k}m, \mathbf{q}^s}^{\mathbf{k}'m', \mathbf{q}'s'} | \phi_{\mathbf{q}'s'}^{j,e} \rangle u_e^j(\mathbf{r}) \\ &\quad - \sqrt{\frac{A_{\text{ph}}^j}{k_B \bar{T}}} \langle \phi_{\mathbf{q}^s}^{i,e} | \Omega_{\mathbf{k}m, \mathbf{q}^s}^{\mathbf{k}'m', \mathbf{q}'s'} | \phi_{\mathbf{q}'s'}^{j,p} \rangle u_p^j(\mathbf{r}). \end{aligned} \quad (\text{C7})$$

As before, we replace the left-hand side with the divergence of the appropriate flux, and scale both sides with  $\sqrt{k_B \bar{T} A_{\text{el}}^i}$ . Here that is the electron momentum flux, as defined in Eq. (B17). However, on the right-hand side

we are left with the  $\Omega^U$  term, since  $|\phi_{\mathbf{k}m}^{i,e}\rangle$  are not eigenvectors of the full collision matrix. However, assuming that  $\Omega^U$  is a small perturbation to  $\Omega^N$ , we keep only the leading order terms within the momentum subspace, as described in Section II C, defining the following dissipation tensors:

$$D_{ee}^{ij} = \sqrt{A_{\text{el}}^i A_{\text{el}}^j} \langle \phi_{\mathbf{q}s}^{i,e} | \Omega_{\mathbf{k}m, \mathbf{k}'m'}^{i,e} | \phi_{\mathbf{q}'s'}^{j,e} \rangle, \quad (\text{C8})$$

$$D_{\text{ep}}^{ij} = \sqrt{A_{\text{el}}^i A_{\text{ph}}^j} \langle \phi_{\mathbf{q}s}^{i,e} | \Omega_{\mathbf{k}m, \mathbf{k}'m'}^{i,e} | \phi_{\mathbf{q}'s'}^{j,p} \rangle. \quad (\text{C9})$$

Finally, we can expand the electron momentum flux as in Eq. (B33), obtaining:

$$\begin{aligned} \chi_e^{ij} \frac{\partial T}{\partial r^j} - \psi^{ij} \frac{\partial V_{\text{eff}}}{\partial r^j} - \eta_{ee}^{ijkl} \frac{\partial u_e^k}{\partial r^j \partial r^l} - \eta_{\text{ep}}^{ijkl} \frac{\partial u_p^k}{\partial r^j \partial r^l} \\ = -D_{ee}^{ij} u_e^j - D_{\text{ep}}^{ij} u_p^j. \end{aligned} \quad (\text{C10})$$

#### b. Momentum in the phononic subspace

Finally, we project Eq. (C2) onto the phonon momentum eigenvectors, we can follow the same steps as for electron momentum. Specifically, using Eq. (B18), we find:

$$\begin{aligned} & \left\langle \phi_{\mathbf{q}s}^{i,p} \left| u_{\mathbf{k}m}^j \cdot \frac{\partial}{\partial r^j} \right| z_{\mathbf{k}m} \right\rangle \\ &= \frac{1}{\sqrt{k_B \bar{T}} A_{\text{ph}}^i} \frac{\partial \Pi_p^{ij}}{\partial r^j} \\ &= - \left\langle \phi_{\mathbf{q}s}^{i,p} \left| \Omega_{\mathbf{k}m, \mathbf{k}'m'}^U \left( |z_{\mathbf{q}'s'}^{\mathbf{u}_e} \rangle + |z_{\mathbf{q}'s'}^{\mathbf{u}_p} \rangle + |z_{\mathbf{q}'s'}^{\delta, O} \rangle \right) \right. \right\rangle \\ &\approx - \left\langle \phi_{\mathbf{q}s}^{i,p} \left| \Omega_{\mathbf{k}m, \mathbf{k}'m'}^U \left( |z_{\mathbf{q}'s'}^{\mathbf{u}_e} \rangle + |z_{\mathbf{q}'s'}^{\mathbf{u}_p} \rangle \right) \right. \right\rangle \\ &= - \sqrt{\frac{A_{\text{ph}}^j}{k_B \bar{T}}} \langle \phi_{\mathbf{q}s}^{i,p} | \Omega_{\mathbf{k}m, \mathbf{k}'m'}^{i,p} | \phi_{\mathbf{q}'s'}^{j,p} \rangle u_p^j(\mathbf{r}) \\ &\quad - \sqrt{\frac{A_{\text{el}}^j}{k_B \bar{T}}} \langle \phi_{\mathbf{q}s}^{i,p} | \Omega_{\mathbf{k}m, \mathbf{k}'m'}^{i,p} | \phi_{\mathbf{q}'s'}^{j,e} \rangle u_e^j(\mathbf{r}). \end{aligned} \quad (\text{C11})$$

As for the electron momentum flux, we define phonon-phonon and phonon-electron momentum dissipation rate tensors:

$$D_{\text{pp}}^{ij} = \sqrt{A_{\text{ph}}^i A_{\text{ph}}^j} \langle \phi_{\mathbf{q}s}^{i,p} | \Omega_{\mathbf{k}m, \mathbf{k}'m'}^{i,p} | \phi_{\mathbf{q}'s'}^{j,p} \rangle, \quad (\text{C12})$$

$$D_{\text{pe}}^{ij} = \sqrt{A_{\text{ph}}^i A_{\text{el}}^j} \langle \phi_{\mathbf{q}s}^{i,p} | \Omega_{\mathbf{k}m, \mathbf{k}'m'}^{i,p} | \phi_{\mathbf{q}'s'}^{j,e} \rangle. \quad (\text{C13})$$

Using Eq. (B34), we express the phonon momentum equation in terms of conjugate variables, obtaining the continuity equation for momentum in the phonon subspace:

$$\chi_p^{ij} \frac{\partial T}{\partial r^j} - \eta_{\text{pp}}^{ijkl} \frac{\partial u_p^k}{\partial r^j \partial r^l} - \eta_{\text{pe}}^{ijkl} \frac{\partial u_e^k}{\partial r^j \partial r^l} = -D_{\text{pp}}^{ij} u_p^j - D_{\text{pe}}^{ij} u_e^j. \quad (\text{C14})$$

#### Appendix D: Computational details

To obtain the electronic and phononic band structures, as well as the electron-phonon and phonon-phonon couplings used in the construction of the scattering matrix, we used a  $32 \times 32 \times 8$  k-point grid and an  $8 \times 8 \times 2$  supercell, a pseudopotential [118] parameterized in the RKKJ [119] method for the local density approximation, and a 70 Ry plane-wave energy cutoff. To compute electron-phonon matrix elements, we utilized the open-source density-functional theory (DFT) JDFTx code [120]. For the generation of third-order phonon-phonon coupling matrix elements, we used the d3q density-functional perturbation theory (DFPT) module of [121] Quantum ESPRESSO [122], as in Refs. [54, 123].

To calculate the transport coefficients from the linear-response solution of the electron-phonon BTE, we computed the electron-phonon scattering-matrix using temperature-dependent discrete grid of  $\mathbf{k}$  and  $\mathbf{q}$  points, as at low temperatures a much finer mesh of electron states is required for convergence. For phonons, we used consistently a  $27 \times 27 \times 11$  q-point mesh, and for electrons, we chose commensurate k-point meshes which resulted in transport properties converged up to 5% of the total value, ranging from  $567 \times 567 \times 231$  at 30 K to  $297 \times 297 \times 121$  at 210 K. We note that to obtain an accurate relaxons solution, these meshes must be odd to respect the wavevector-inversion symmetry. To broaden the Dirac delta functions appearing in the scattering rate expressions, we applied a Gaussian smearing approximation, with a broadening of 5 meV for all scattering involving electrons (el-ph, ph-el, and drag calculations) and 2 meV for phonons (phonon-phonon, phonon-isotope).

These inputs were then read in by the Phoebe code, where the calculation of the coupled Boltzmann transport equation was performed. From the output of this calculation, we obtained JSON files containing  $\zeta_{\text{ee, ep, pe, pp}}, \alpha, S, \sigma$ , and  $\kappa$ , as well as the  $D_{\text{ee, ep, pe, pp}}^{ij}, \chi_{\text{p, e}}^{ij}, \psi^{ij}$  tensors. Then, these were post-processed with the SolViTE toolkit to solve the VTE with finite-element simulation.

- 
- [1] L. Mezhev-Deglin, Measurement of the thermal conductivity of crystalline He<sup>4</sup>, Soviet Phys. JETP **22** (1966).  
 [2] C. C. Ackerman, B. Bertman, H. A. Fairbank, and R. A.

- Guyer, Second sound in solid helium, Phys. Rev. Lett. **16**, 789–791 (1966).  
 [3] R. N. Gurzhi, Hydrodynamic effects in solids at low tem-



- perature, Soviet Physics Uspekhi **11**, 255 (1968).
- [4] H. E. Jackson, C. T. Walker, and T. F. McNelly, Second sound in naf, Phys. Rev. Lett. **25**, 26–28 (1970).
- [5] D. W. Pohl and V. Irniger, Observation of second sound in naf by means of light scattering, Phys. Rev. Lett. **36**, 480–483 (1976).
- [6] B. Hehlen, A.-L. Pérou, E. Courtens, and R. Vacher, Observation of a doublet in the quasielastic central peak of quantum-paraelectric  $\text{SrTiO}_3$ , Phys. Rev. Lett. **75**, 2416–2419 (1995).
- [7] Y. K. Koh and D. G. Cahill, Frequency dependence of the thermal conductivity of semiconductor alloys, Phys. Rev. B **76**, 075207 (2007).
- [8] D. D. Joseph and L. Preziosi, Heat waves, Rev. Mod. Phys. **61**, 41–73 (1989).
- [9] J. Dragašević and M. Simoncelli, Viscous heat backflow and temperature resonances in extreme thermal conductors (2025 revision in preparation.), ”” (2023).
- [10] M. J. M. de Jong and L. W. Molenkamp, Hydrodynamic electron flow in high-mobility wires, Phys. Rev. B **51**, 13389–13402 (1995).
- [11] L. Levitov and G. Falkovich, Electron viscosity, current vortices and negative nonlocal resistance in graphene, Nature Physics **12**, 672 (2016).
- [12] D. A. Bandurin, I. Torre, R. K. Kumar, M. B. Shalom, A. Tomadin, A. Principi, G. H. Auton, E. Khestanova, K. S. Novoselov, I. V. Grigorieva, L. A. Ponomarenko, A. K. Geim, and M. Polini, Negative local resistance caused by viscous electron backflow in graphene, Science **351**, 1055–1058 (2016), <https://www.science.org/doi/pdf/10.1126/science.aad0201>.
- [13] J. Crossno, J. K. Shi, K. Wang, X. Liu, A. Harzheim, A. Lucas, S. Sachdev, P. Kim, T. Taniguchi, K. Watanabe, *et al.*, Observation of the dirac fluid and the breakdown of the wiedemann-franz law in graphene, Science **351**, 1058–1061 (2016).
- [14] P. J. Moll, P. Kushwaha, N. Nandi, B. Schmidt, and A. P. Mackenzie, Evidence for hydrodynamic electron flow in  $\text{pdcO}_2$ , Science **351**, 1061–1064 (2016).
- [15] J. A. Sulpizio, L. Ella, A. Rozen, J. Birkbeck, D. J. Perello, D. Dutta, M. Ben-Shalom, T. Taniguchi, K. Watanabe, T. Holder, *et al.*, Visualizing poiseuille flow of hydrodynamic electrons, Nature **576**, 75–79 (2019).
- [16] S. Huberman, R. A. Duncan, K. Chen, B. Song, V. Chiloyan, Z. Ding, A. A. Maznev, G. Chen, and K. A. Nelson, Observation of second sound in graphite at temperatures above 100 k, Science **364**, 375–379 (2019).
- [17] Y. Machida, N. Matsumoto, T. Isono, and K. Behnia, Phonon hydrodynamics and ultrahigh-room-temperature thermal conductivity in thin graphite, Science **367**, 309–312 (2020).
- [18] J. Jeong, X. Li, S. Lee, L. Shi, and Y. Wang, Transient Hydrodynamic Lattice Cooling by Picosecond Laser Irradiation of Graphite, Physical Review Letters **127**, 085901 (2021).
- [19] X. Huang, Y. Guo, Y. Wu, S. Masubuchi, K. Watanabe, T. Taniguchi, Z. Zhang, S. Volz, T. Machida, and M. Nomura, Observation of phonon poiseuille flow in isotopically purified graphite ribbons, Nature Communications **14**, 2044 (2023).
- [20] X. Huang, R. Anufriev, L. Jalabert, K. Watanabe, T. Taniguchi, Y. Guo, Y. Ni, S. Volz, and M. Nomura, A graphite thermal Tesla valve driven by hydrodynamic phonon transport, Nature , 1–5 (2024), publisher: Nature Publishing Group.
- [21] M. L. Palm, C. Ding, W. S. Huxter, T. Taniguchi, K. Watanabe, and C. L. Degen, Observation of current whirlpools in graphene at room temperature, Science **384**, 465–469 (2024), publisher: American Association for the Advancement of Science.
- [22] Z. Ding, K. Chen, B. Song, J. Shin, A. A. Maznev, K. A. Nelson, and G. Chen, Observation of second sound in graphite over 200 k, Nature communications **13**, 1–9 (2022).
- [23] A. Tomadin, G. Vignale, and M. Polini, Corbino Disk Viscometer for 2D Quantum Electron Liquids, Physical Review Letters **113**, 235901 (2014).
- [24] I. Torre, A. Tomadin, A. K. Geim, and M. Polini, Non-local transport and the hydrodynamic shear viscosity in graphene, Physical Review B - Condensed Matter and Materials Physics **92**, 1–11 (2015).
- [25] A. Aharon-Steinberg, T. Völkl, A. Kaplan, A. K. Pariari, I. Roy, T. Holder, Y. Wolf, A. Y. Meltzer, Y. Myasoedov, M. E. Huber, B. Yan, G. Falkovich, L. S. Levitov, M. Hücker, and E. Zeldov, Direct observation of vortices in an electron fluid, Nature **607**, 74–80 (2022).
- [26] G. Varnavides, A. Yacoby, C. Felser, and P. Narang, Charge transport and hydrodynamics in materials, Nature Reviews Materials , 1–16 (2023), publisher: Nature Publishing Group.
- [27] R. A. Guyer and J. Krumhansl, Solution of the linearized phonon boltzmann equation, Physical Review **148**, 766 (1966).
- [28] R. J. Hardy and D. L. Albers, Hydrodynamic approximation to the phonon boltzmann equation, Phys. Rev. B **10**, 3546–3551 (1974).
- [29] J. A. Sussmann and A. Thellung, Thermal Conductivity of Perfect Dielectric Crystals in the Absence of Umklapp Processes, Proc. Phys. Soc. **81**, 1122 (1963).
- [30] C. P. Enz, One-particle densities, thermal propagation, and second sound in dielectric crystals, Annals of Physics **46**, 114–173 (1968).
- [31] S. Poncé, W. Li, S. Reichardt, and F. Giustino, First-principles calculations of charge carrier mobility and conductivity in bulk semiconductors and two-dimensional materials, Reports on Progress in Physics **83**, 036501 (2020).
- [32] F. Giustino, Electron-phonon interactions from first principles, Reviews of Modern Physics **89**, 015003 (2017).
- [33] S. Poncé, E. Margine, C. Verdi, and F. Giustino, EPW: Electron-phonon coupling, transport and superconducting properties using maximally localized Wannier functions, Computer Physics Communications **209**, 116–133 (2016).
- [34] A. Cepellotti, J. Coulter, A. Johansson, N. S. Fedorova, and B. Kozinsky, Phoebe: a high-performance framework for solving phonon and electron Boltzmann transport equations, Journal of Physics: Materials **5**, 035003 (2022).
- [35] J.-J. Zhou and M. Bernardi, *Ab initio* electron mobility and polar phonon scattering in GaAs, Physical Review B **94**, 201201 (2016).
- [36] L. Chaput, Direct Solution to the Linearized Phonon Boltzmann Equation, Phys. Rev. Lett. **110**, 265506 (2013).
- [37] G. Fugallo, M. Lazzeri, L. Paulatto, and F. Mauri, Ab

- initio variational approach for evaluating lattice thermal conductivity, *Phys. Rev. B* **88**, 045430 (2013).
- [38] L. Paulatto, F. Mauri, and M. Lazzeri, Anharmonic properties from a generalized third-order ab initio approach: Theory and applications to graphite and graphene, *Phys. Rev. B* **87**, 214303 (2013).
- [39] L. Lindsay, First principles peierls-boltzmann phonon thermal transport: a topical review, *Nanoscale and Microscale Thermophysical Engineering* **20**, 67–84 (2016).
- [40] P. B. Allen and V. Perebeinos, Temperature in a Peierls-Boltzmann treatment of nonlocal phonon heat transport, *Physical Review B* **98**, 085427 (2018).
- [41] M. Puligheddu, Y. Xia, M. Chan, and G. Galli, Computational prediction of lattice thermal conductivity: A comparison of molecular dynamics and Boltzmann transport approaches, *Physical Review Materials* **3**, 085401 (2019).
- [42] Y. Guo, Z. Zhang, M. Nomura, S. Volz, and M. Wang, Phonon vortex dynamics in graphene ribbon by solving Boltzmann transport equation with ab initio scattering rates, *Int. J. Heat Mass Transf.* **169**, 120981 (2021).
- [43] M. Raya-Moreno, X. Cartoixà, and J. Carrete, BTE-Barna: An extension of almaBTE for thermal simulation of devices based on 2D materials, *Computer Physics Communications* **281**, 108504 (2022).
- [44] C. Zhang, S. Huberman, and L. Wu, On the emergence of heat waves in the transient thermal grating geometry, *J. Appl. Phys.* **132**, 085103 (2022).
- [45] Z. Han and X. Ruan, Thermal conductivity of monolayer graphene: Convergent and lower than diamond, *Phys. Rev. B* **108**, L121412 (2023).
- [46] J. Zhou, B. Liao, B. Qiu, S. Huberman, K. Esfarjani, M. S. Dresselhaus, and G. Chen, Ab initio optimization of phonon drag effect for lower-temperature thermoelectric energy conversion, *Proceedings of the National Academy of Sciences* **112**, 14777–14782 (2015), publisher: Proceedings of the National Academy of Sciences.
- [47] N. H. Protik and B. Kozinsky, Electron-phonon drag enhancement of transport properties from a fully coupled *ab initio* Boltzmann formalism, *Physical Review B* **102**, 245202 (2020).
- [48] N. H. Protik and D. A. Broido, Coupled transport of phonons and carriers in semiconductors: A case study of n-doped GaAs, *Physical Review B* **101**, 075202 (2020).
- [49] N. H. Protik, C. Li, M. Pruneda, D. Broido, and P. Ordejón, The elphbolt ab initio solver for the coupled electron-phonon Boltzmann transport equations, *npj Computational Materials* **8**, 28 (2022).
- [50] C. Hua, L. Lindsay, X. Chen, and A. J. Minnich, Generalized Fourier’s law for nondiffusive thermal transport: Theory and experiment, *Physical Review B* **100**, 085203 (2019), publisher: American Physical Society.
- [51] C. Hua and L. Lindsay, Space-time dependent thermal conductivity in nonlocal thermal transport, *Physical Review B* **102**, 104310 (2020).
- [52] L. Sendra, A. Beardo, P. Torres, J. Bafaluy, F. X. Alvarez, and J. Camacho, Derivation of a hydrodynamic heat equation from the phonon Boltzmann equation for general semiconductors, *Phys. Rev. B* **103**, L140301 (2021).
- [53] L. Sendra, A. Beardo, J. Bafaluy, P. Torres, F. X. Alvarez, and J. Camacho, Hydrodynamic heat transport in dielectric crystals in the collective limit and the drifting/driftless velocity conundrum, *Phys. Rev. B* **106**, 155301 (2022).
- [54] M. Simoncelli, N. Marzari, and A. Cepellotti, Generalization of Fourier’s law into viscous heat equations, *Phys. Rev. X* **10**, 011019 (2020).
- [55] H.-Y. Yang, X. Yao, V. Plisson, S. Mozaffari, J. P. Scheifers, A. F. Savvidou, E. S. Choi, G. T. McCandless, M. F. Padlewski, C. Putzke, P. J. W. Moll, J. Y. Chan, L. Balicas, K. S. Burch, and F. Tafti, Evidence of a coupled electron-phonon liquid in NbGe<sub>2</sub>, *Nature Communications* **12**, 5292 (2021).
- [56] A. Levchenko and J. Schmalian, Transport properties of strongly coupled electron-phonon liquids, *Annals of Physics* **419**, 168218 (2020).
- [57] X. Huang and A. Lucas, Electron-phonon hydrodynamics, *Physical Review B* **103**, 155128 (2021).
- [58] A. Jaoui, A. Gourgout, G. Seyfarth, A. Subedi, T. Lorenz, B. Fauqué, and K. Behnia, Formation of an electron-phonon bifluid in bulk Antimony, *Phys. Rev. X* **12**, 031023 (2022).
- [59] A. Cepellotti, G. Fugallo, L. Paulatto, M. Lazzeri, F. Mauri, and N. Marzari, Phonon hydrodynamics in two-dimensional materials, *Nat. Commun.* **6**, 6400 (2015).
- [60] L. D. Landau, E. M. Lifshitz, and L. P. Pitaevskii, *Physical Kinetics. Course of theoretical physics, Vol. 10* (Pergamon Press, 1981).
- [61] Y. Quan, Y. Chen, and B. Liao, Significant phonon drag effect in wide band gap GaN and AlN, *Physical Review B* **107**, 245202 (2023).
- [62] T. Takezawa, T. Tsuzuku, A. Ono, and Y. Hishiyama, Thermoelectric power of single-crystal graphite at low temperatures, *Philosophical Magazine* **19**, 623–628 (1969).
- [63] K. Sugihara, Phonon Drag Thermoelectric Power in Graphite, *Journal of the Physical Society of Japan* **29**, 1465–1470 (1970).
- [64] J. P. Jay-Gerin and R. Maynard, Phonon drag in graphite, *Journal of Low Temperature Physics* **3**, 377–392 (1970).
- [65] A. De Combarieu, J. Jay-Gerin, and R. Maynard, Thermoelectric power of electron-irradiated graphite at low temperatures, *Journal of Physics and Chemistry of Solids* **34**, 189–195 (1973).
- [66] C. Ayache, A. De Combarieu, and J. P. Jay-Gerin, Observation of a new anomaly in the low-temperature thermoelectric power of graphite: Interpretation by a phonon-drag effect acting on the H-point minority holes, *Physical Review B* **21**, 2462–2465 (1980).
- [67] M. Elzinga, D. T. Morelli, and C. Uher, Thermal transport properties of SbCl<sub>5</sub> graphite, *Physical Review B* **26**, 3312–3319 (1982), publisher: American Physical Society.
- [68] C. Uher, Thermopower of exfoliated graphites between 1.7 and 300 K, *Physical Review B* **25**, 4167–4172 (1982).
- [69] K. Sugihara, Thermoelectric power of graphite intercalation compounds, *Physical Review B* **28**, 2157–2165 (1983), publisher: American Physical Society.
- [70] A. Cepellotti and N. Marzari, Thermal transport in crystals as a kinetic theory of relaxons, *Phys. Rev. X* **6**, 041013 (2016).
- [71] M. Fiorentini and N. Bonini, Thermoelectric coefficients of n-doped silicon from first principles via the solution of the Boltzmann transport equation, *Phys. Rev. B* **94**,

- 085204 (2016).
- [72] F. T. Vas'ko and O. E. Raichev, *Quantum kinetic theory and applications: electrons, photons, phonons* (Springer, New York, 2005).
- [73] J. M. Ziman, *Electrons and phonons: the theory of transport phenomena in solids* (Oxford university press, 1960).
- [74] T. Sohler, M. Calandra, C.-H. Park, N. Bonini, N. Marzari, and F. Mauri, Phonon-limited resistivity of graphene by first-principles calculations: Electron-phonon interactions, strain-induced gauge field, and boltzmann equation, *Physical Review B* **90**, 125414 (2014).
- [75] C.-H. Park, N. Bonini, T. Sohler, G. Samsonidze, B. Kozinsky, M. Calandra, F. Mauri, and N. Marzari, Electron-phonon interactions and the intrinsic electrical resistivity of graphene, *Nano letters* **14**, 1113–1119 (2014).
- [76] Rigorously speaking, in the presence of electron-electron collision integral one would obtain the eBTE for electrons interacting among themselves and with a phonon bath. However, we note that the calculation of the full electron-electron collision integral, accounting for both normal and Umklapp electron-electron processes, is still beyond the reach of state-of-the-art methods [124].
- [77] W. Li, J. Carrete, N. A. Katcho, and N. Mingo, ShengBTE: A solver of the Boltzmann transport equation for phonons, *Comput. Phys. Commun.* **185**, 1747 – 1758 (2014).
- [78] J. Carrete, B. Vermeersch, A. Katre, A. van Roekeghem, T. Wang, G. K. Madsen, and N. Mingo, almaBTE : A solver of the space-time dependent Boltzmann transport equation for phonons in structured materials, *Comput. Phys. Commun.* **220**, 351 – 362 (2017).
- [79] A. Togo, L. Chaput, and I. Tanaka, Distributions of phonon lifetimes in Brillouin zones, *Phys. Rev. B* **91**, 094306 (2015).
- [80] T. Tadano, Y. Gohda, and S. Tsuneyuki, Anharmonic force constants extracted from first-principles molecular dynamics: applications to heat transfer simulations, *Journal of Physics: Condensed Matter* **26**, 225402 (2014).
- [81] B. Liao, B. Qiu, J. Zhou, S. Huberman, K. Esfarjani, and G. Chen, Significant Reduction of Lattice Thermal Conductivity by the Electron-Phonon Interaction in Silicon with High Carrier Concentrations: A First-Principles Study, *Physical Review Letters* **114**, 115901 (2015).
- [82] A. Tomadin and M. Polini, Theory of the plasma-wave photoresponse of a gated graphene sheet, *Phys. Rev. B* **88**, 205426 (2013).
- [83] T. V. Phan, J. C. W. Song, and L. S. Levitov, Ballistic heat transfer and energy waves in an electron system, arxiv preprint , 1–4 (2013), arXiv:1306.4972.
- [84] M. E. Tuckerman, *Statistical mechanics: theory and molecular simulation* (Oxford University Press, Oxford ; New York, 2010) oCLC: ocn551495372.
- [85] This similarity transformation is a generalization of the one performed in Refs. [36, 93].
- [86] H. Spohn, The Phonon Boltzmann Equation, Properties and Link to Weakly Anharmonic Lattice Dynamics, *Journal of Statistical Physics* **124**, 1041–1104 (2006).
- [87] This decomposition has been employed, e.g., in Refs. [27, 54, 93] for phonon transport, and in [56] for a simplified electron-phonon problem.
- [88] H. Brenner, Navier–Stokes revisited, *Physica A* **349**, 60–132 (2005).
- [89] R. Sambasivam, S. Chakraborty, and F. Durst, Numerical predictions of backward-facing step flows in microchannels using extended Navier–Stokes equations, *Microfluid. Nanofluid.* **16**, 757–772 (2014).
- [90] J. Schwarz, K. Axelsson, D. Anheuer, M. Richter, J. Adam, M. Heinrich, and R. Schwarze, An OpenFOAM solver for the extended Navier–Stokes equations, *SoftwareX* **22**, 101378 (2023).
- [91] J. Maurer, P. Tabeling, P. Joseph, and H. Willaime, Second-order slip laws in microchannels for helium and nitrogen, *Phys. Fluids* **15**, 2613–2621 (2003).
- [92] N. Dongari, A. Sharma IITK, and F. Durst, Pressure-driven diffusive gas flows in micro-channels: From the Knudsen to the continuum regimes, *Microfluid. Nanofluid.* **6**, 679–692 (2009).
- [93] R. J. Hardy, Phonon Boltzmann equation and second sound in solids, *Phys. Rev. B* **2**, 1193–1207 (1970).
- [94] R. J. Hardy, Energy-Flux Operator for a Lattice, *Phys. Rev.* **132**, 168–177 (1963).
- [95] M. J. Rice, Theory of Viscosity in Nearly Ferromagnetic Fermi Liquids, *Physical Review* **162**, 189–191 (1967).
- [96] Energy and charge terms,  $|z_{\mathbf{q}s}^T\rangle$  and  $|z_{\mathbf{q}s}^\mu\rangle$ , vanish from the right-hand side because energy and charge are conserved also for  $\Omega$ , so  $|\theta_{\mathbf{q}s}^0\rangle$  and  $|\theta_{\mathbf{q}s}^e\rangle$  are still zero eigenvectors.
- [97] E. D. Lucente, F. Libbi, and N. Marzari, Vortices and backflow in hydrodynamic heat transport (2025), arXiv:2501.16580 [physics].
- [98] A. Akrap, T. Weller, M. Ellerby, S. S. Saxena, G. Csányi, and L. Forró, C 6 Yb and graphite: A comparative high-pressure transport study, *Physical Review B* **76**, 045426 (2007).
- [99] C. Zhang and Z. Guo, A transient heat conduction phenomenon to distinguish the hydrodynamic and (quasi) ballistic phonon transport, *International Journal of Heat and Mass Transfer* **181**, 121847 (2021).
- [100] In this work we neglect electron-electron scattering, since by focusing on the regime where phonon-phonon is dominant and progressively enhancing the role of electrons via doping, we expect that and electron-phonon scattering will be dominant over electron-electron scattering.
- [101] M. Raya-Moreno, J. Carrete, and X. Cartoixa, Hydrodynamic signatures in thermal transport in devices based on two-dimensional materials: An *ab initio* study, *Phys. Rev. B* **106**, 014308 (2022).
- [102] This formally follows from the DTE constraint that  $T(\mathbf{r})$  and  $V(\mathbf{r})$  have to be harmonic functions, and also from the requirement that the boundaries have to be electrically insulating and adiabatic.
- [103] V. K. Michalis, A. N. Kalarakis, E. D. Skouras, and V. N. Burganos, Rarefaction effects on gas viscosity in the Knudsen transition regime, *Microfluidics and Nanofluidics* **9**, 847–853 (2010).
- [104] K. Balasubramanian, F. Hayot, and W. F. Saam, Darcy's law from lattice-gas hydrodynamics, *Phys. Rev. A* **36**, 2248–2253 (1987).
- [105] O. Dardis and J. McCloskey, Lattice Boltzmann scheme with real numbered solid density for the simulation of flow in porous media, *Phys. Rev. E* **57**, 4834–4837

- (1998).
- [106] D. Bresch and B. Desjardins, Existence of Global Weak Solutions for a 2D Viscous Shallow Water Equations and Convergence to the Quasi-Geostrophic Model, *Commun. Math. Phys.* **238**, 211–223 (2003).
- [107] X. Cai and Q. Jiu, Weak and strong solutions for the incompressible Navier–Stokes equations with damping, *J. Math. Anal.* **343**, 799–809 (2008).
- [108] Z. Zhang, X. Wu, and M. Lu, On the uniqueness of strong solution to the incompressible Navier–Stokes equations with damping, *J. Math. Anal.* **377**, 414–419 (2011).
- [109] V. Goblot, K. Wu, E. D. Lucente, Y. Zhu, E. Losero, Q. Jobert, C. J. Concha, N. Marzari, M. Simoncelli, and C. Galland, Imaging heat transport in suspended diamond nanostructures with integrated spin defect thermometers (2024), arXiv:2411.04065.
- [110] Y. Zeng, H. Guo, O. M. Ghosh, K. Watanabe, T. Taniguchi, L. S. Levitov, and C. R. Dean, Quantitative measurement of viscosity in two-dimensional electron fluids (2024), arXiv:2407.05026 [cond-mat] version: 1.
- [111] S. Xu, Y. Li, R. A. Vitalone, R. Jing, A. J. Sternbach, S. Zhang, J. Ingham, M. Delor, J. W. McIver, M. Yankowitz, R. Queiroz, A. J. Millis, M. M. Fogler, C. R. Dean, A. N. Pasupathy, J. Hone, M. Liu, and D. N. Basov, Electronic interactions in Dirac fluids visualized by nano-terahertz spacetime interference of electron-photon quasiparticles, *Science Advances* **10**, eado5553 (2024), publisher: American Association for the Advancement of Science.
- [112] U. Vool, A. Hamo, G. Varnavides, Y. Wang, T. X. Zhou, N. Kumar, Y. Dovzhenko, Z. Qiu, C. A. C. Garcia, A. T. Pierce, J. Gooth, P. Anikeeva, C. Felser, P. Narang, and A. Yacoby, Imaging phonon-mediated hydrodynamic flow in WTe<sub>2</sub>, *Nature Physics* **17**, 1216–1220 (2021).
- [113] M. M. Glazov and L. E. Golub, Valley Hall effect caused by the phonon and photon drag, *Physical Review B* **102**, 155302 (2020), publisher: American Physical Society.
- [114] T. Yamaguchi, H. Kohno, and R. A. Duine, Microscopic theory of magnon-drag electron flow in ferromagnetic metals, *Physical Review B* **99**, 094425 (2019), publisher: American Physical Society.
- [115] H. Pan, Z.-K. Ding, B.-W. Zeng, N.-N. Luo, J. Zeng, L.-M. Tang, and K.-Q. Chen, *Ab initio* Boltzmann approach to coupled magnon-phonon thermal transport in ferromagnetic crystals, *Physical Review B* **107**, 104303 (2023).
- [116] Note that, due to inversion symmetry of the phonon Brillouin zone, the state  $-\mathbf{q}, s$  has the same energy as  $\mathbf{q}, s$  and we can replace  $\mathbf{q}$  with  $-\mathbf{q}$  under the sum over  $\mathbf{q}$ .
- [117] We also note that in deriving the VTE we will consider the divergence of these fluxes, thus these constant terms will contribute zero to the balance equations.
- [118] A. Dal Corso, Pseudopotentials periodic table: From h to pu, *Computational Materials Science* **95**, 337–350 (2014).
- [119] A. M. Rappe, K. M. Rabe, E. Kaxiras, and J. Joannopoulos, Optimized pseudopotentials, *Physical Review B* **41**, 1227 (1990).
- [120] R. Sundararaman, K. Letchworth-Weaver, K. A. Schwarz, D. Gunceler, Y. Ozhages, and T. A. Arias, Jdftx: Software for joint density-functional theory, *SoftwareX* **6**, 278–284 (2017).
- [121] L. Paulatto, I. Errea, M. Calandra, and F. Mauri, First-principles calculations of phonon frequencies, lifetimes, and spectral functions from weak to strong anharmonicity: The example of palladium hydrides, *Phys. Rev. B* **91**, 054304 (2015).
- [122] P. Giannozzi, O. Andreussi, T. Brumme, O. Bunau, M. B. Nardelli, M. Calandra, R. Car, C. Cavazzoni, D. Ceresoli, M. Cococcioni, *et al.*, Advanced capabilities for materials modelling with quantum espresso, *Journal of physics: Condensed matter* **29**, 465901 (2017).
- [123] G. Fugallo, A. Cepellotti, L. Paulatto, M. Lazzeri, N. Marzari, and F. Mauri, Thermal Conductivity of Graphene and Graphite: Collective Excitations and Mean Free Paths, *Nano Letters* **14**, 6109–6114 (2014).
- [124] D. J. Abramovitch, J. Mravlje, J.-J. Zhou, A. Georges, and M. Bernardi, Respective Roles of Electron-Phonon and Electron-Electron Interactions in the Transport and Quasiparticle Properties of SrVO<sub>3</sub>, *Physical Review Letters* **133**, 186501 (2024), publisher: American Physical Society.